Coastal Protection and Restoration Authority
150 Terrace Avenue, Baton Rouge, LA 70802 | coastal@la.gov | www.coastal.la.gov

2017 Coastal Master Plan

Attachment C3-25.1: Storm Surge

Report: Final

Date: April 2017

Prepared By: Hugh Roberts and Zachary Cobell

Coastal Protection and Restoration Authority

This document was prepared in support of the 2017 Coastal Master Plan being prepared by the Coastal Protection and Restoration Authority (CPRA). CPRA was established by the Louisiana Legislature in response to Hurricanes Katrina and Rita through Act 8 of the First Extraordinary Session of 2005. Act 8 of the First Extraordinary Session of 2005 expanded the membership, duties, and responsibilities of CPRA and charged the new authority to develop and implement a comprehensive coastal protection plan, consisting of a master plan (revised every five years) and annual plans. CPRA's mandate is to develop, implement, and enforce a comprehensive coastal protection and restoration master plan.

Suggested Citation:

Roberts, H. and Cobell, Z. (2017). *2017 Coastal Master Plan: Attachment C3-25.1: Storm Surge*. Version Final. (pp. 1-110). Baton Rouge, Louisiana: Coastal Protection and Restoration Authority.

Table of Contents

List of Tables

List of Figures

List of Abbreviations

ADCIRC	ADvanced CIRCulation Model
CLARA	Coastal Louisiana Risk Assessment Model
CPRA	Coastal Protection and Restoration Authority
CRMS	Coastwide Reference Monitoring System
CSI	Coastal Studies Institute
FEMA	Federal Emergency Management Agency
FIRM	Flood Insurance Rate Map
FIS	Flood Insurance Study
FWOA	future without action
HSDRRS	Hurricane and Storm Damage Risk Reduction System
ICM	Integrated Compartment Model
JPM-OS	Joint Probability Method Optimal Sampling
NAVD88	North American Vertical Datum of 1988
NDBC	National Data Buoy Center
NOAA	National Oceanographc and Atmospheric Administration
PBL	Planetary Boundary Layer
SWAN	Simulating Waves Nearshore Model
USACE	U.S. Army Corps of Engineers
USGS	U.S. Geological Survey

Appendix 1: ADCIRC+SWAN Model Updates and Validation

Introduction

As part of the 2017 Coastal Master Plan improvement process, the CPRA 2012 (Cobell et al., 2013) ADvanced CIRCulation (ADCIRC) and Simulating Waves Nearshore (SWAN) models, referred to as the ADCIRC+SWAN model, were updated to improve the representation of storm surge across Louisiana while maintaining the mission of providing a high-speed, physics-based modeling approach. The model geometry was updated in three critical ways: geometry enhancements to account for features that were underrepresented, additional model resolution in areas that enhance model skill, and inclusion of protected areas. With these enhancements in place, the model is now referred to as the CPRA 2017 ADCIRC+SWAN model.

After applying the aforementioned updates, the model was validated using Hurricane Ike (Ike; 2008) and Hurricane Gustav (Gustav; 2008) observations like the CPRA 2012 ADCIRC+SWAN model. Additionally, the CPRA 2017 model was compared to observations collected during Hurricane Katrina (Katrina; 2005) and Hurricane Rita (Rita; 2005). For the purposes of validation, the geometry of the CPRA 2017 model was altered to remove major features that have been constucted since the storms occurred, such as the Seabrook Gate, the Inner Harbor Navigation Canal Lake Borgne Surge Barrier, and the Gulf Intracoastal Waterway West Closure Complex.

Model Geometry Updates

Model geometry was updated to enhance the representation of Louisiana's coast in the model. The geometry was specifically updated in the following ways:

1. **Texas and the Louisiana-Texas Shelf** – Additional model resolution on the continental shelf improves SWAN model performance, specifically in transforming waves from deep water to the more shallow coastal areas. Additionally, increased model resolution in Coastal Texas improves model performance in southwestern Louisiana. Figure 1 shows the change in model resolution between CPRA 2012 and CPRA 2017.

2. **Coastal Mississippi and Alabama** – The model boundary was extended inland to mimic the extent used in the Federal Emergency Management Agency (FEMA) models developed for the Flood Insurance Rate Map (FIRM) development in this area (U.S. Army Corps of Engineers [USACE], 2008b). This allows surge to propagate inland naturally, enhancing model performance for storms and scenarios that result in high flood levels in these areas. Figure 2 shows the model with and without the extended model boundary.

3. **Protected Areas** – Areas that were previously excluded from the model in order to reduce computational costs have been introduced to provide both additional numerical accuracy and better visual understanding of model outputs. With the protected areas included, a more accurate head differential across the protection system can be computed in ADCIRC, thereby enhancing the exterior calculation while providing results on the interior as well. (Note: The Coastal Louisiana Risk Assessment [CLARA] model does not directly use ADCIRC model results in protected areas.) Figure 3 shows the model with and without the protected areas included.

4. **West Shore of Lake Pontchartrain** – Under high sea level rise conditions, the CPRA 2012 model boundary was near the edge of surge inundation limits. To prevent possible

boundary effects, the boundary was extended further to the west, and the Mississippi River was extended north to Baton Rouge. Figures 1 and 3 show this model extension.

5. **Feedback** – Relatively minor changes were made to select areas that were specifically recommended for updates by individuals familiar with the CPRA 2012 model or as part of CPRA studies since the 2012 Coastal Master Plan. Updates were based upon available survey and satellite images. The most noteworthy update is near Des Allemandes, which was upgraded as part of a separate CPRA study in the Upper Barataria Basin.

Upon completion of these updates, the CPRA 2017 model contained 1.39 million vertices. This is a significant reduction from the current high-resolution model in Louisiana, SL18, which contains 6.9 million vertices. In the following sections, validation results for the CPRA 2017 model are analyzed and compared to the SL16 model, the predecessor to SL18. The SL16 model contains 5.0 million vertices, and its validation has been published in multiple journal articles (Dietrich et al., 2011; Dietrich et al., 2012).

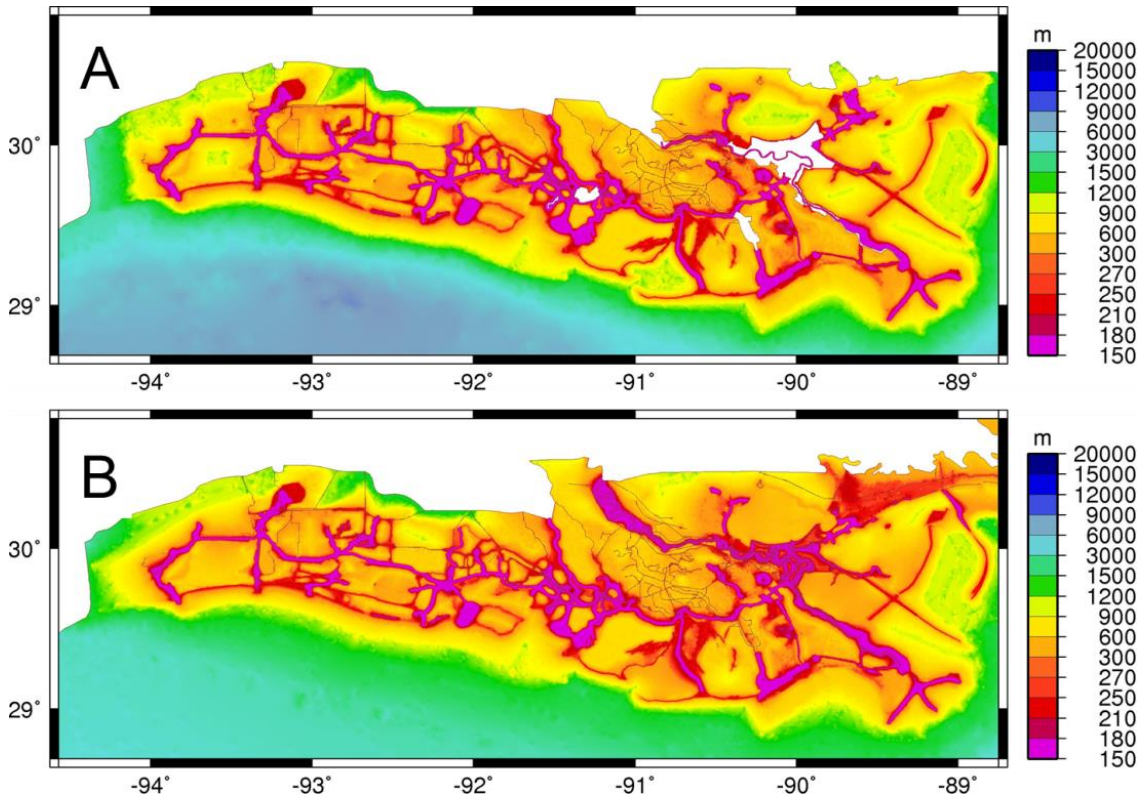

Figure 1: A) CPRA 2012 Model Resolution and B) CPRA 2017 Model Resolution. Warmer colors indicate greater model resolution.

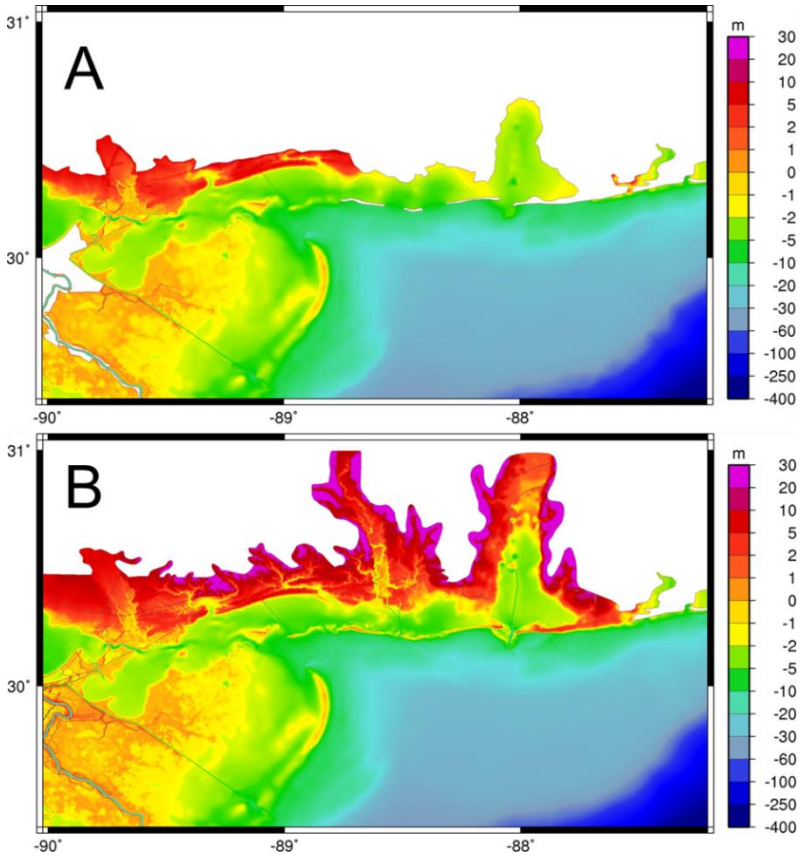

Figure 2: Model Domain in Mississippi and Alabama for the A) CPRA 2012 and B) CPRA 2017 Models. Warmer colors indicate greater elevations.

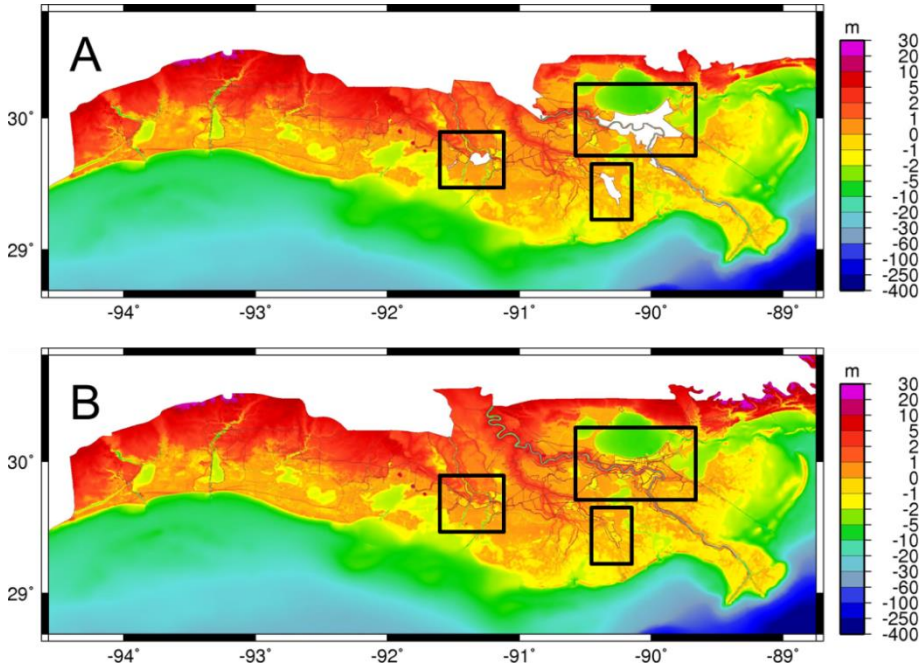

Figure 3: Protected Areas in the A) CPRA 2012 and B) CPRA 2017 Models. Warmer colors indicate greater elevations. Black boxes identify areas of model improvement for CPRA 2017.

Model Validation

The 2017 CPRA model validation was conducted using the same two storms as were used for the 2012 Coastal Master Plan, Gustav and Ike, as well as two additional storms, Katrina and Rita. Oceanweather, Inc., produced data-assimilated wind, and pressure fields were applied. These Katrina and Rita wind and pressure fields were created during the 2007 FEMA Flood Insurance Study (FIS) in Louisiana, and the Gustav and Ike wind and pressure fields were created during the 2011 FEMA FIS in Texas. The studies were conducted to develop coastal FIRMs in both states (USACE, 2008a; USACE, 2008b; USACE, 2008c; USACE, 2011).

Tidal forcing for the model was provided by the Oregon State University Tidal Database (TPXO 7.2). The constituents Q1, O1, P1, K1, N2, M2, S2, and K2 were used to force the model open boundary as well as tidal potential forcing throughout the model.

River discharges were applied for both the Mississippi and Atchafalaya Rivers. Currently, the ADCIRC model only allows a single flow rate to be applied for the entire simulation and, therefore, an averaged flow rate was applied from measured discharges during the individual events. The Mississippi River discharge was applied at Baton Rouge, Louisiana with measurement from United States Geological Survey (USGS) Station 07374000. The Atchafalaya River flowrate was applied near Splice Island with the discharge measurement at Simmesport, Louisiana from USGS Station 07381490.

The model tidal and river forcings were allowed to reach a dynamic equilibrium for a minimum of 18 days before wind and pressure forcing was applied, during which time the SWAN wave model was not active. Once the wind and pressure information was applied to the model, ADCIRC and SWAN computed hydrodynamic and wave calculations, respectively, passing information between the models every 10 minutes. The wind velocity vectors were applied to the water surface in both the ADCIRC and SWAN model using the wind drag formulation described in Appendix 4.

Note that the 2005 and 2008 model versions removed various newly constructed protection features to reflect the conditions under which these storms occurred.

The model was validated with data from the following sources:

- National Oceanographc and Atmospheric Administration (NOAA) water level measurement time series;
- USACE water level measurement time series;
- Coastal Studies Institute (CSI) wave information and water level information;
- Andrew Kennedy (Kennedy et al., 2011) deployed gages in the path of both Gustav and Ike in 2008. These gages measure both wave information and water level information;
- USGS water level measurement time series;
- Coastwide Reference Monitoring System (CRMS) water level measurement time series; and
- High water mark measurements collected post-storm by FEMA, USACE, and their contractors.

Unless otherwise noted, the data used in this study are the same as used in Dietrich et al., 2012.

Hurricane Katrina (2005)

Katrina entered the Gulf of Mexico (Gulf) and quickly became a Category 5 storm while approaching Louisiana. Shortly after weakening to a Category 3 storm, Katrina turned north across the Mississippi River Delta, making landfall and building surge against the Mississippi River levees and the Greater New Orleans hurricane protection system. The storm continued north before making another landfall in Mississippi and eventually degrading while moving north across the southern United States.

The CPRA 2017 model simulation of Katrina began on August 7, 2005, and concluded on August 31, 2005. River discharges of 4,842 cubic meters per second (m^3/s) and 2,067 m^3/s were applied for the Mississippi and Atchafalaya River model boundaries, respectively. Other freshwater inputs such as the Pearl River are not included in the model setup due to model resolution limitations. The lack of freshwater inputs may impact water surface elevation calculations locally. However, the Mississippi and Atchafalaya Rivers are included to ensure that regional impacts from the large river basins are included in the analyses.

Katrina provides an excellent test for the updated model, particularly because of the observed storm surge elevations in Mississippi and Alabama, which can be used to validate the recently added portions of the model domain. Many of the measured high water marks are concentrated in this region.

Figure 4 shows the maximum computed surge from the ADCIRC+SWAN model, and Figure 5 shows the maximum computed significant wave height. Figure 6 show gage locations used for the validation of all four storms. Table 1 reflects the station names as they relate to the numbers shown in these figures. Figures 7 through 9 show the comparison to National Data Buoy Center (NDBC) wave gages. Figures 10 and 11 show the water level comparisons to gage data. Comparisons to high water mark information are shown in Figures 12 and 13. For this storm, high water mark data were available in Mississippi as well as Louisiana. Figures 12 and 13 include high water marks west of I-110 near Biloxi, Mississippi. The ADCIRC model resolution east of Biloxi Bay is more coarse than areas west of the bay in order to minimize computational costs. Previous studies, including analyses of a barrier from New Orleans to the Pearl River Basin, have shown that projects in Louisiana have very limited, if any, impacts on storm surge levels east of Biloxi Bay (Ben C. Gerwick, Inc., 2012).

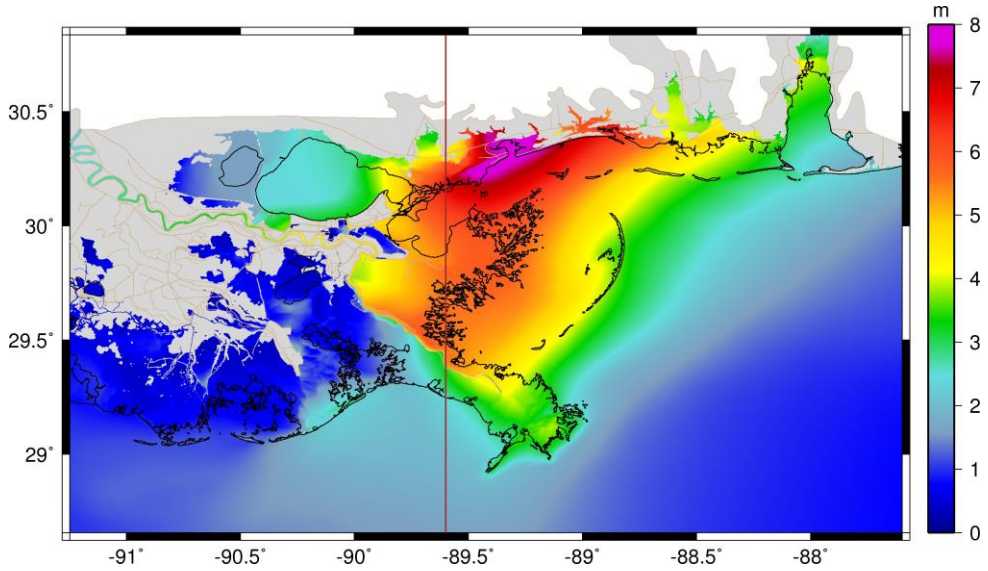

Figure 4: Maximum Storm Surge Elevation (meters [m], North American Vertical Datum of 1988 [NAVD88]) during the 2017 CPRA Hurricane Katrina Simulation. Storm track shown in brown.

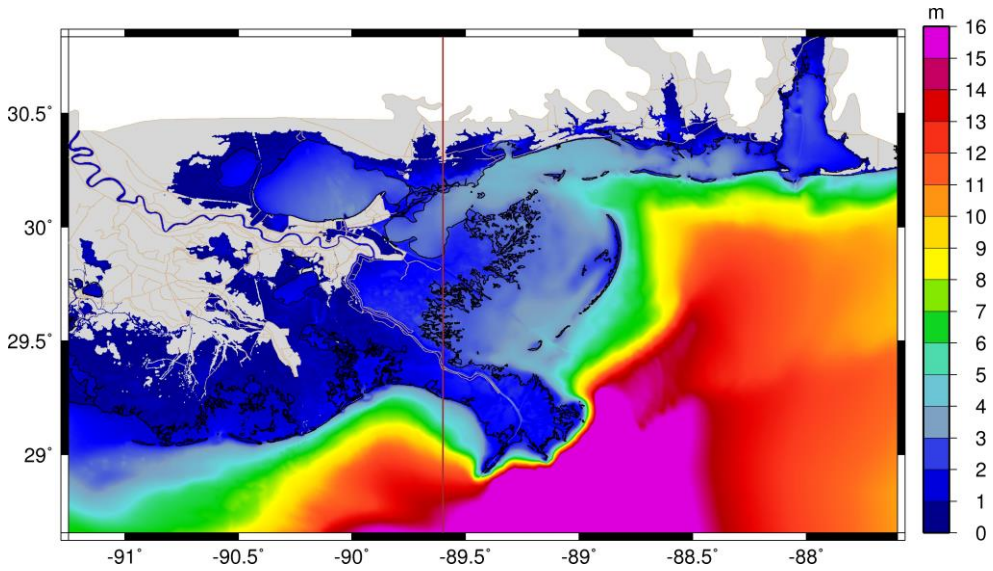

Figure 5: Maximum Significant Wave Height (m) during the 2017 CPRA Hurricane Katrina Simulation. Storm track shown in brown.

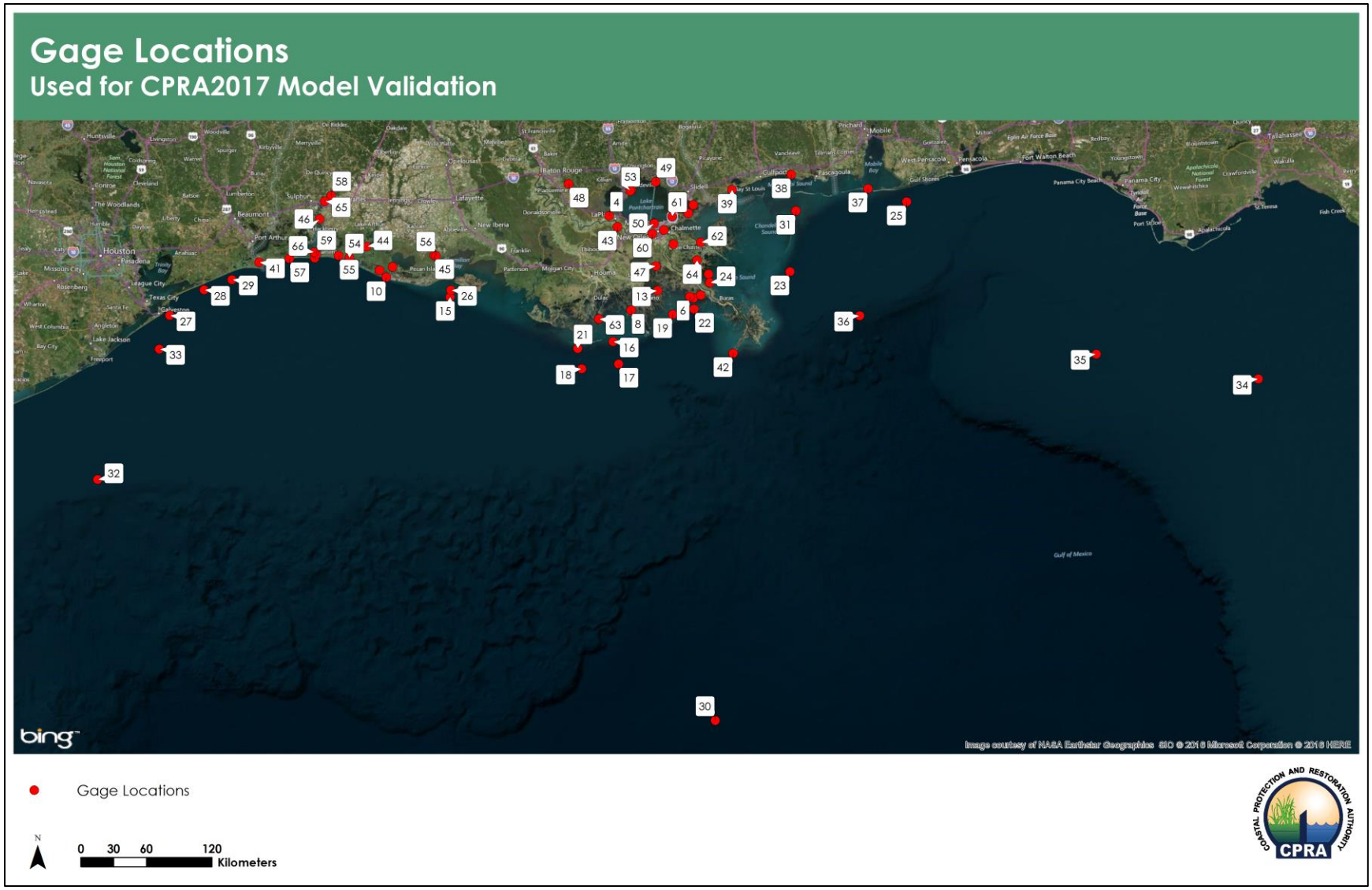

Figure 6: Gage Locations used for CPRA 2017 Model Validation.

Table 1: CPRA 2017 Validation Gages.

Station Number	Longitude	Latitude	Name
1	-90.117000	30.025000	17th Street Canal (USACE)
2	-89.791547	30.100333	CRMS 0002-H01
3	-90.325165	30.303964	CRMS 0030-H01
4	-90.543070	30.093135	CRMS 0059-W01
5	-89.765495	29.397287	CRMS 0174-H01
6	-89.796239	29.408751	CRMS 0176-H01
7	-89.692874	29.419984	CRMS 0272-H01
8	-90.355854	29.311394	CRMS 0337-H01
9	-92.728166	29.665219	CRMS 0581-H01
10	-92.665070	29.606958	CRMS 0599-H01
11	-92.604395	29.693726	CRMS 0626-W01
12	-89.937500	29.847779	CRMS BS08-30
13	-90.100000	29.466667	CRMS DCPBA07
14	-89.614445	29.592222	CRMS DCPBS03
15	-92.061333	29.441167	CSI 03
16	-90.533333	29.053333	CSI 05
17	-90.483333	28.866667	CSI 06
18	-90.832000	28.833167	CSI 15
19	-89.963300	29.267100	Grand Isle (NOAA)
20	-90.026397	29.966639	IHNC Lock(USACE)
21	-90.865100	29.001033	Kennedy 1
22	-89.759817	29.306183	Kennedy 11
23	-88.844850	29.590567	Kennedy 12
24	-89.605633	29.520317	Kennedy 13
25	-87.715150	30.127117	Kennedy 19
26	-92.053183	29.499367	Kennedy 6
27	-94.708950	29.281267	Kennedy X
28	-94.388400	29.496333	Kennedy Y
29	-94.125333	29.584683	Kennedy Z
30	-89.667000	25.900000	NDBC 42001
31	-88.769000	30.090000	NDBC 42007
32	-95.360000	27.913000	NDBC 42019
33	-94.803000	29.003000	NDBC 42035
34	-84.517000	28.500000	NDBC 42036
35	-86.008000	28.791000	NDBC 42039
36	-88.205000	29.205000	NDBC 42040
37	-88.075000	30.250000	NOAA 8735180
38	-88.798330	30.391670	NOAA 8743281
39	-89.366700	30.281700	NOAA 8747766

Station Number	Longitude	Latitude	Name
40	-93.341670	29.766670	NOAA 8768094
41	-93.870000	29.728330	NOAA 8770570
42	-89.406700	28.931700	Southwest Pass (NOAA)
43	-90.466131	30.001667	USACE 01275
44	-92.849242	29.862933	USACE 70750
45	-92.209250	29.787019	USACE 76800
46	-93.294886	30.088719	USACE 76960
47	-90.110556	29.669444	USACE 82875
48	-90.922888	30.365797	USACE 85575
49	-90.092289	30.365797	USACE 85575
50	-90.115644	30.022164	USACE 85625
51	-89.861900	30.141700	USGS 300830089515000
52	-89.740600	30.166900	USGS 301001089442600
53	-90.336000	30.296400	USGS 301748090200900
54	-93.014730	29.770570	USGS DEP-LA11
55	-93.114940	29.786100	USGS DEP-LA12
56	-92.192500	29.783110	USGS DEP-LA9B
57	-93.582580	29.761980	USGS DEP-LC11
58	-93.187500	30.284920	USGS DEP-LC2B
59	-93.328860	29.797640	USGS DEP-LC8A
60	-90.135430	29.936750	USGS DEP-SSS-LA-ORL-001
61	-89.943340	30.077170	USGS DEP-SSS-LA-ORL-014
62	-89.678340	29.855790	USGS DEP-SSS-LA-STB-004
63	-90.660810	29.243140	USGS DEP-SSS-LA-TER-024
64	-89.719444	29.708056	USGS PERM-73745257
65	-93.247222	30.236944	USGS PERM-8017044
66	-93.348800	29.815500	USGS PERM-8017118

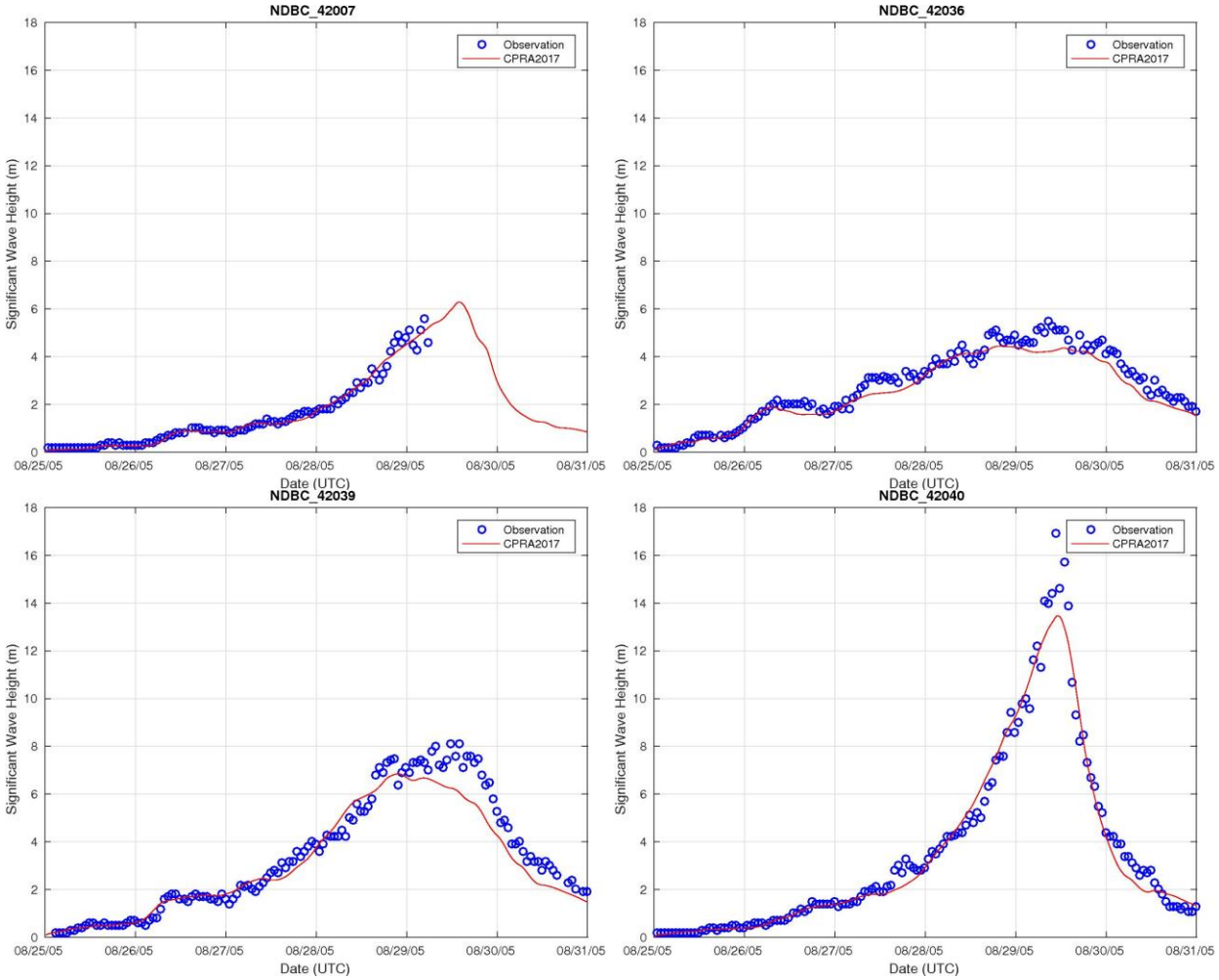

Figure 7: NDBC Significant Wave Height Comparisons for Hurricane Katrina. Observations are in blue; CPRA 2017 model results are in red.

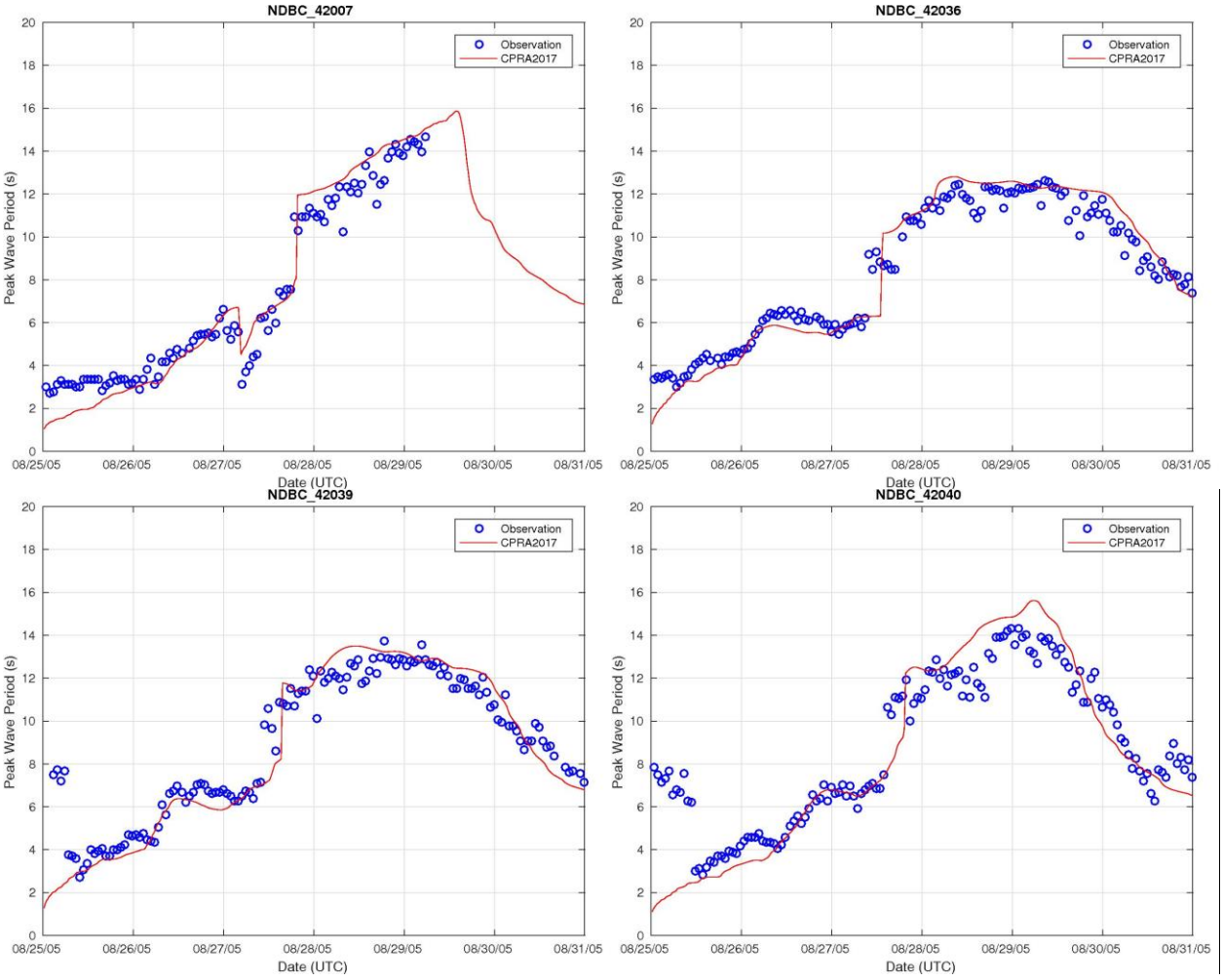

Figure 8: NDBC Peak Wave Period Comparisons for Hurricane Katrina. Observations are in blue; CPRA 2017 model results are in red.

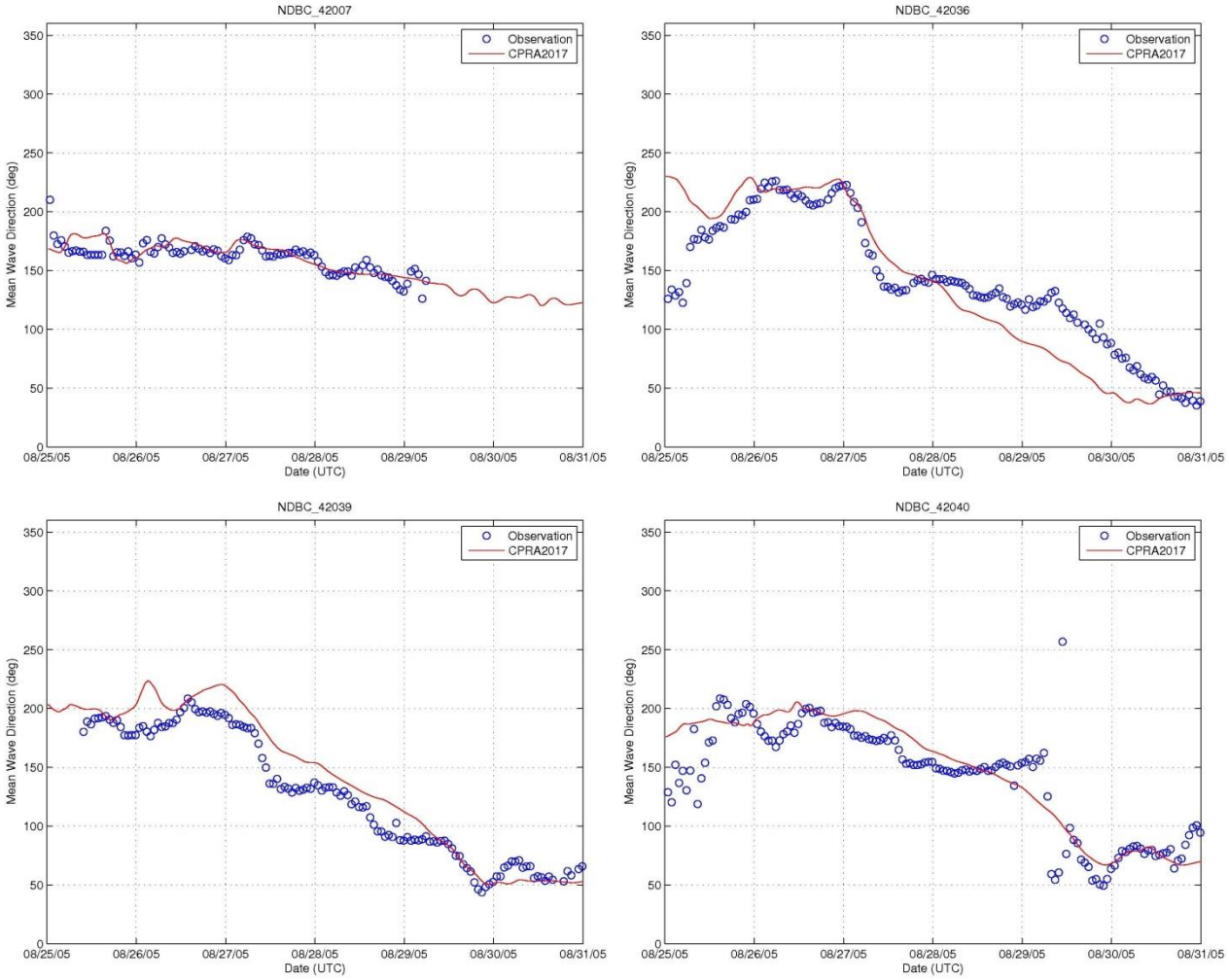

Figure 9: NDBC Mean Wave Direction Comparisons for Hurricane Katrina. Observations are in blue; CPRA 2017 model results are in red.

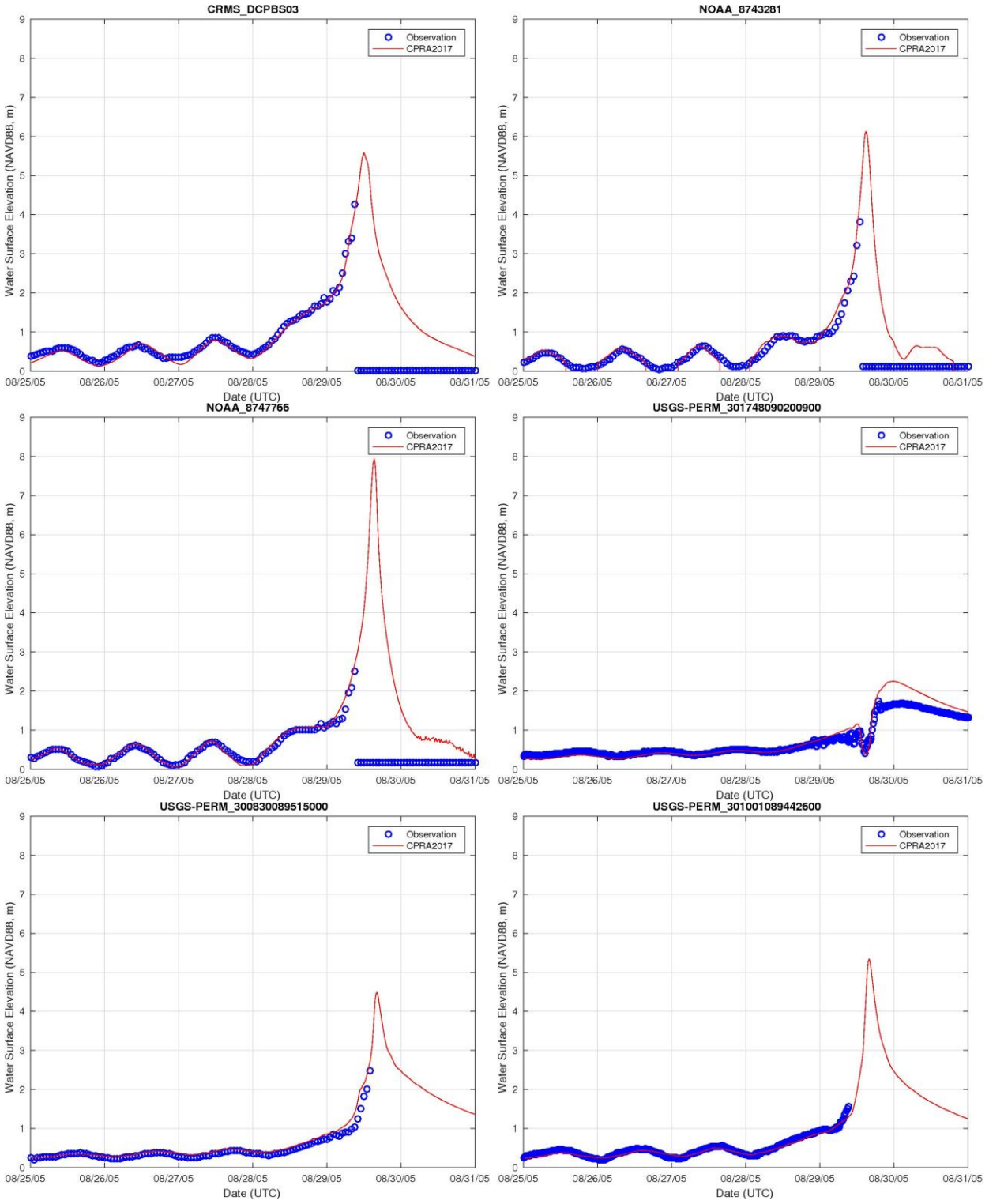

Figure 10: Water Elevation (m, NAVD88) Comparisons for Hurricane Katrina. Observations are in blue; CPRA 2017 model results are in red.

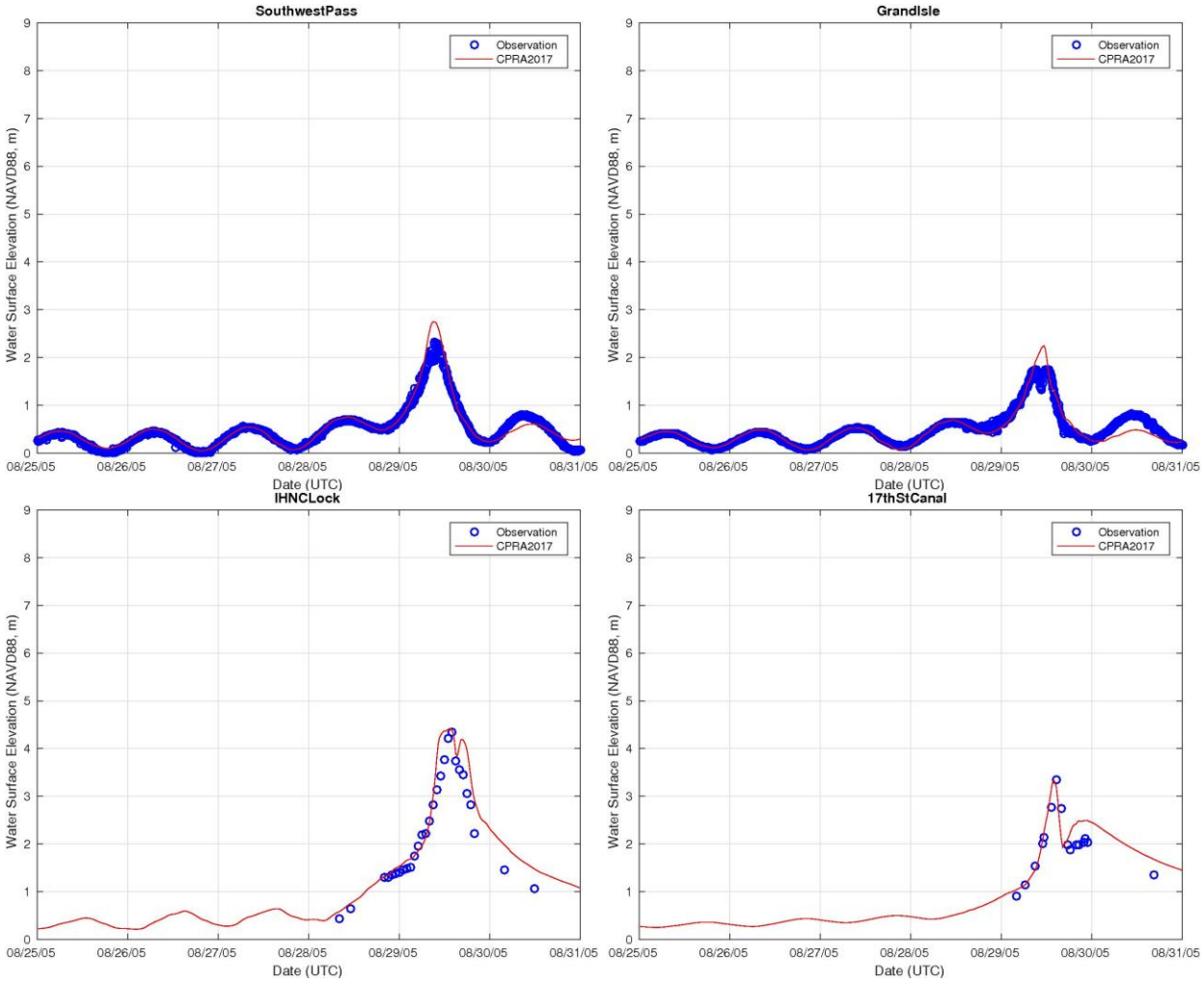

Figure 11: Water Elevation (m, NAVD88) Comparisons for Hurricane Katrina. Observations are in blue; CPRA 2017 model results are in red.

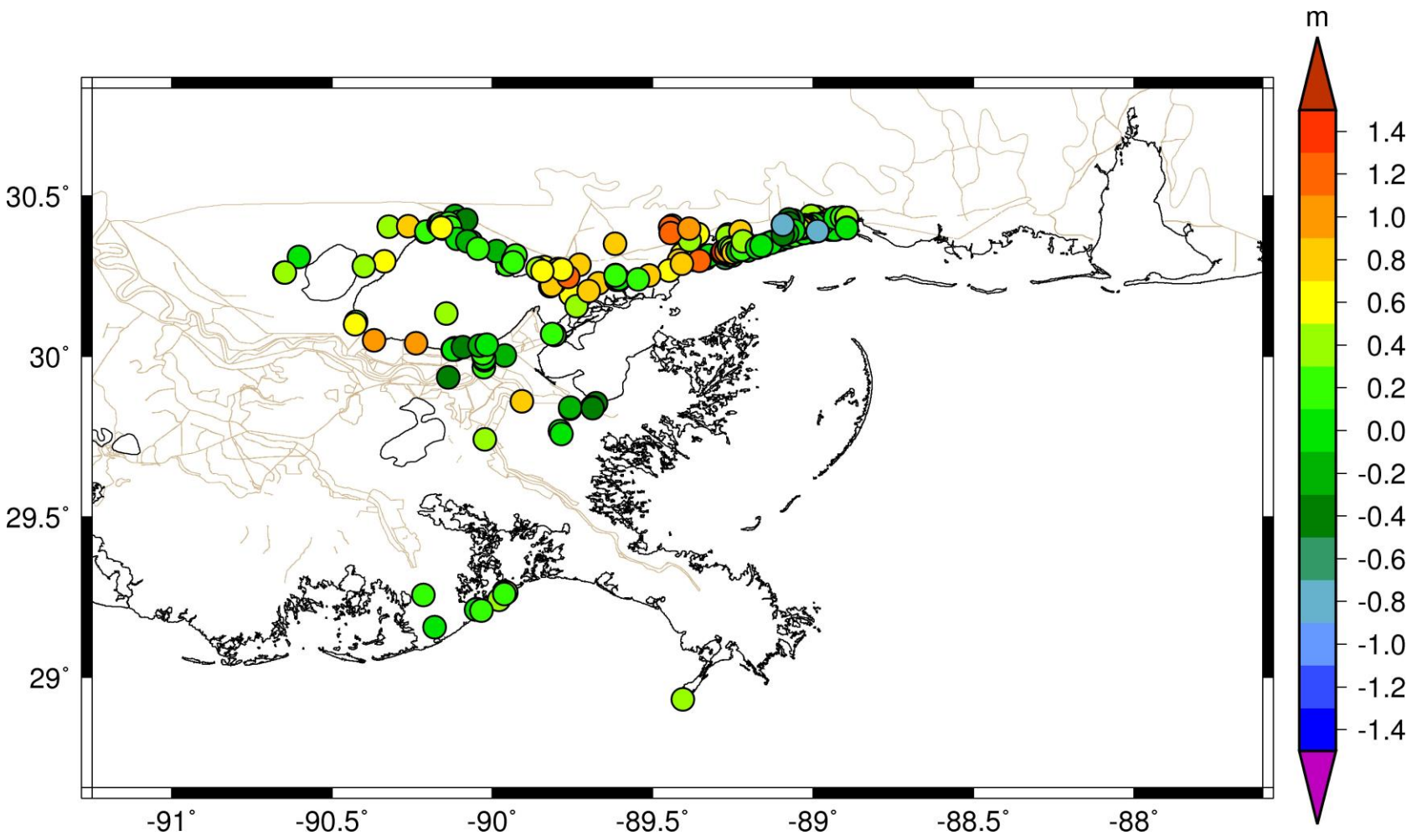

Figure 12: CPRA 2017 Model Hurricane Katrina Comparison to Measured High Water Marks. Warm colors indicate the model results are greater than measurement; cool colors indicate the model results are lower than measurement.

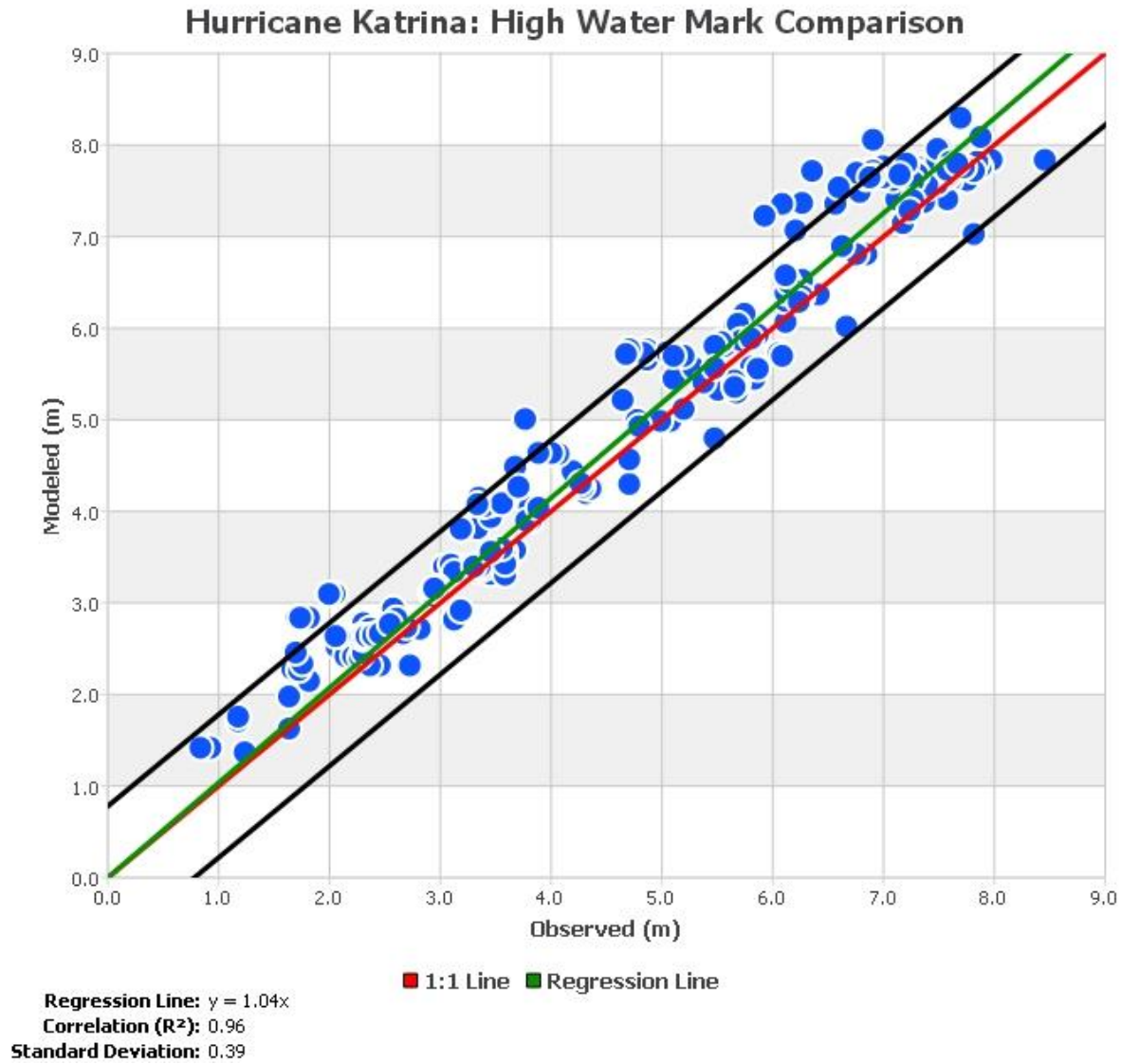

Figure 13: Hurricane Katrina Regression Plot Comparing Measured High Water Marks to CPRA 2017 Model Results.

Hurricane Rita (2005)

Rita entered the Gulf, passing between Florida and Cuba. While moving northwest toward Louisiana, warm waters strengthened the storm to Category 5 intensity. However, the storm weakened to a Category 3 before making landfall in western Louisiana near Sabina Pass approximately one month after Katrina.

The CPRA 2017 model simulation of Rita began on August 31, 2005, and concluded September 5, 2005. River discharges of 5,437 m^3/s and 2,322 m^3/s were used for the Mississippi and Atchafalaya River model boundaries, respectively. Other freshwater inputs such as the Calcasieu River are not included in the model setup due to model resolution limitations.

Figure 14 shows the maximum computed surge from the ADCIRC+SWAN model, and Figure 15 shows the maximum computed significant wave height. Figures 16 through 18 show the comparisons to wave measurements. Figure 19 shows the comparison to water level measurements. Finally, Figures 20 and 21 show the comparisons to measured high water marks. One notable deviation from the measurement is seen in the high water mark comparisons west of Lake Calcasieu near where the eye of the storm made landfall. Previous studies have shown simliar trends (Dietrich et al., 2012). The overpredicted water levels have been attributed to wind speeds greater than those which actually occurred during the storm. Unlike the other storms applied for model calibration, the best available Hurricane Rita winds were not developed using data assimilaton in the eye of the storm. Instead parametric wind fields have been applied, which are generally less accurate than data assimilated winds.

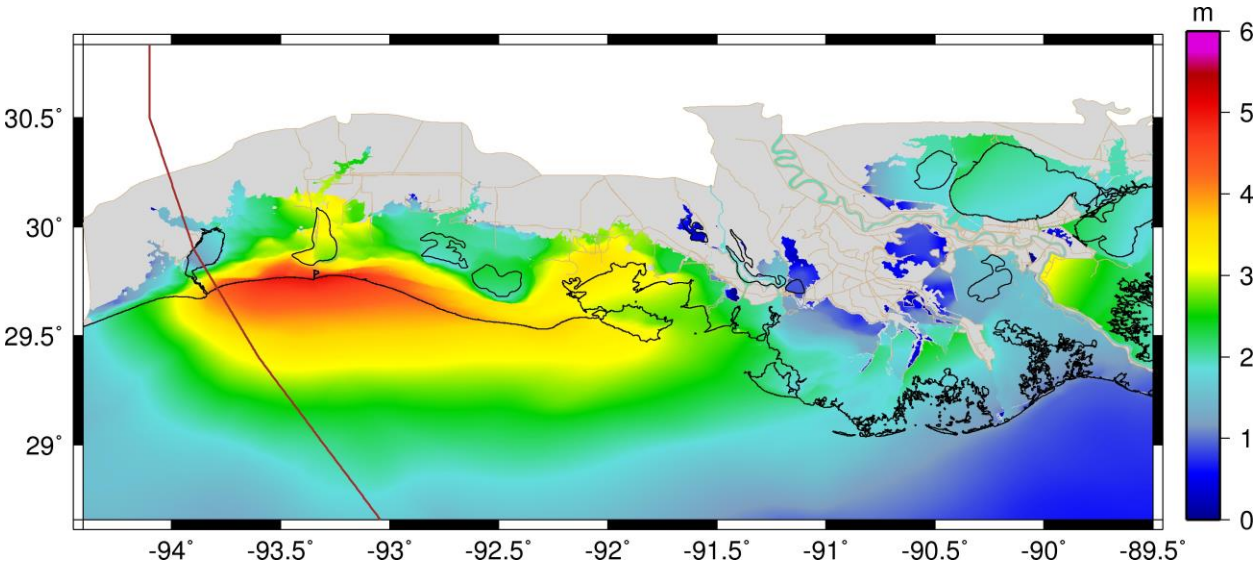

Figure 14: Maximum Storm Surge Elevation (m, NAVD88) During the 2017 CPRA Hurricane Rita Simulation. Storm track shown in brown.

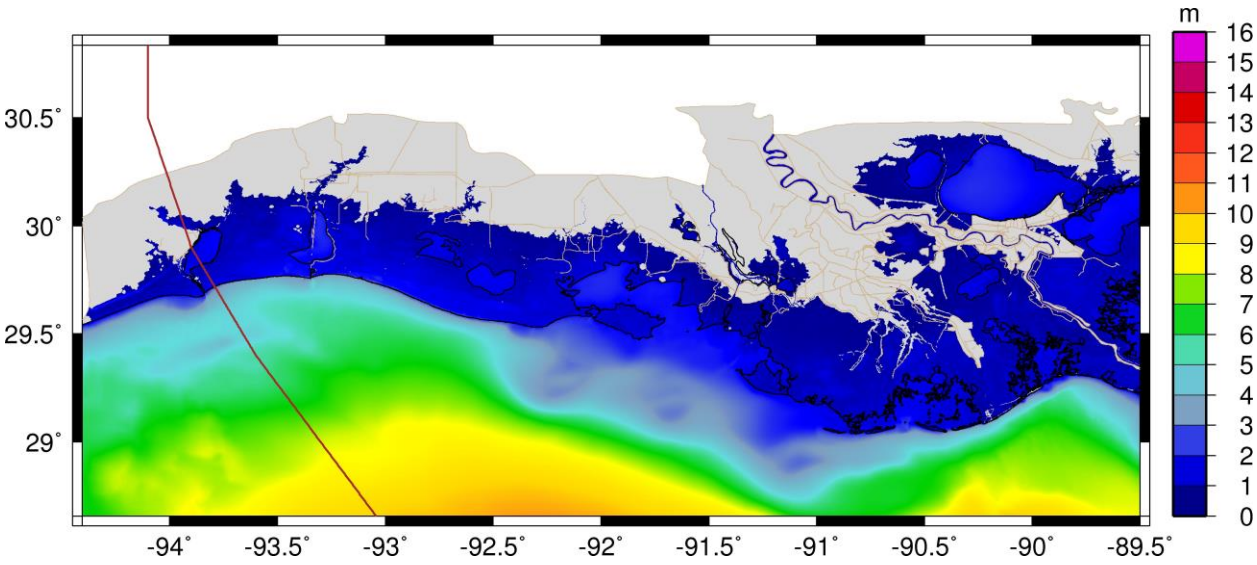

Figure 15: Maximum Significant Wave Height (m) During the 2017 CPRA Hurricane Rita Simulation. Storm track shown in brown.

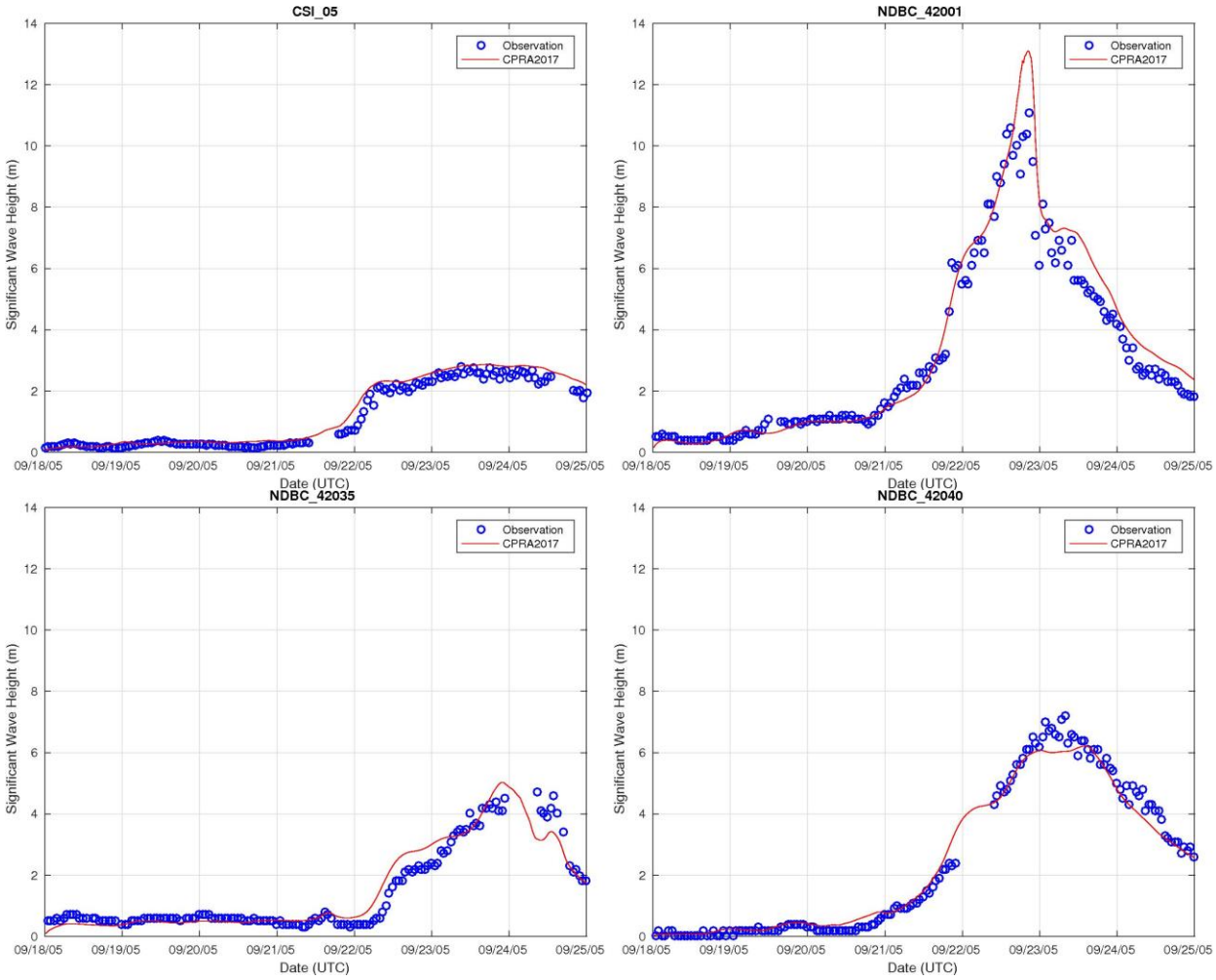

Figure 16: NDBC Significant Wave Height Comparisons for Hurricane Rita. Observations are in blue; CPRA 2017 model results are in red.

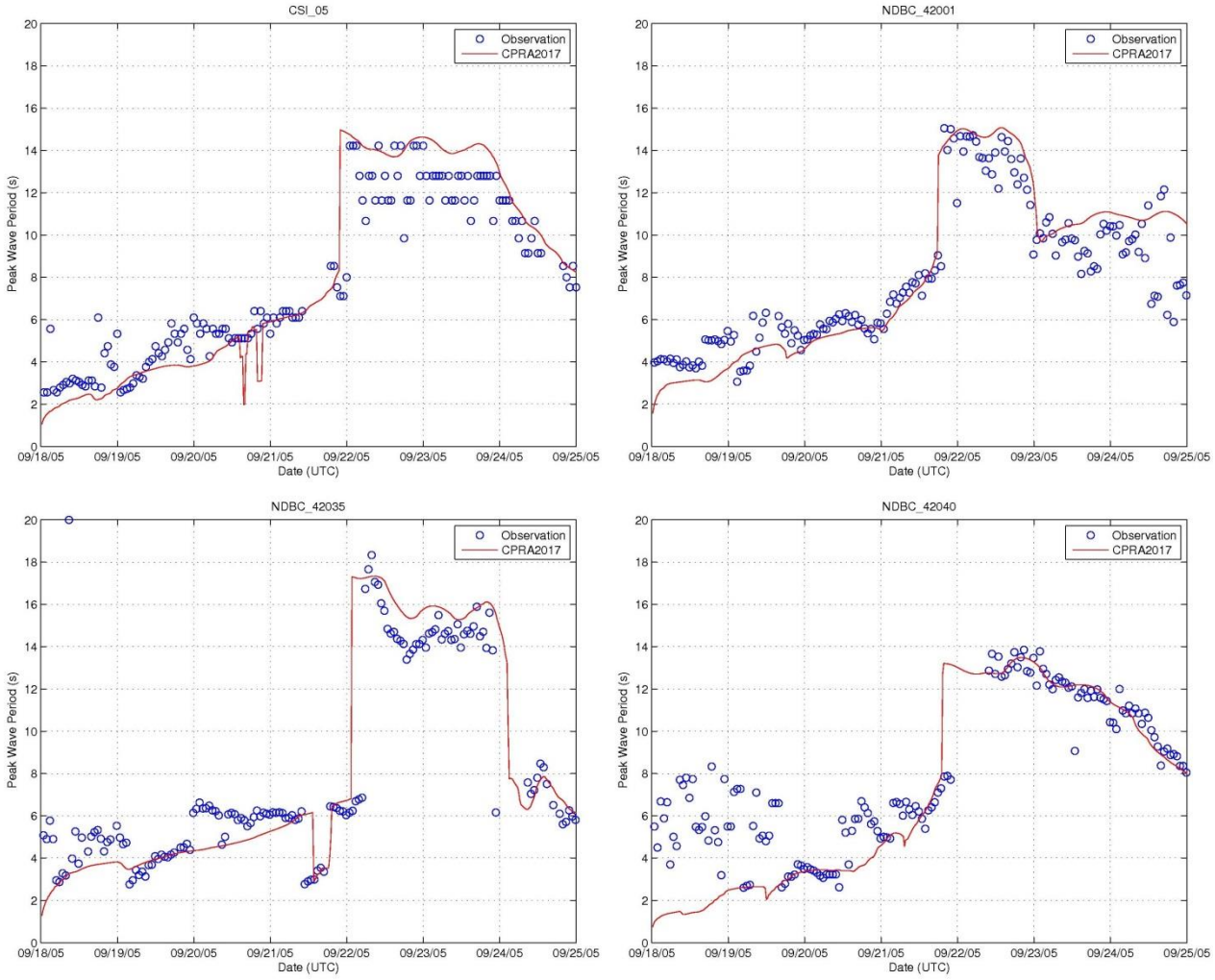

Figure 17: NDBC Peak Wave Period Comparisons for Hurricane Rita. Observations are in blue; CPRA 2017 model results are in red.

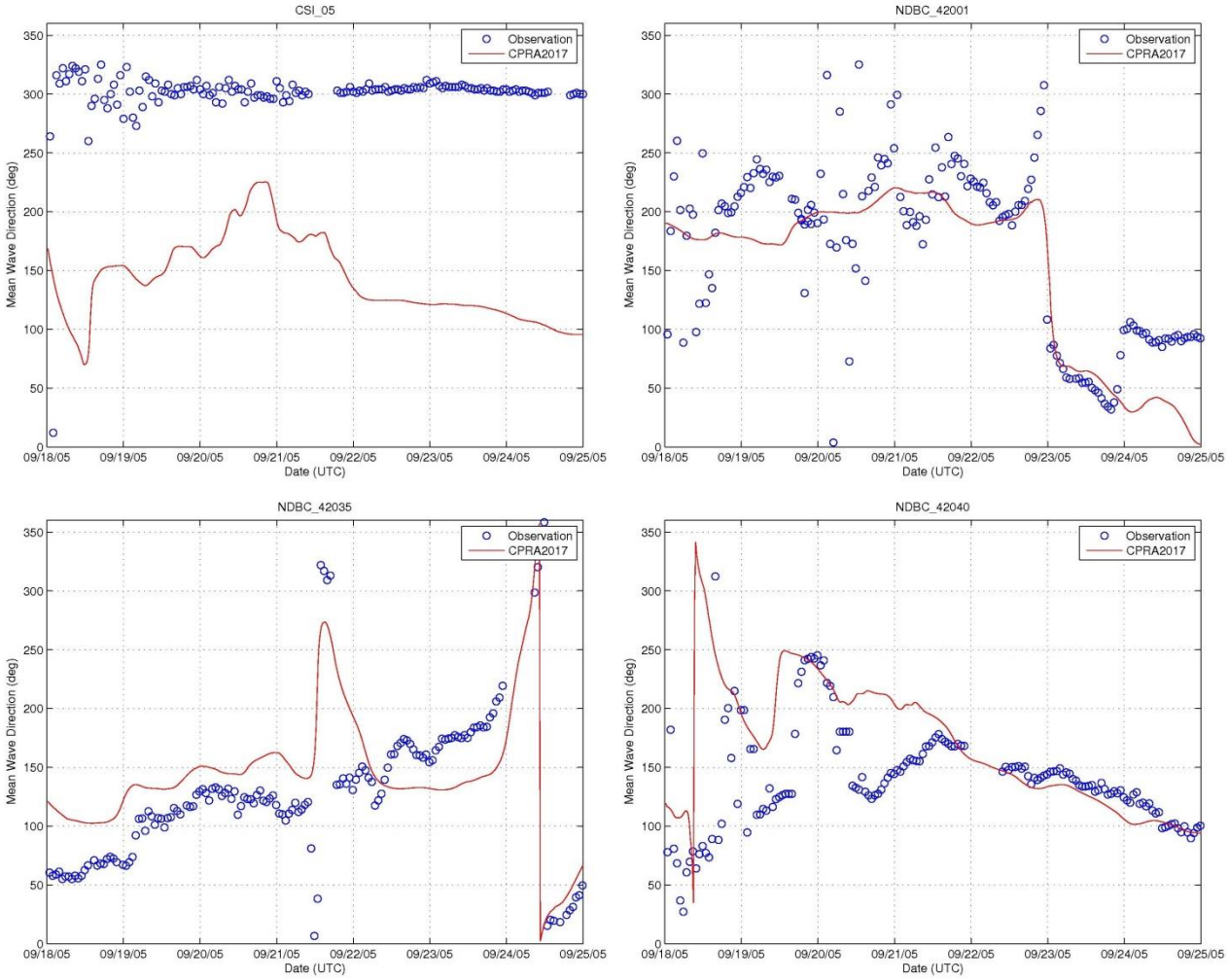

Figure 18: NDBC Mean Wave Direction Comparisons for Hurricane Rita. Observations are in blue; CPRA 2017 model results are in red. Note that observed wave directions at CSI_05 are believed to be a result of incorrect measurement.

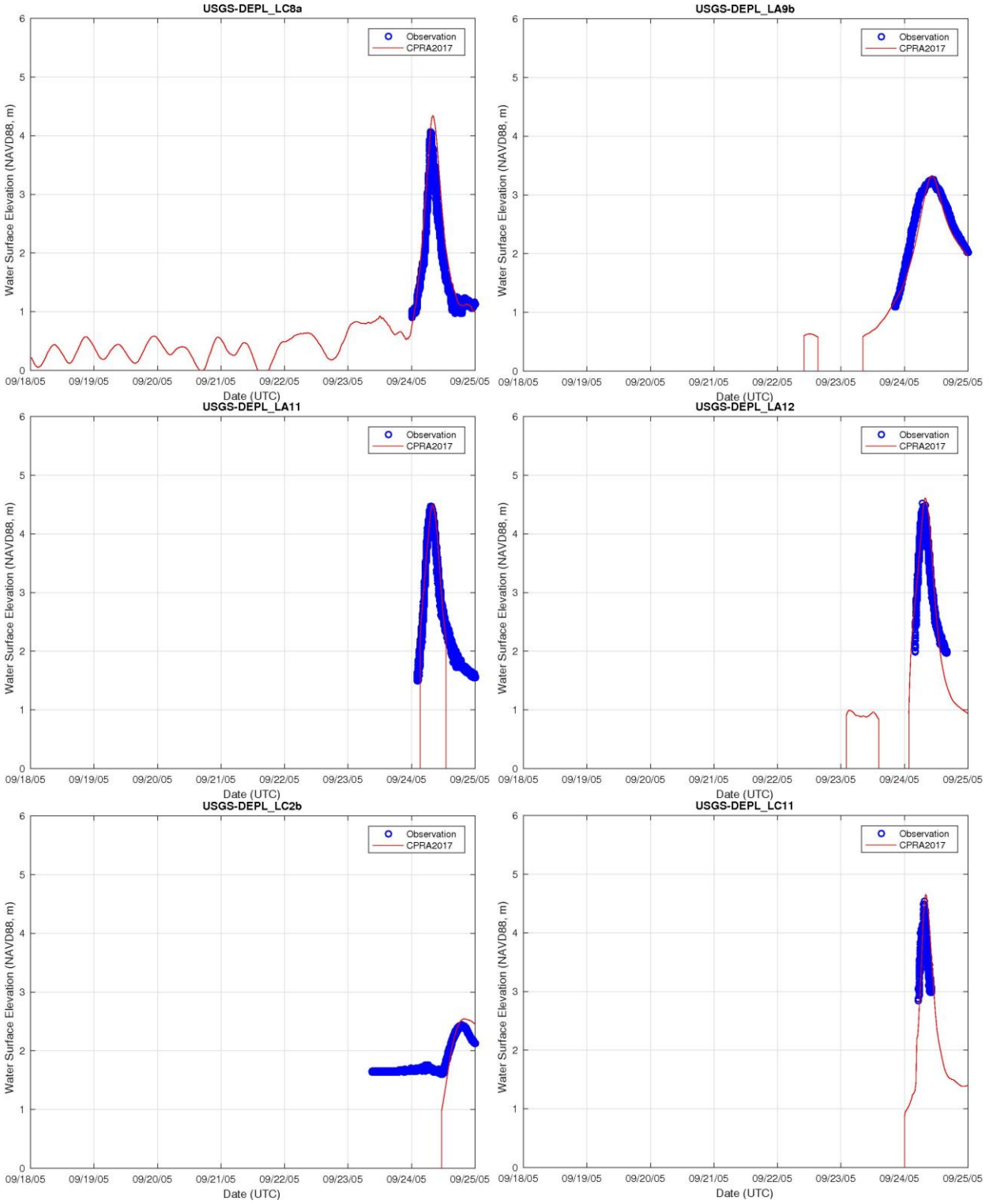

Figure 19: Water Elevation (m, NAVD88) Comparisons for Hurricane Rita. Observations are in blue; CPRA 2017 model results are in red.

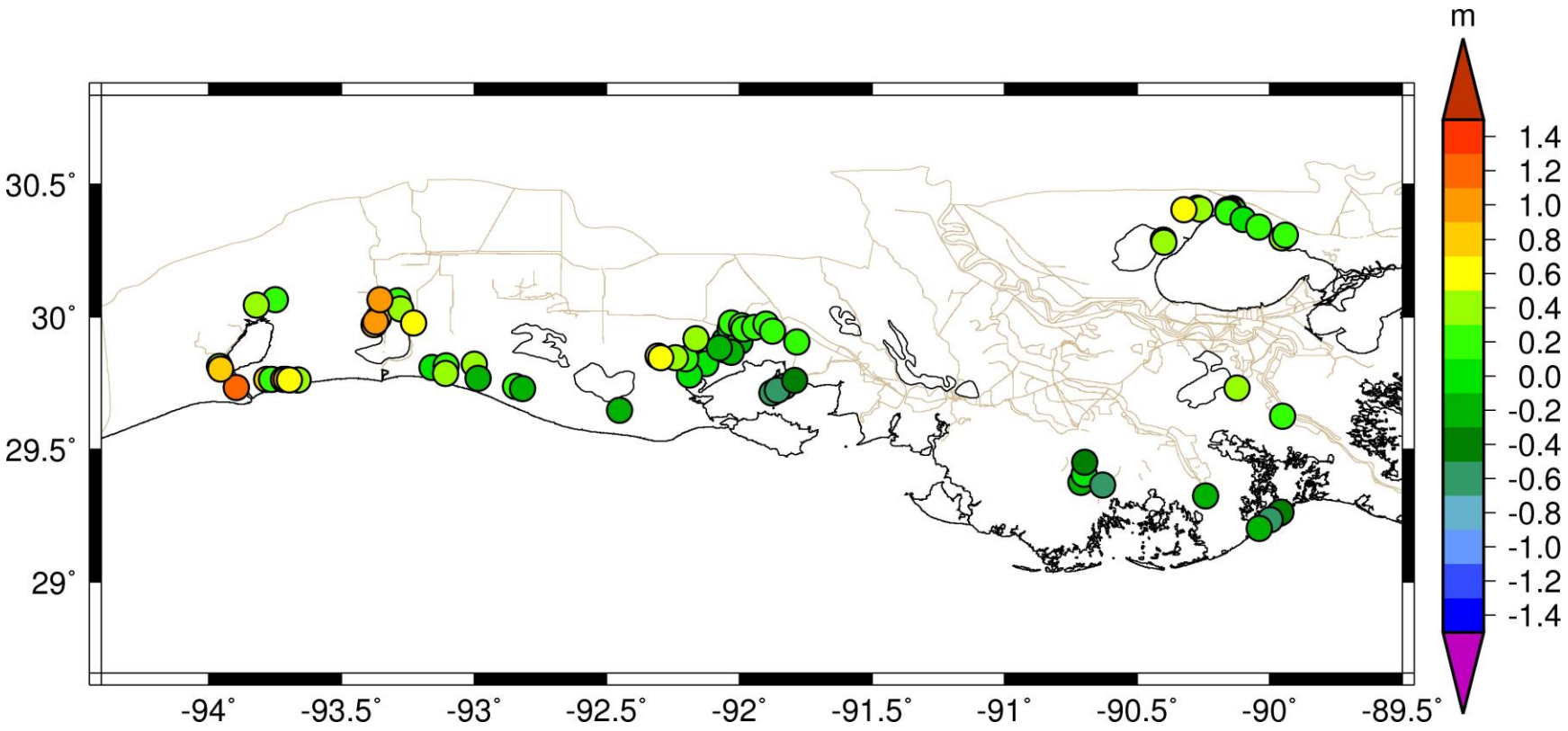

Figure 20: CPRA 2017 Model Hurricane Rita Comparison to Measured High Water Marks. Warm colors indicate the model results are greater than measurement; cool colors indicate the model results are lower than measurement.

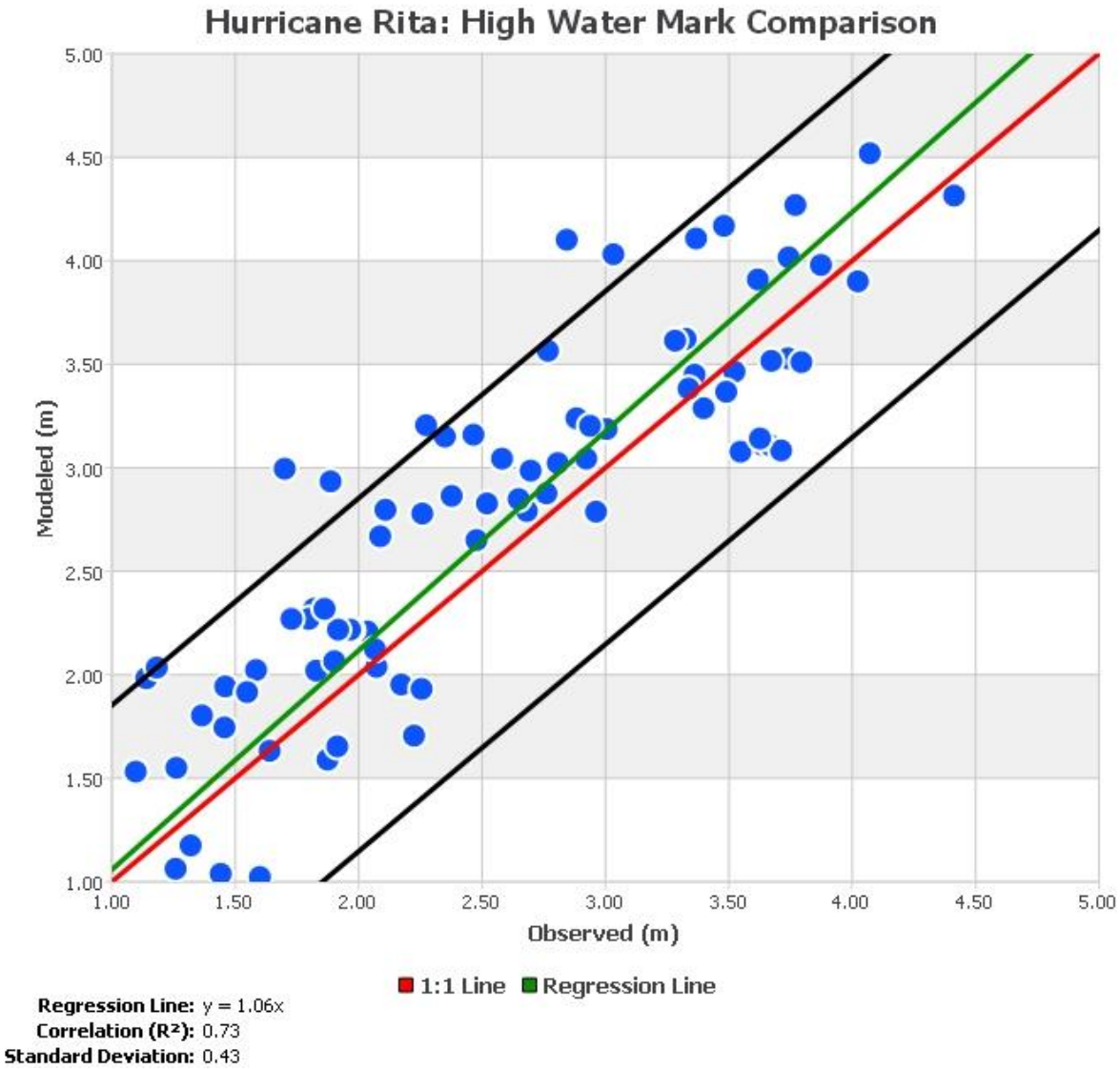

Figure 21: Hurricane Rita Regression Plot Comparing Measured High Water Marks to CPRA 2017 Model Results.

Hurricane Gustav (2008)

Gustav spent a short time as a Category 4 hurricane before weakening as it crossed Cuba. On August 31, 2008, three years and two days after Katrina made landfall, Gustav weakened to a Category 2 storm and made landfall near Terrebonne Bay. Gustav continued its northwestern track across the state as a tropical storm until finally making a turn toward the northeast over Arkansas as a tropical depression.

The CPRA 2017 model simulation of Gustav began on July 21, 2008, and concluded on September 4, 2008. River discharges of 4,729 m^3/s and 1,982 m^3/s were applied to the Mississippi and Atchafalaya River model boundaries, respectively. Other freshwater inputs are not included in the model setup due to model resolution limitations.

Figure 22 shows the maximum computed surge from the ADCIRC+SWAN model, and Figure 23 shows the maximum computed significant wave height. Figures 24 through 28 show the time series comparisons of wave data. Figures 29 and 30 show the comparisons to measured time series water level measurements. Finally, Figures 31 and 32 show the comparisons to measured high water marks.

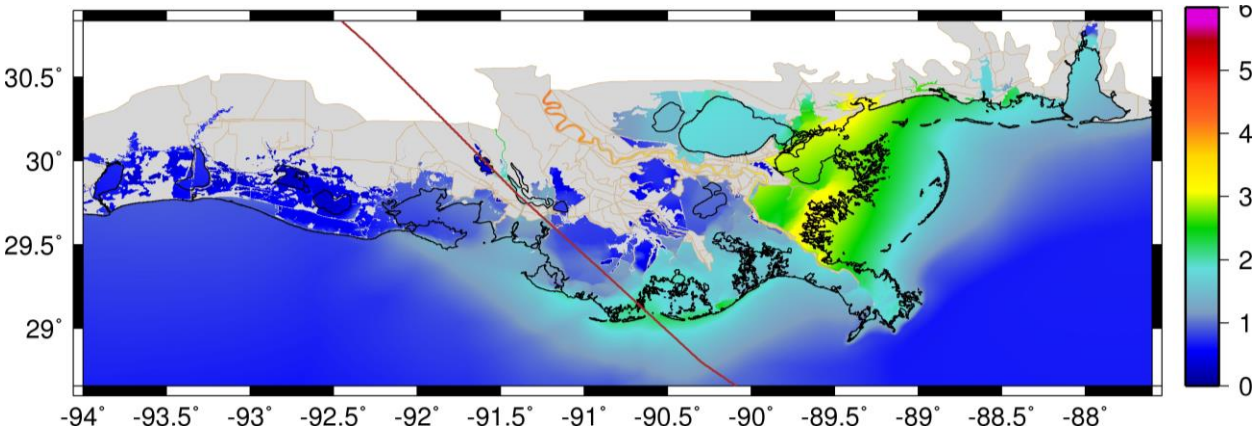

Figure 22: Maximum Storm Surge Elevation (m, NAVD88) During the 2017 CPRA Hurricane Gustav Simulation. Storm track shown in brown.

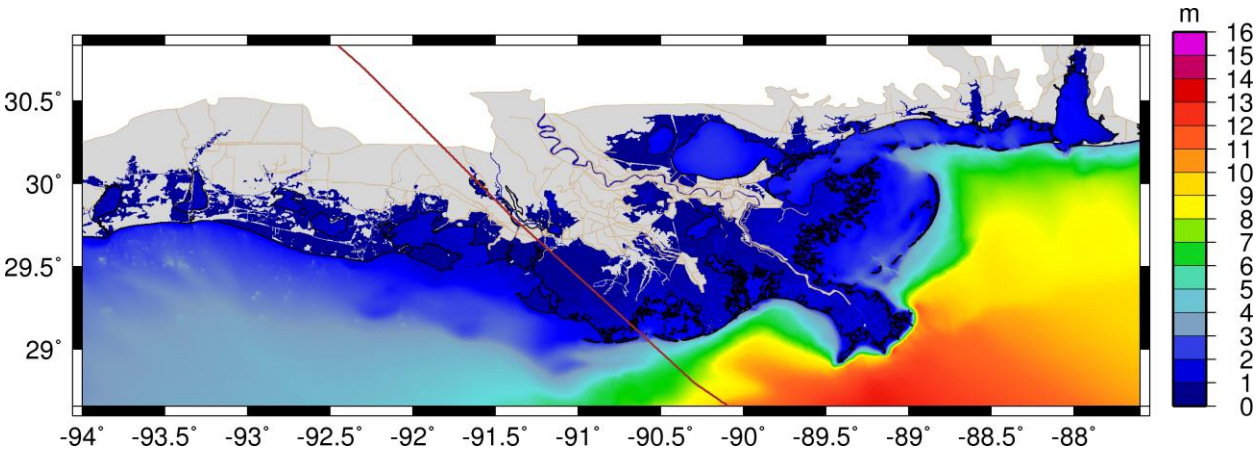

Figure 23: Maximum Significant Wave Height (m) During the 2017 CPRA Hurricane Gustav Simulation. Storm track shown in brown.

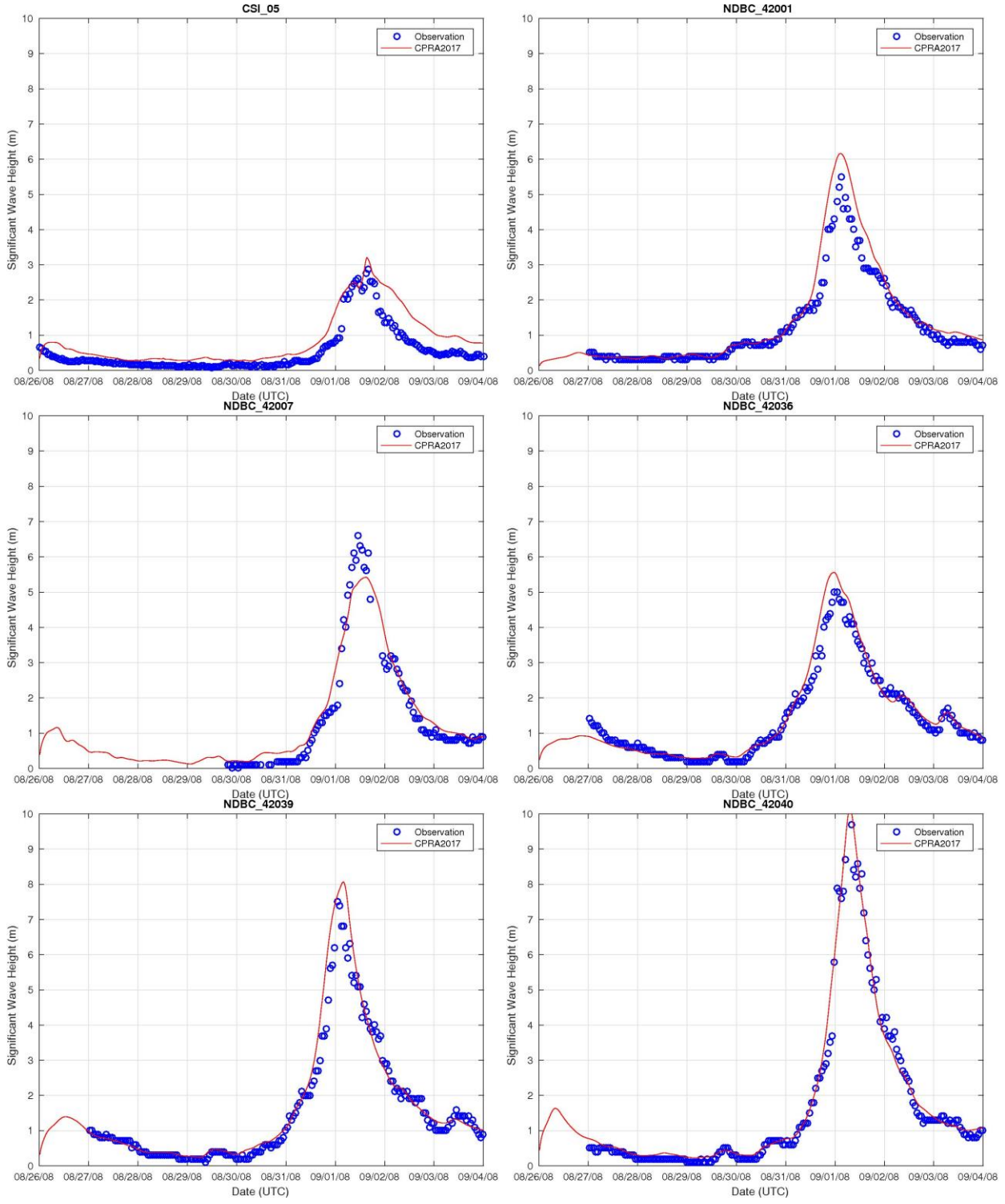

Figure 24: NDBC and CSI Significant Wave Height Comparisons for Hurricane Gustav.
Observations are in blue; CPRA 2017 model results are in red.

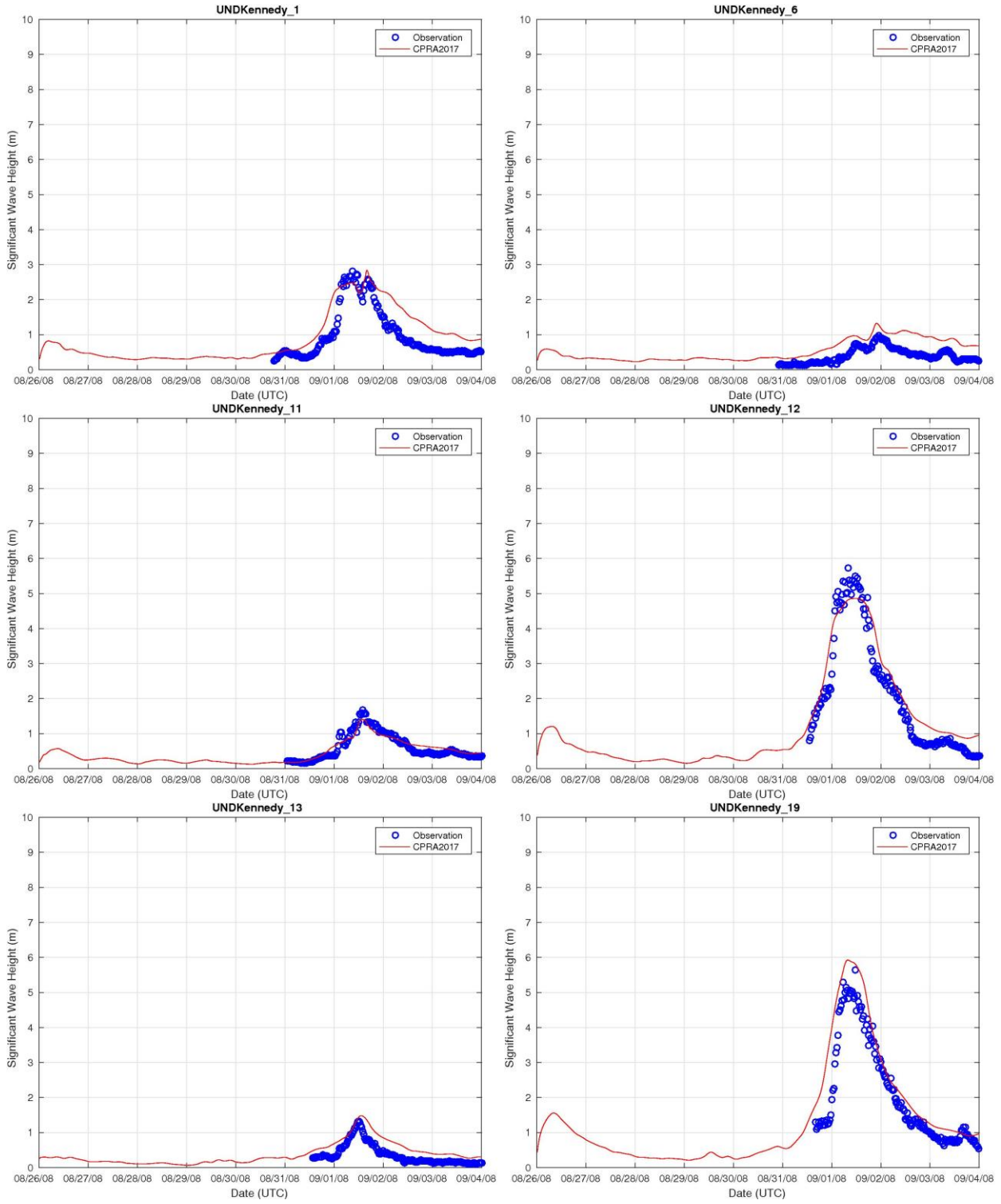

Figure 25: Significant Wave Height Comparisons at Andrew Kennedy Locations for Hurricane Gustav. Observations are in blue; CPRA 2017 model results are in red.

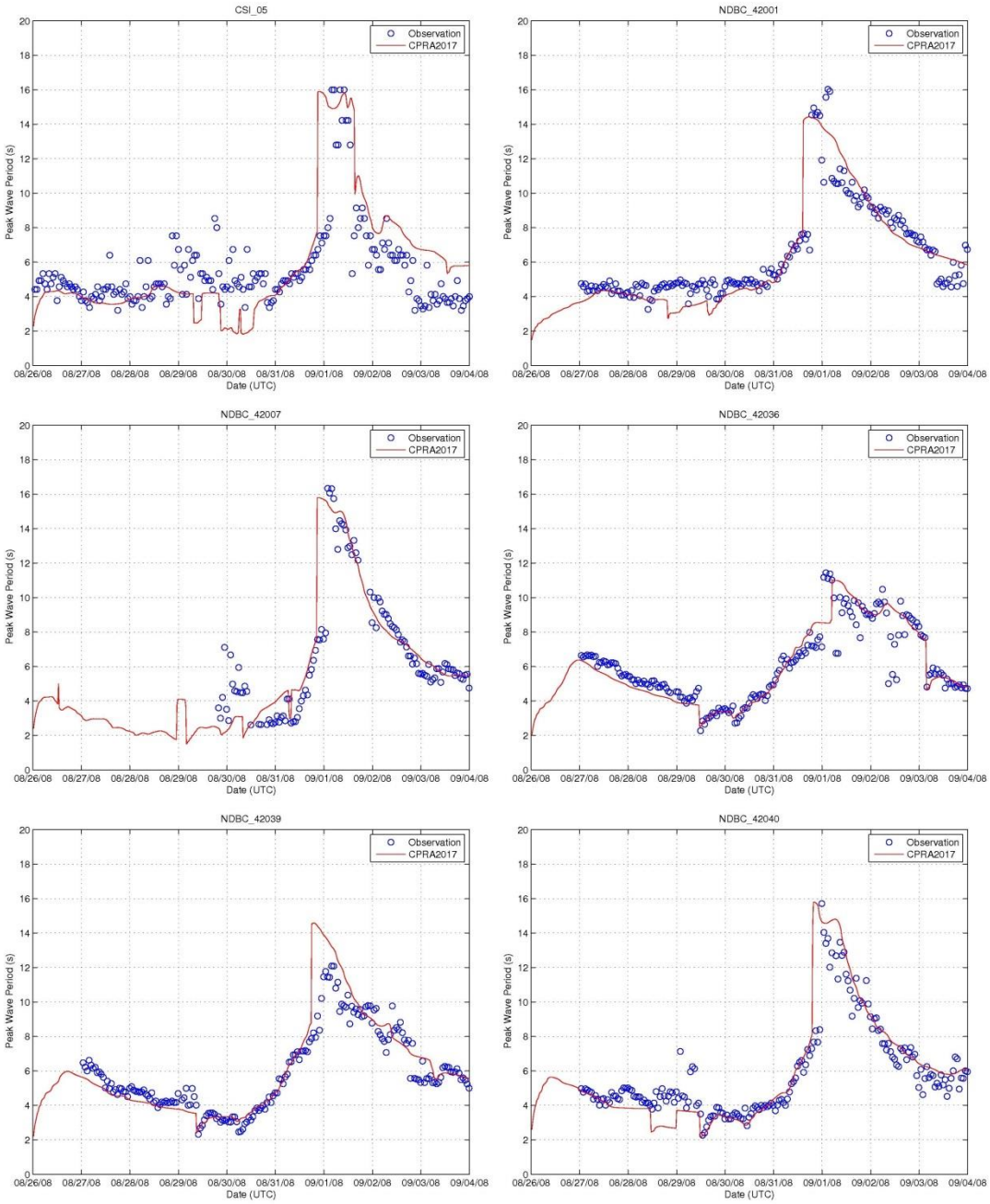

Figure 26: NDBC and CSI Peak Wave Period Comparisons for Hurricane Gustav. Observations are in blue; CPRA 2017 model results are in red.

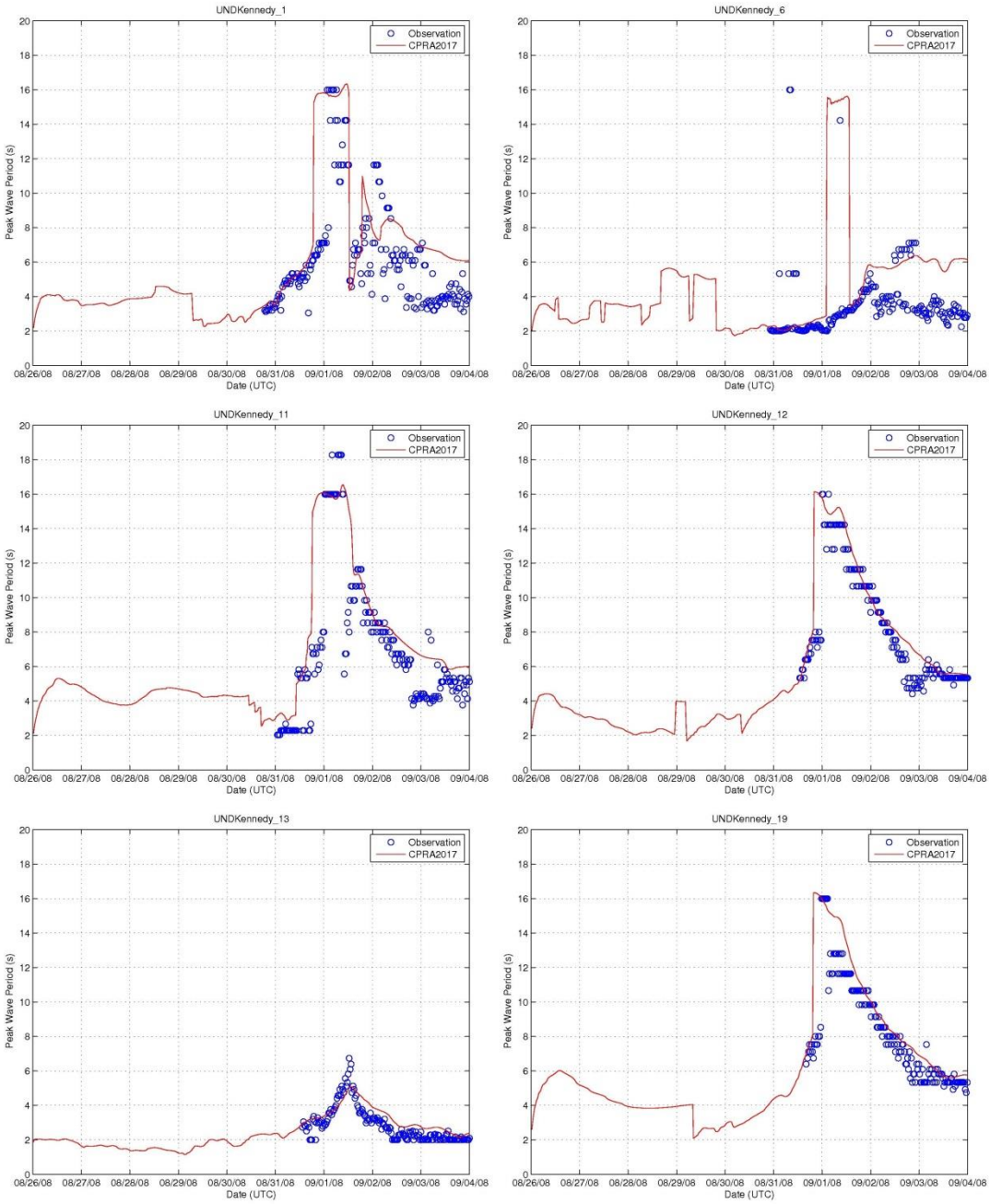

Figure 27: Peak Wave Period Comparisons at Andrew Kennedy Locations for Hurricane Gustav. Observations are in blue; CPRA 2017 model results are in red.

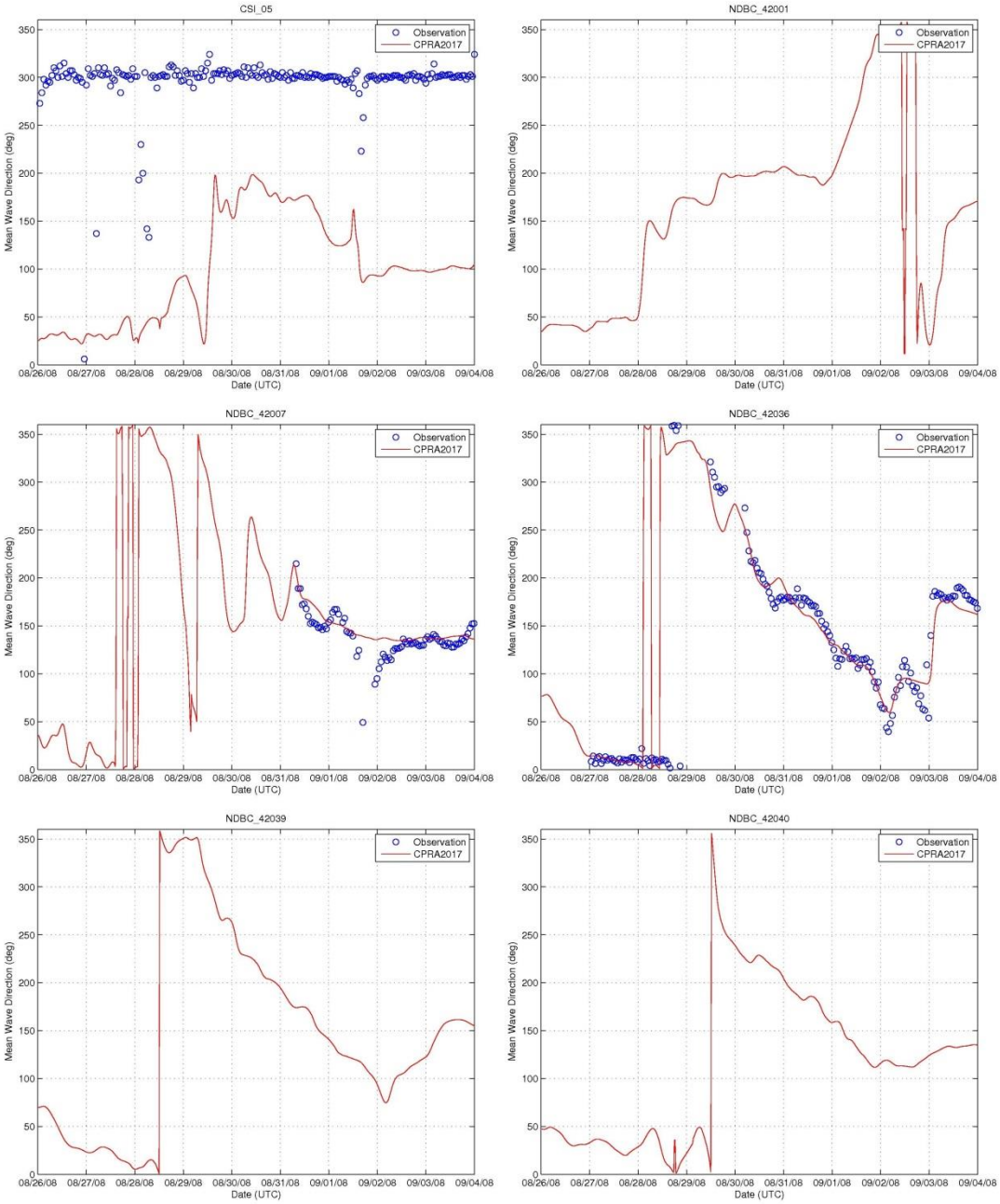

Figure 28: NDBC and CSI Mean Wave Direction Comparisons for Hurricane Gustav. Observations are in blue; CPRA 2017 model results are in red. Note that observed wave directions at CSI_05 are believed to be a result of incorrect measurement.

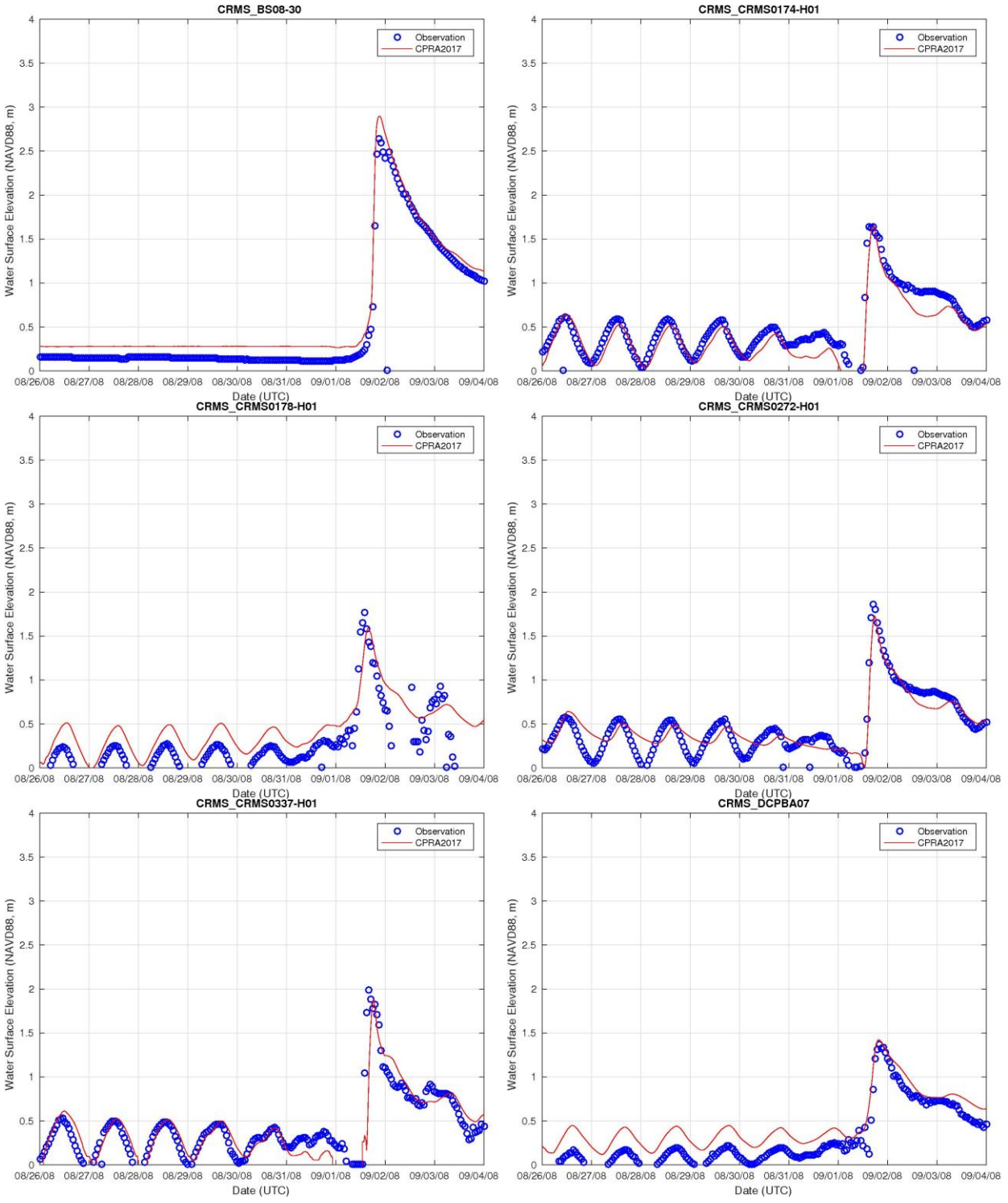

Figure 29: Water Elevation (m, NAVD88) Comparisons at CRMS Stations for Hurricane Gustav. Observations are in blue; CPRA 2017 model results are in red.

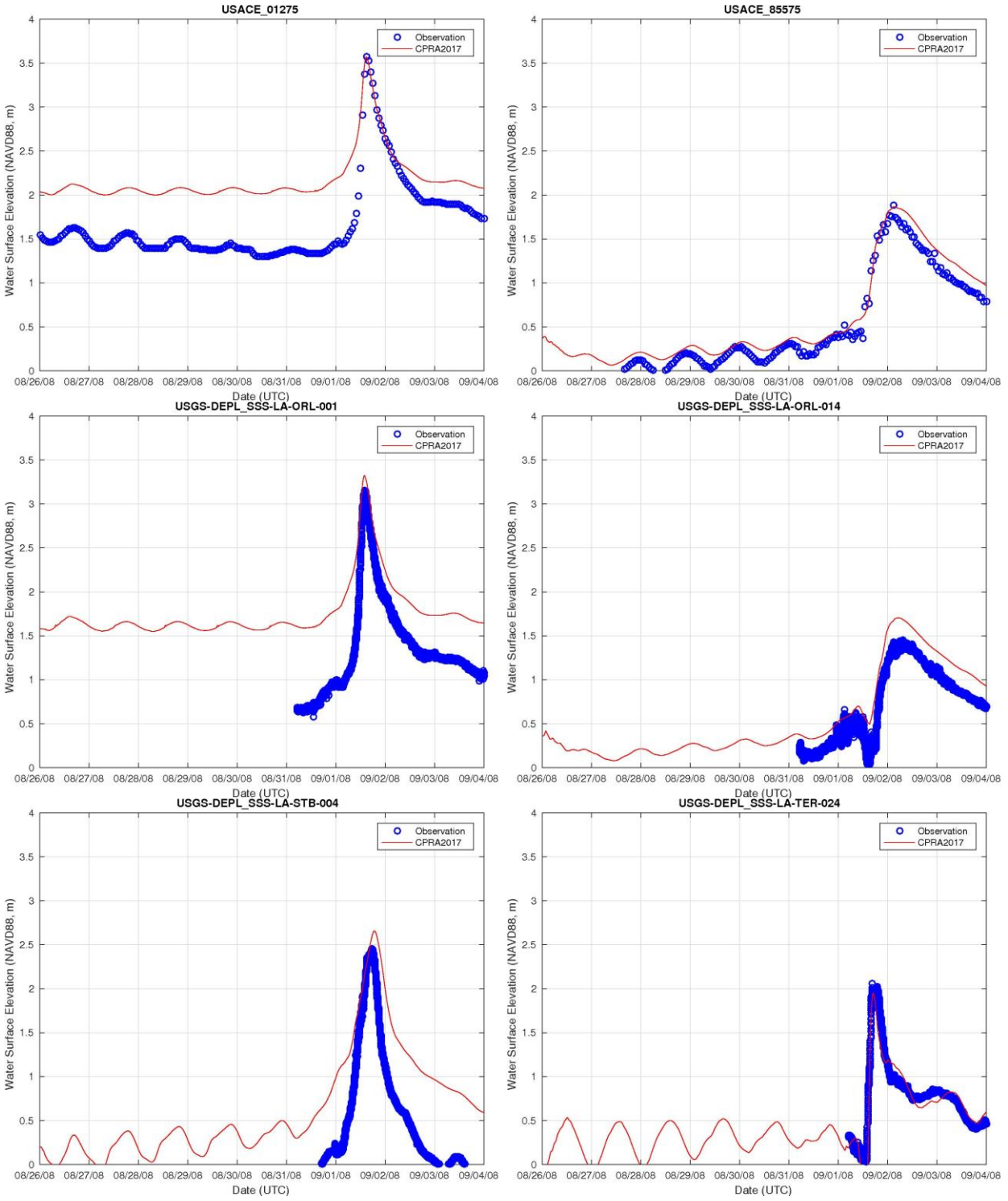

Figure 30: Water Elevation (m, NAVD88) Comparisons at USGS and USACE Stations for Hurricane Gustav. Observations are in blue; CPRA 2017 model results are in red. Note that Station 01275 and SSS-LA-ORL-001 lie in the Mississippi River. Because a constant flow rate is used, the pre-storm river stage is not captured; however, an accurate maximum water level is maintained once the surge overwhelms the river flow.

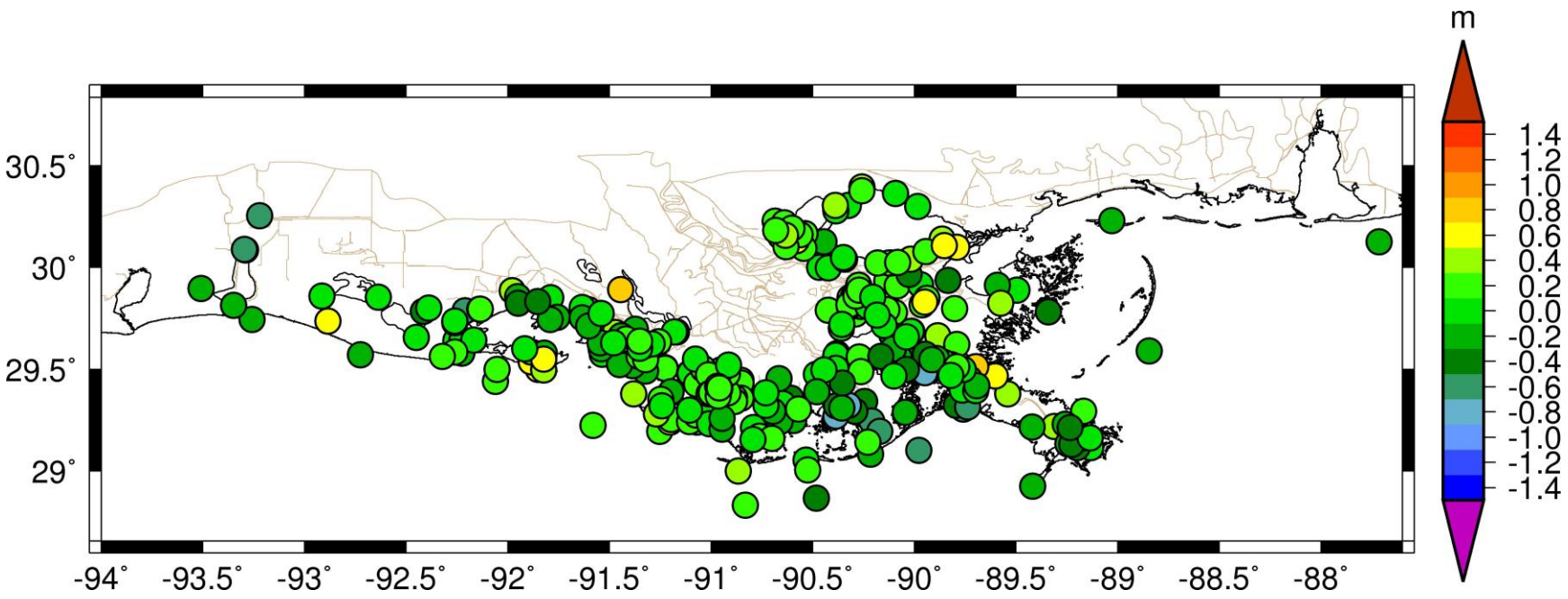

Figure 31: CPRA 2017 Model Hurricane Gustav Comparison to Measured High Water Marks. Warm colors indicate the model results are greater than measurement; cool colors indicate the model results are lower than measurement.

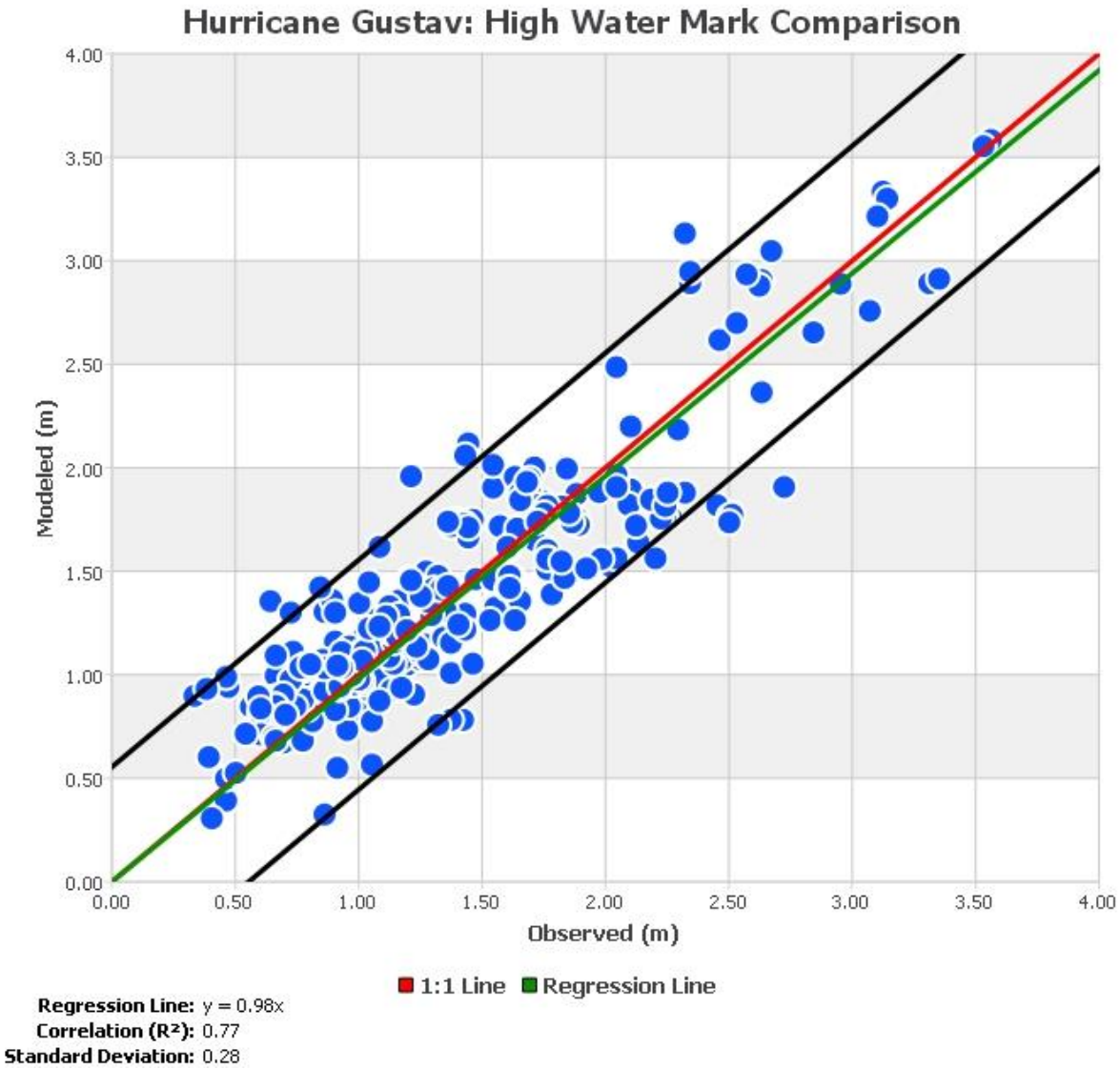

Figure 32: Hurricane Gustav Regression Plot Comparing Measured High Water Marks to CPRA 2017 Model Results.

Hurricane Ike (2008)

Before Ike entered the Gulf and made landfall in Cuba, it was a Category 4 hurricane. By the time it entered the Gulf, however, it was a Category 1 storm. Warm currents in the Gulf reintensified the storm to a Category 2 hurricane before making landfall on September 13, 2008, in Galveston, Texas, just two weeks after Gustav made landfall in Louisiana.

Ike provides an interesting test of model ability. Shore parallel currents caused waters to rise nearly a full day before landfall in western Louisiana and Texas. This can be attributed to an Ekman setup (Kennedy et al., 2011). This extra setup is driven by a combination of the Coriolis force and current velocities. As Kennedy points out, these velocities, especially in shallower waters like those on the Louisiana-Texas shelf, are highly dependent upon properly selected bottom friction coefficients and are very difficult to determine, given the size and inaccessibility of the Louisiana-Texas shelf. However, applying a similar model setup as Kennedy et al. (2011) and Hope et al. (2013), much of this extra setup is achieved. Figure 33 shows the water level as measured by the NOAA gage at Sabine Lake, the computed surge in the CPRA 2017 model, and the computed surge from the newly developed 9.1 million vertex SL18+TX model used by Hope et al. (2013) for validation of Ike. The plot shows much of the forerunner is captured by CPRA 2017 between midnight on September 12, 2008, and midnight on September 13, 2008. The plot additinally shows excellent agreement with the state of the art SL18+TX model. Notice that the surge hits the first peak during the forerunner, followed by a small dip. Then a second, larger peak is observed as the storm passes through the area. This early forerunner provides the initial water level necessary to generate the measured surge.

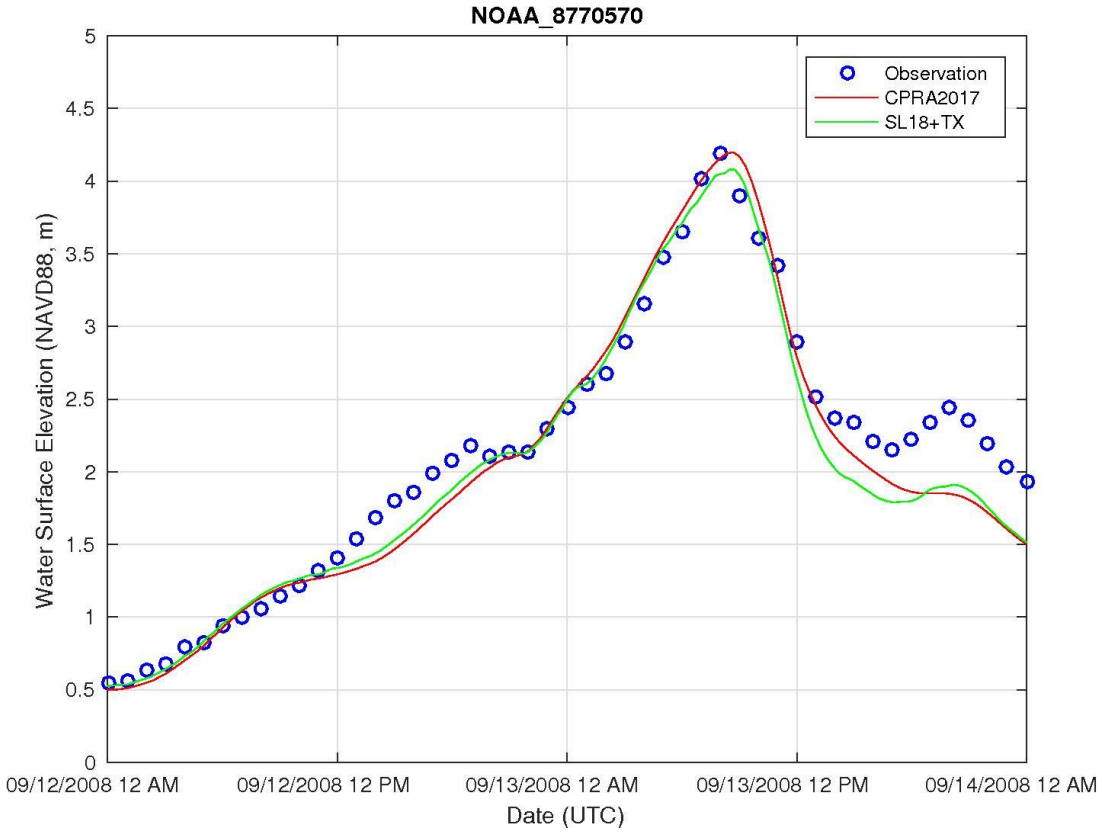

Figure 33: Hurricane Ike Forerunner Surge (m, NAVD88; Hope et al., 2013). Observations are shown in blue; CPRA 2017 is shown in red; SL18+TX is shown in green.

The simulation of Ike uses Gustav as an initial condition. Because the storms occur so near each other in time, the dynamic solution already computed from Gustav creates the initial condition for Ike. The initial conditions for both circulation and waves are applied. The simulation concludes on September 14, 2008.

River flow rates from Gustav are carried forward and used during the Ike simulation.

Figure 34 shows the maximum computed surge from the ADCIRC+SWAN model, and Figure 35 shows the maximum computed significant wave height during the simulation of Ike. Figures 36 through 40 show the wave comparisons to measured data. Figures 41 through 43 show the water level comparisons to measured data. Finally, Figures 44 and 45 show the comparisons to measured high water marks.

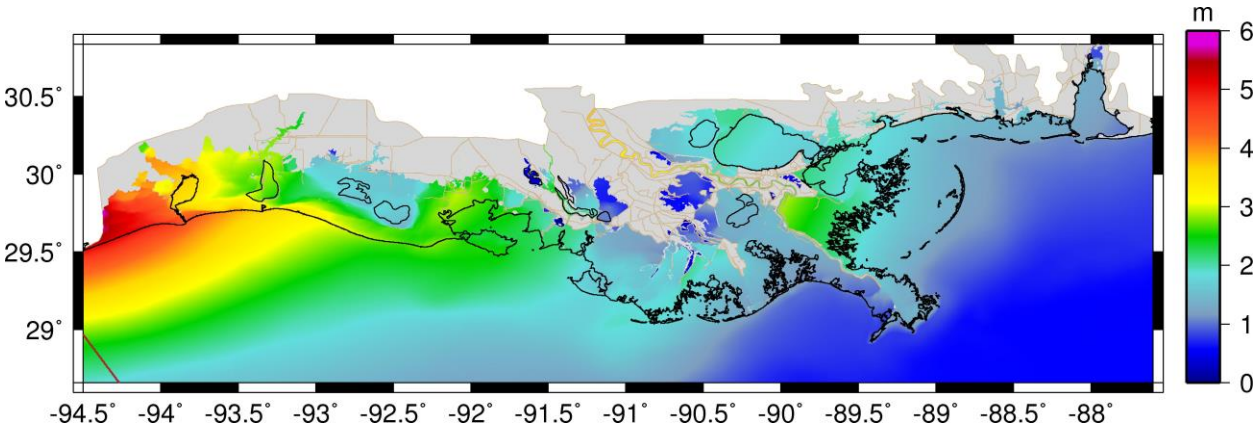

Figure 34: Maximum Storm Surge Elevation (m, NAVD88) During the 2017 CPRA Hurricane Ike Simulation. Storm track shown in brown.

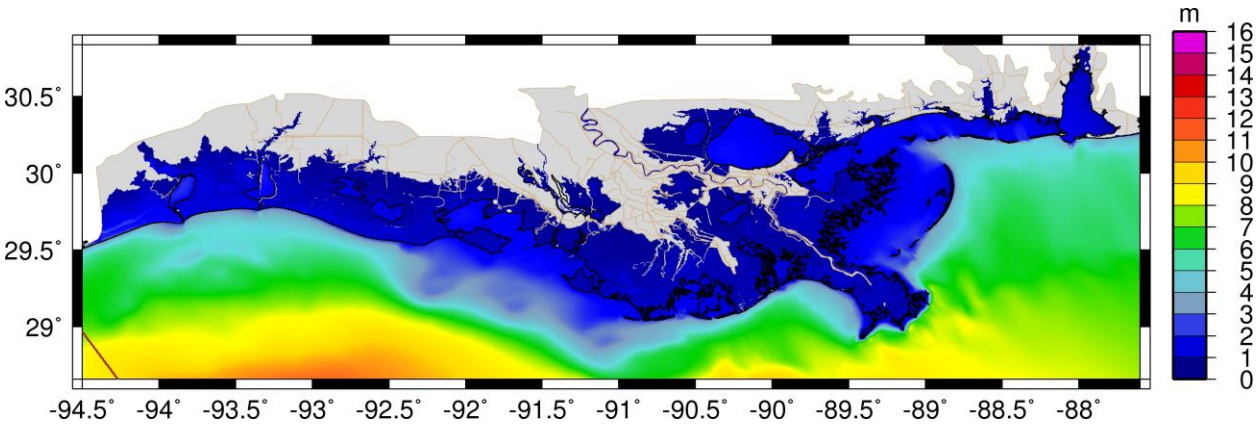

Figure 35: Maximum Significant Wave Height (m) During the 2017 CPRA Hurricane Ike Simulation. Storm track shown in brown.

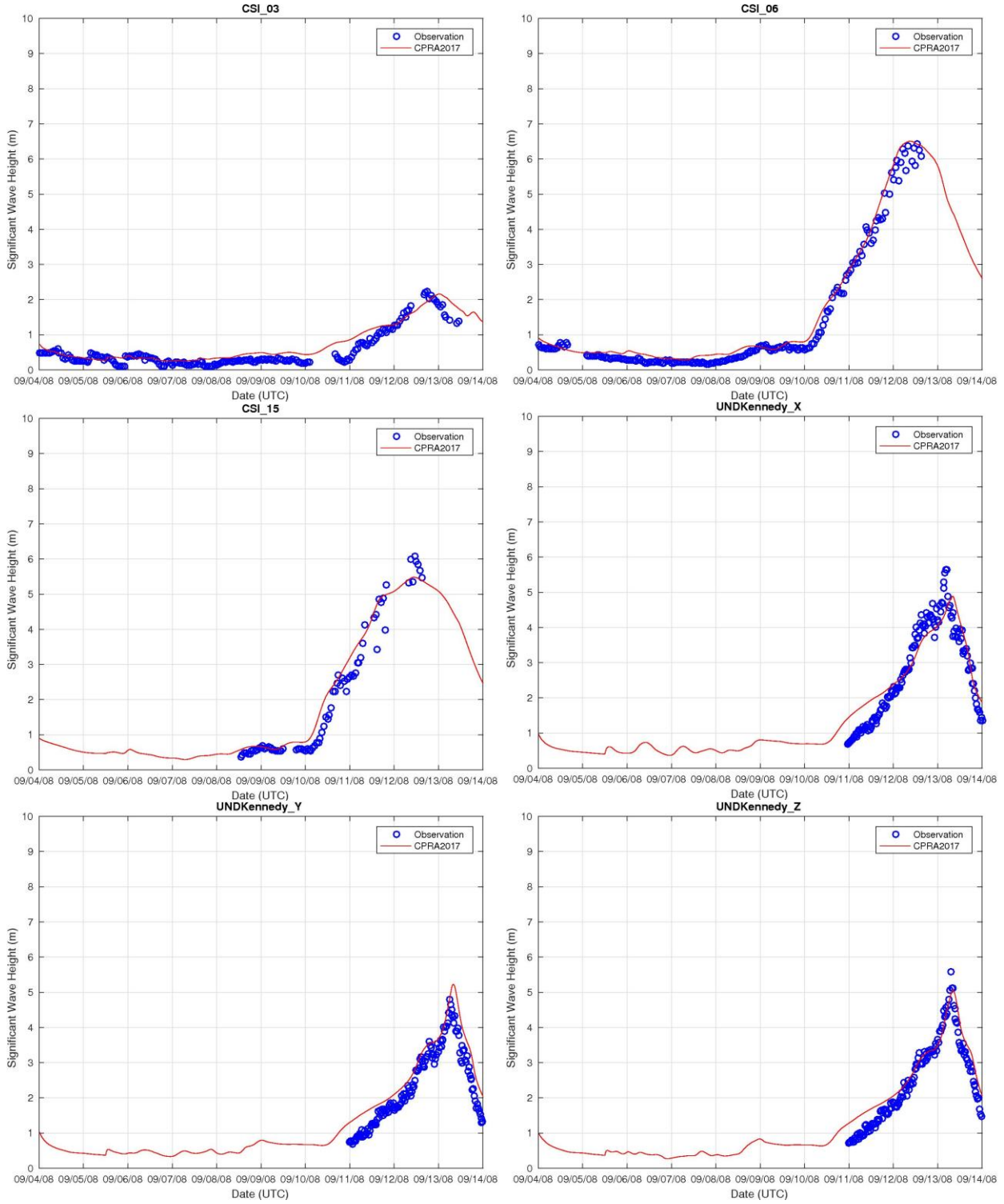

Figure 36: Significant Wave Height Comparisons at CSI and Andrew Kennedy Locations for Hurricane Ike. Observations are in blue; CPRA 2017 model results are in red.

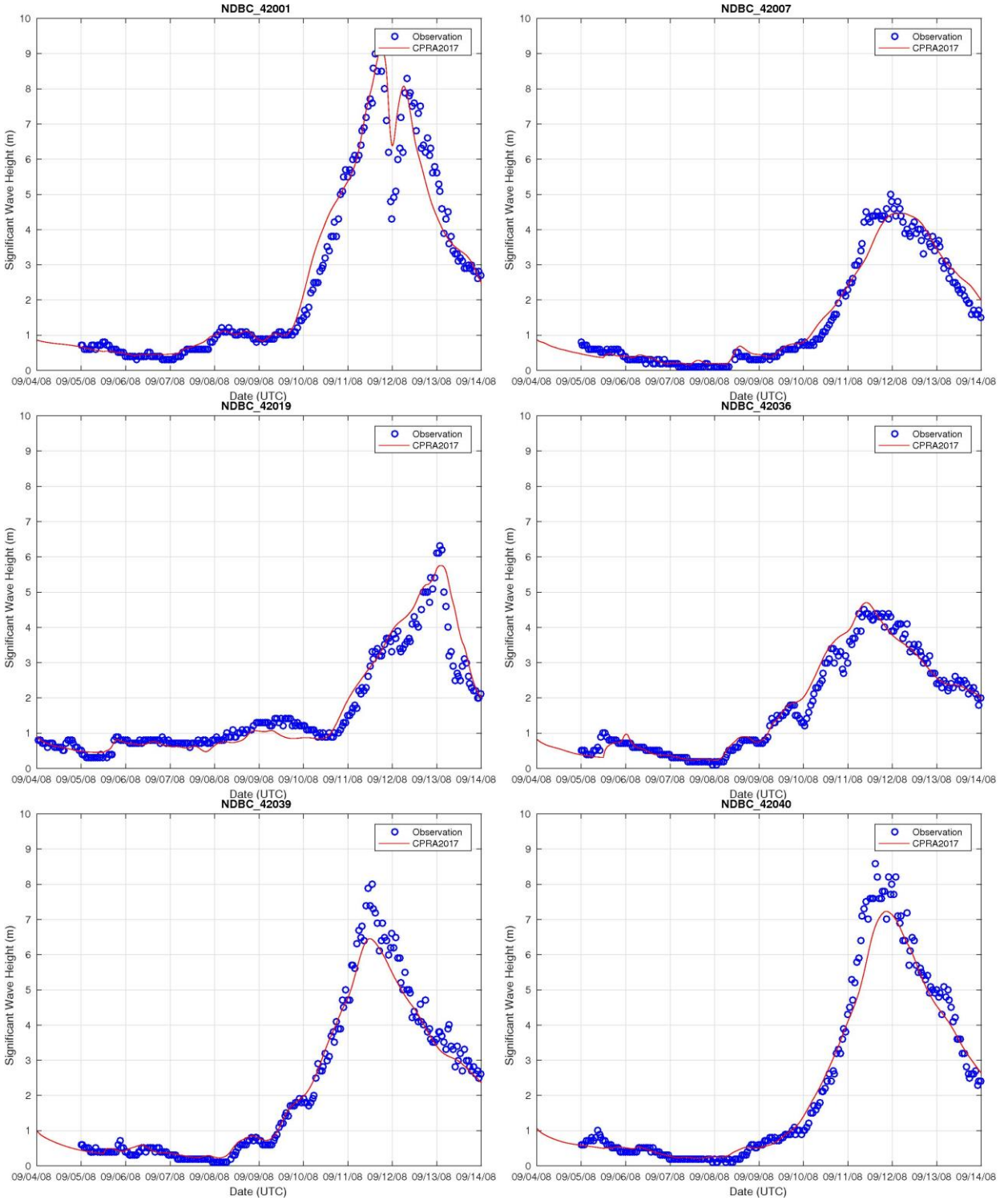

Figure 37: Significant Wave Height Comparisons at NDBC Locations for Hurricane Ike.
Observations are in blue; CPRA 2017 model results are in red.

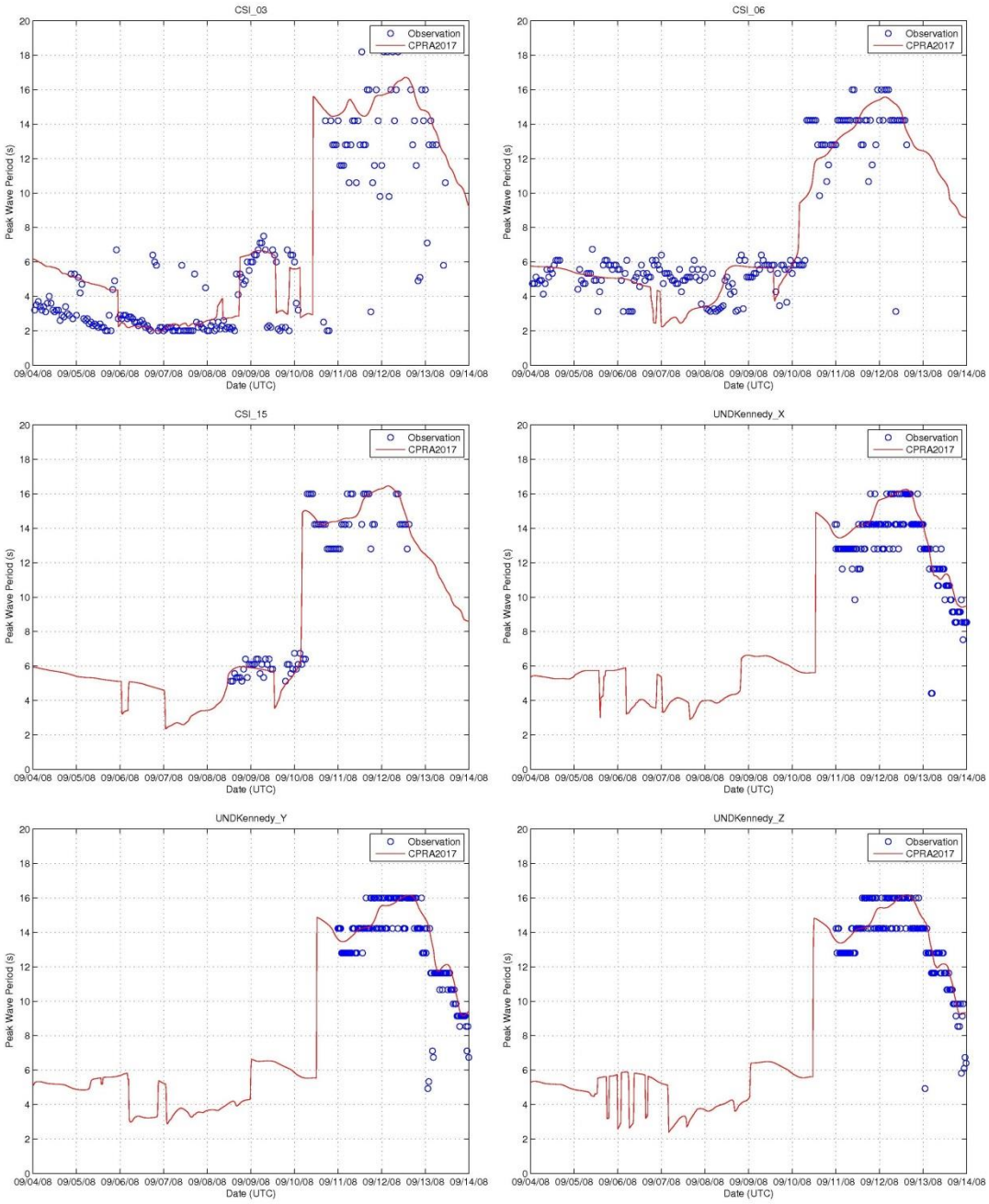

Figure 38: Peak Wave Period Comparisons at CSI and Andrew Kennedy Locations for Hurricane Ike. Observations are in blue; CPRA 2017 model results are in red.

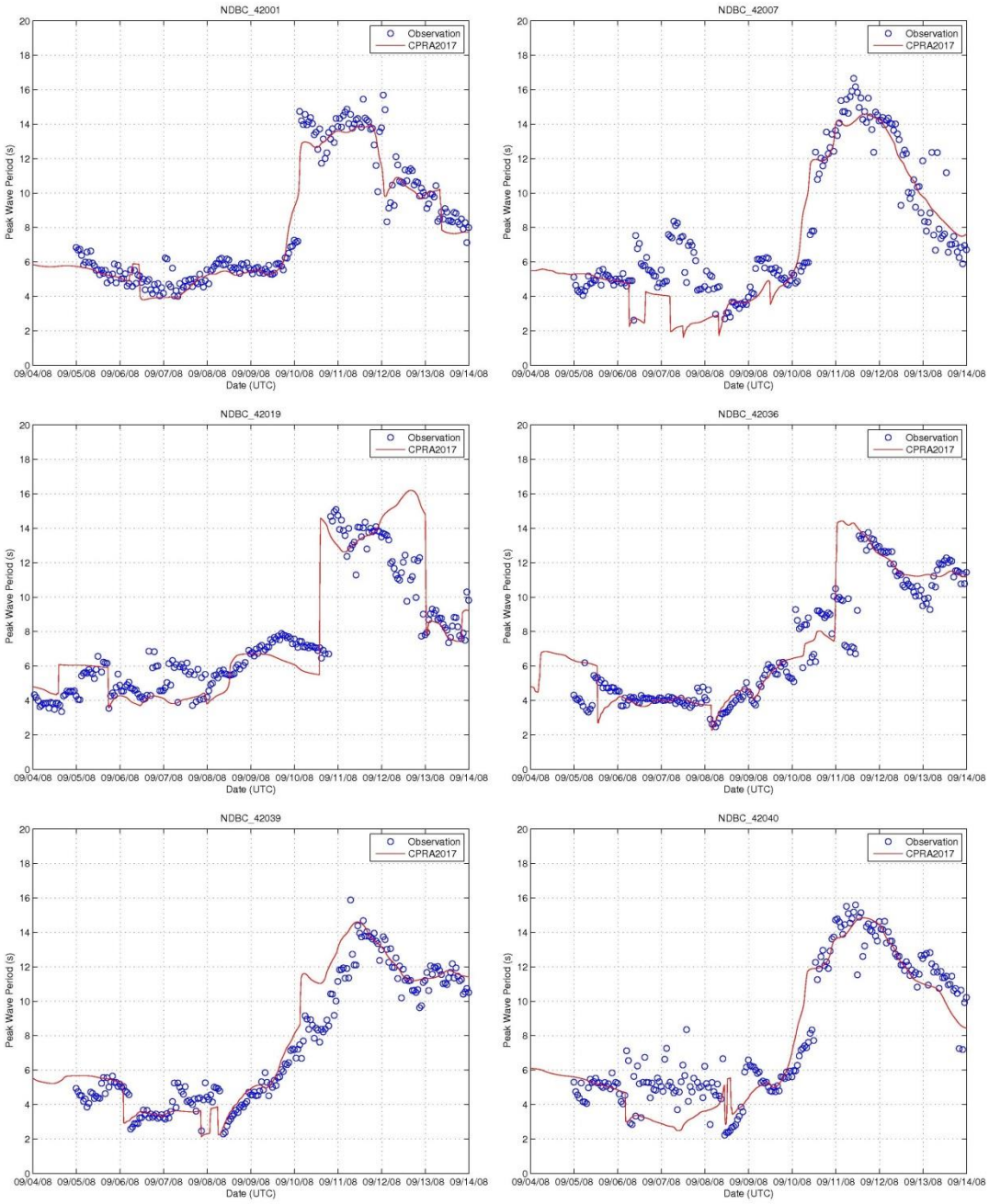

Figure 39: Peak Wave Period Comparisons at NDBC Locations for Hurricane Ike. Observations are in blue; CPRA 2017 model results are in red.

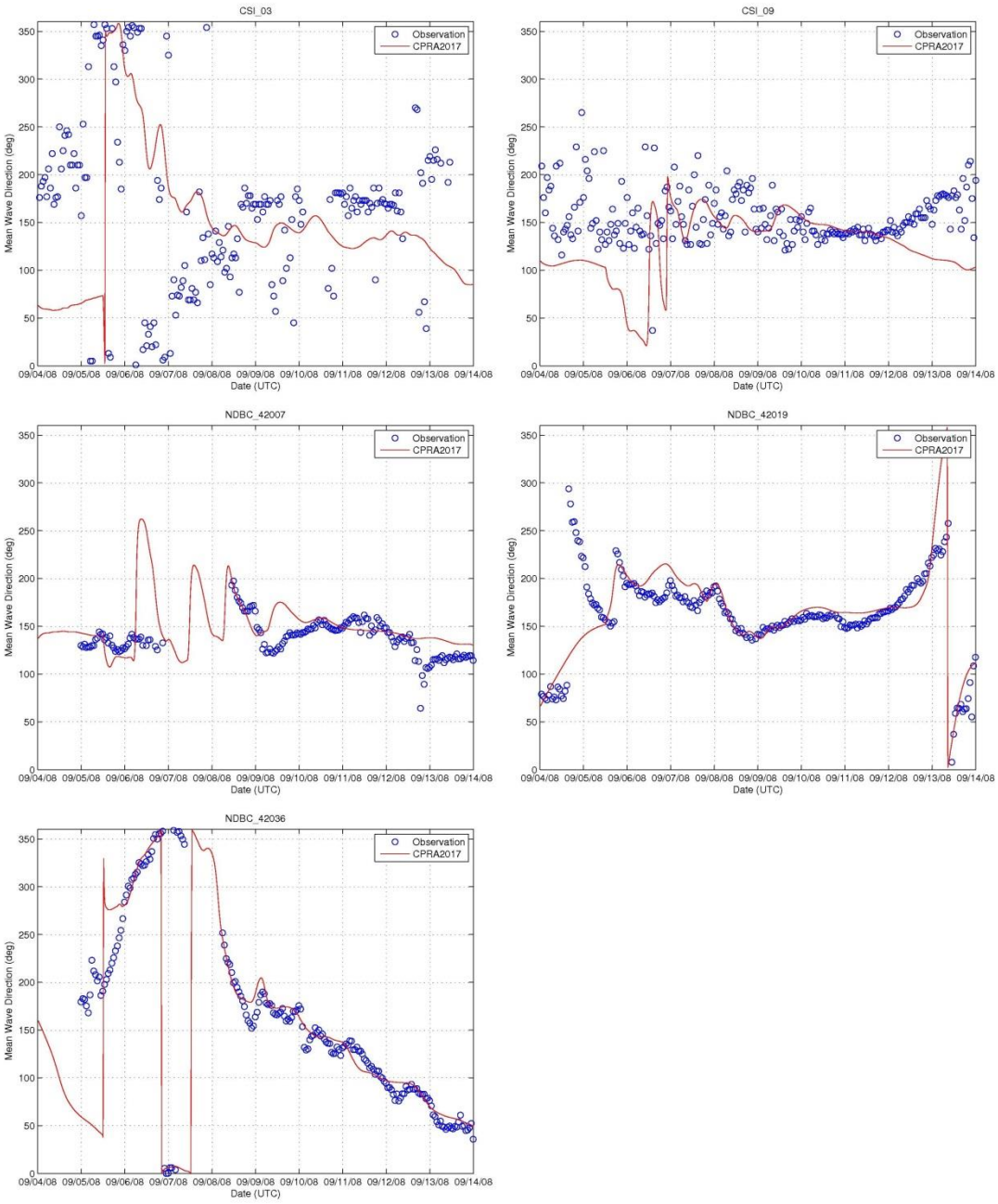

Figure 40: Mean Wave Direction Comparisons for Hurricane Ike at NDBC and CSI Locations. Observations are in blue; CPRA 2017 model results are in red.

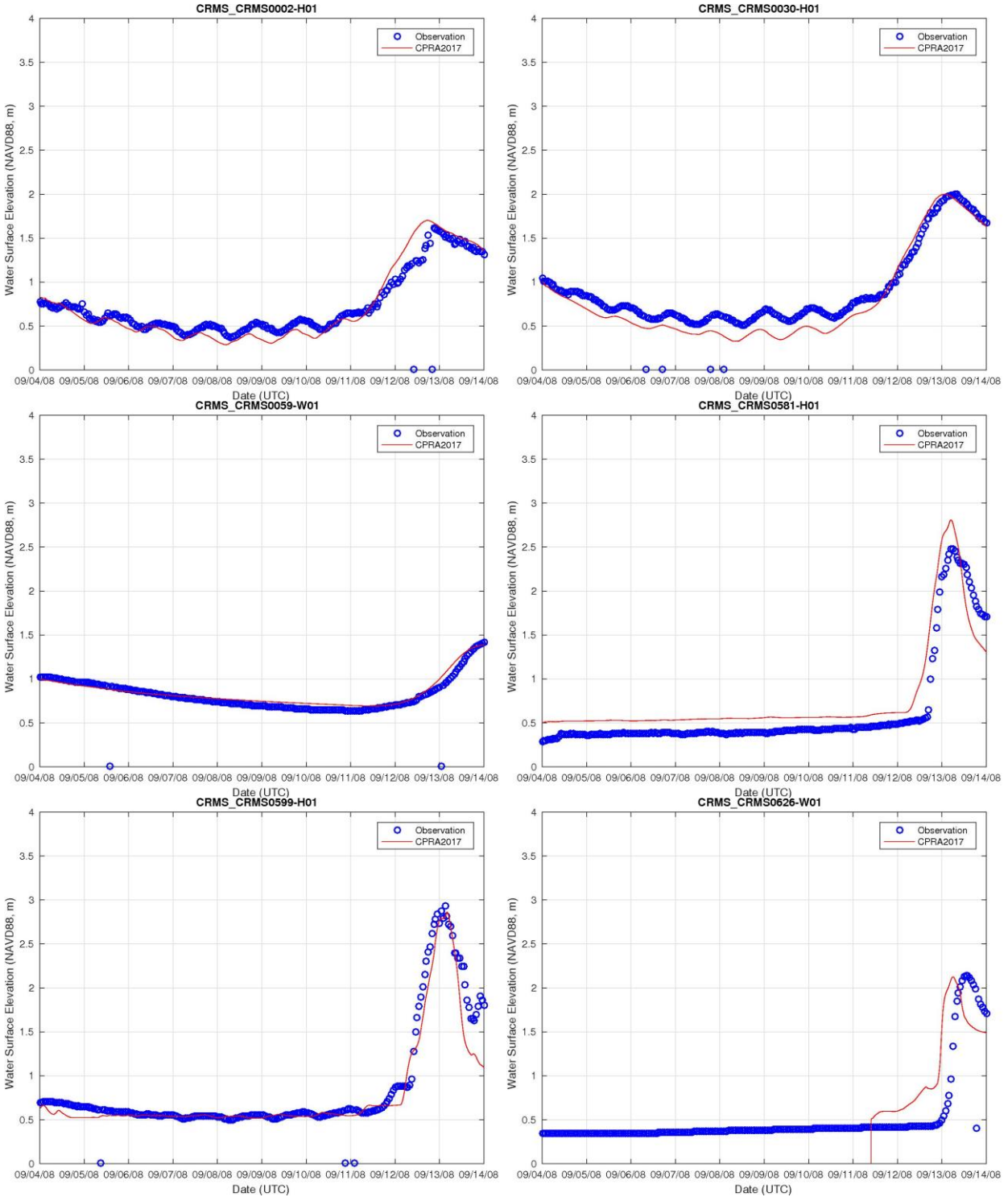

Figure 41: Water Elevation (m, NAVD88) Comparisons for Hurricane Ike at CRMS Locations. Observations are in blue; CPRA 2017 model results are in red.

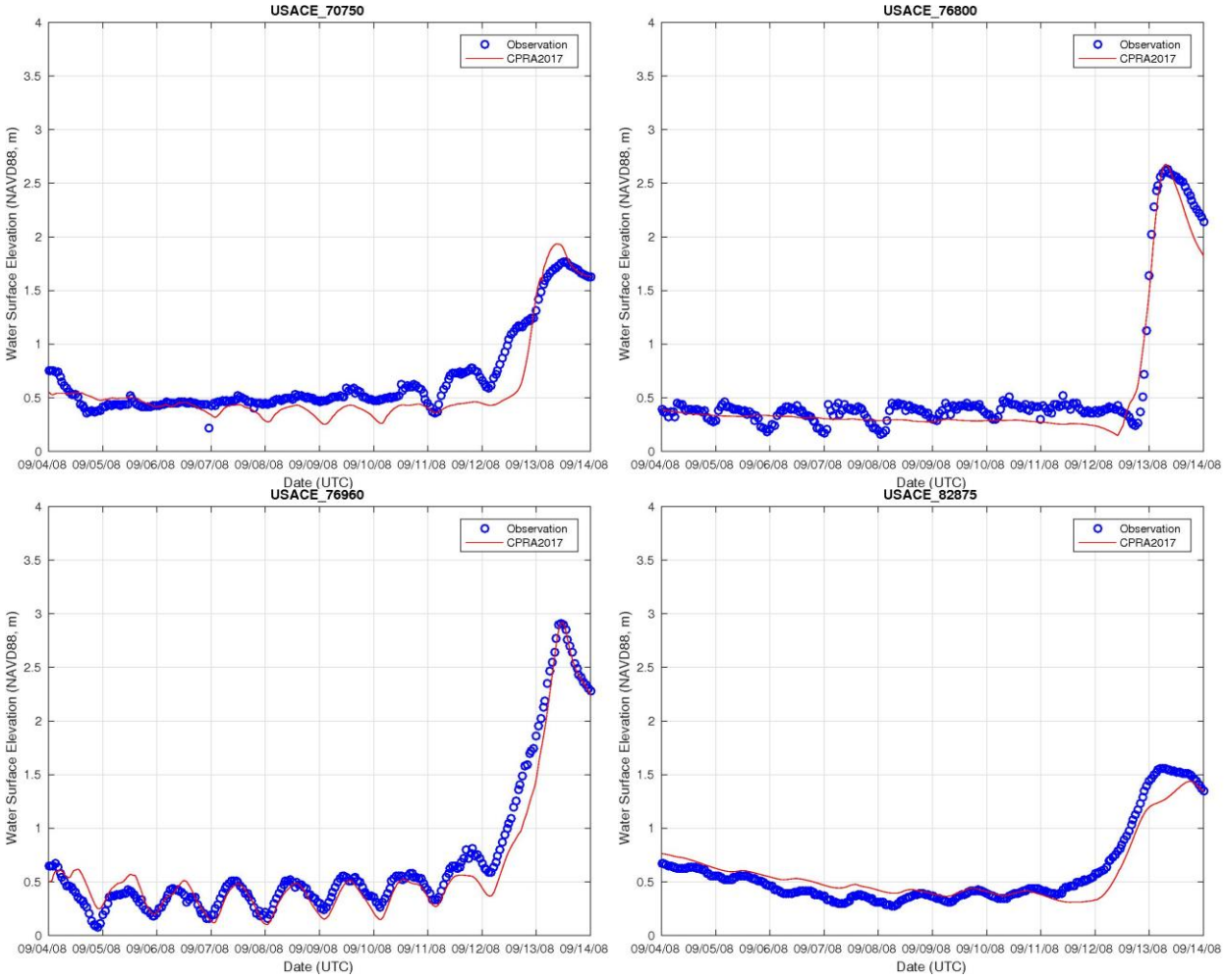

Figure 42: Water Elevation (m, NAVD88) Comparisons for Hurricane Ike at USACE Locations. Observations are in blue; CPRA 2017 model results are in red.

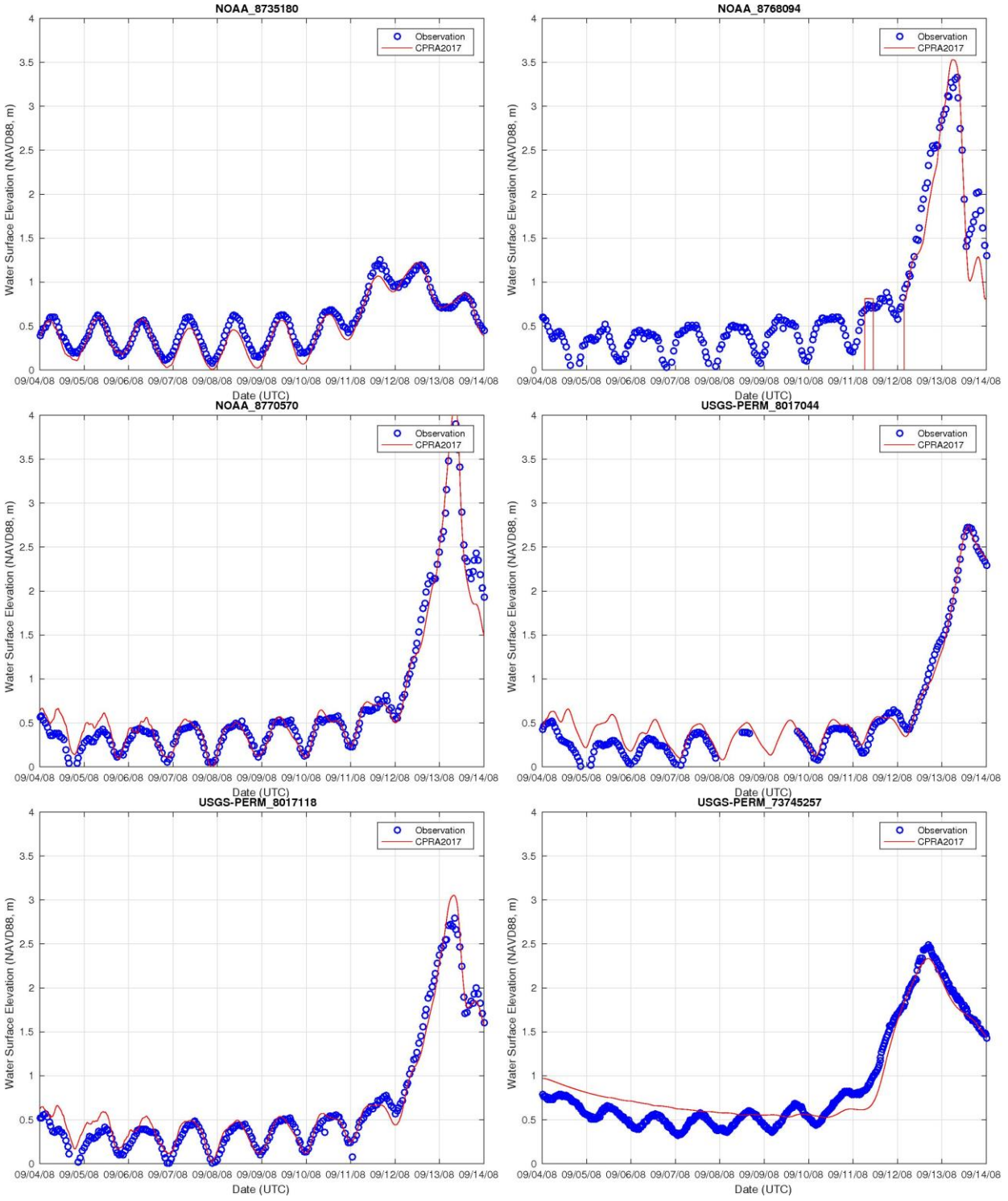

Figure 43: Water Elevation (m, NAVD88) Comparisons for Hurricane Ike at NOAA and USGS Locations. Observations are in blue; CPRA 2017 model results are in red.

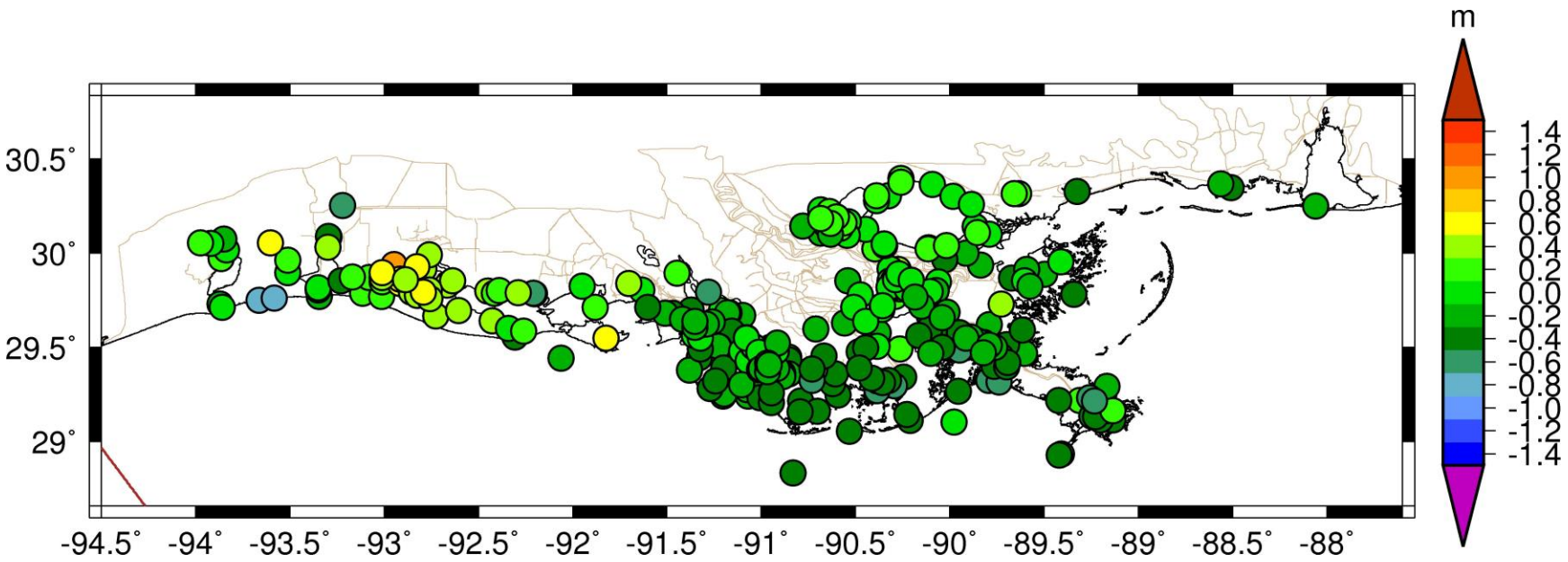

Figure 44: CPRA 2017 Model Hurricane Ike Comparison to Measured High Water Marks. Warm colors indicate the model results are greater than measurement; cool colors indicate the model results are lower than measurement.

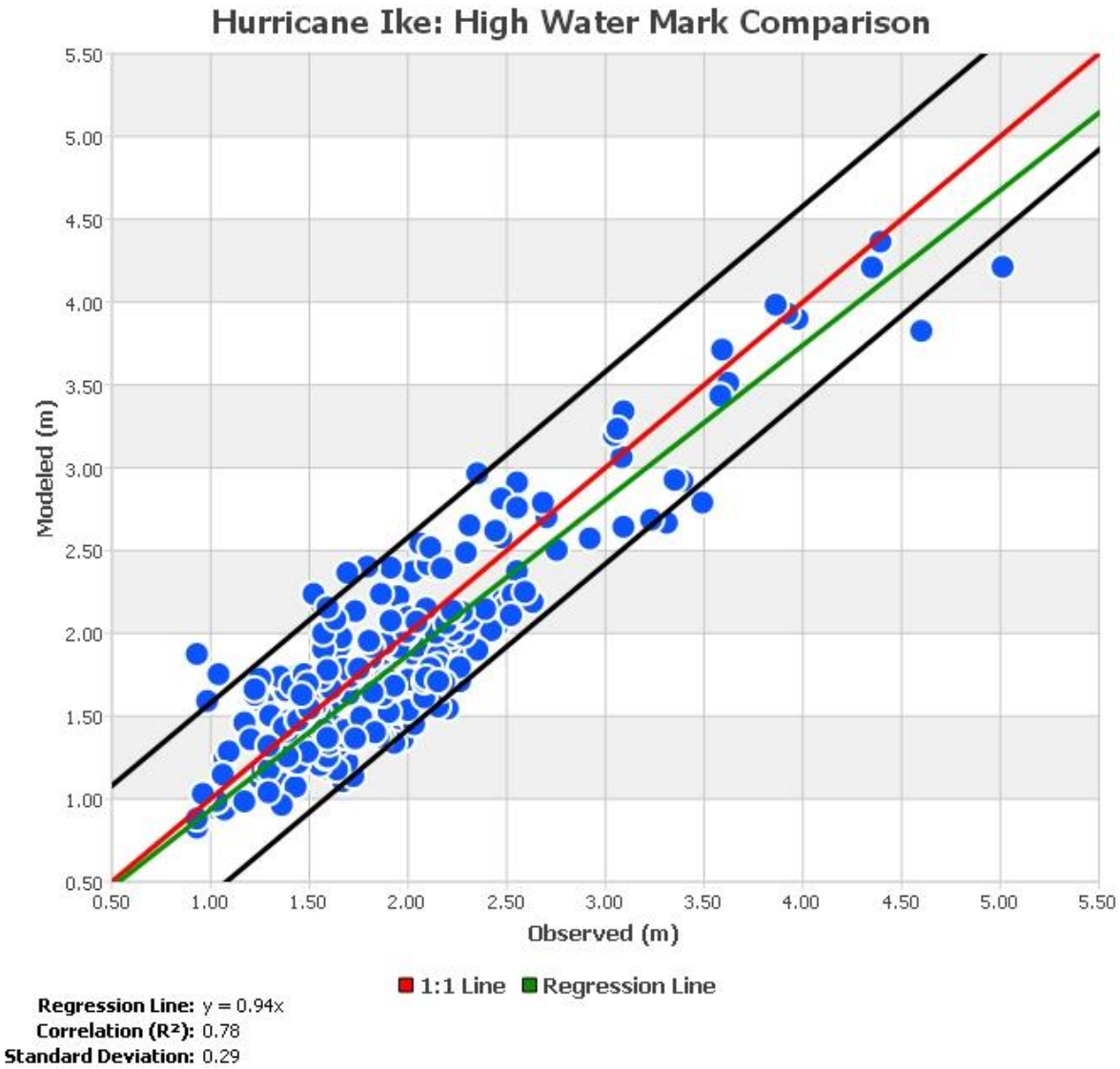

Figure 45: Hurricane Ike Regression Plot Comparing Measured High Water Marks to CPRA 2017 Model Results.

Validation Simulations Performance Summary

2017 CPRA model comparisons to high water marks are summarized in Table 2. The 2017 CPRA model demonstrates a high skill level simlar to the Dietrich et al. study performed on the five million vertex SL16 mesh (2012). Figure 46 shows a regression plot for all four storms combined. When comparing measured high water marks to model results for all four storms, the overall regression slope is 1.02, the correlation coefficient is 0.97, and the standard deviation is 0.36 meters.

Table 2: Summary of High Water Mark Comparisons.

	CPRA 2017		*Dietrich et al. 2012*	
Storm	**Regression Slope**	**Correlation Coefficient**	**Regression Slope**	**Correlation Coefficient**
Katrina	1.04	0.96	1.00	0.93
Rita	1.06	0.73	1.08	0.79
Gustav	0.98	0.77	0.95	0.80
Ike*	0.94	0.78	0.93	0.77

*Note: Not compared to Hope et al. (2013) because domain coverage is significantly different.

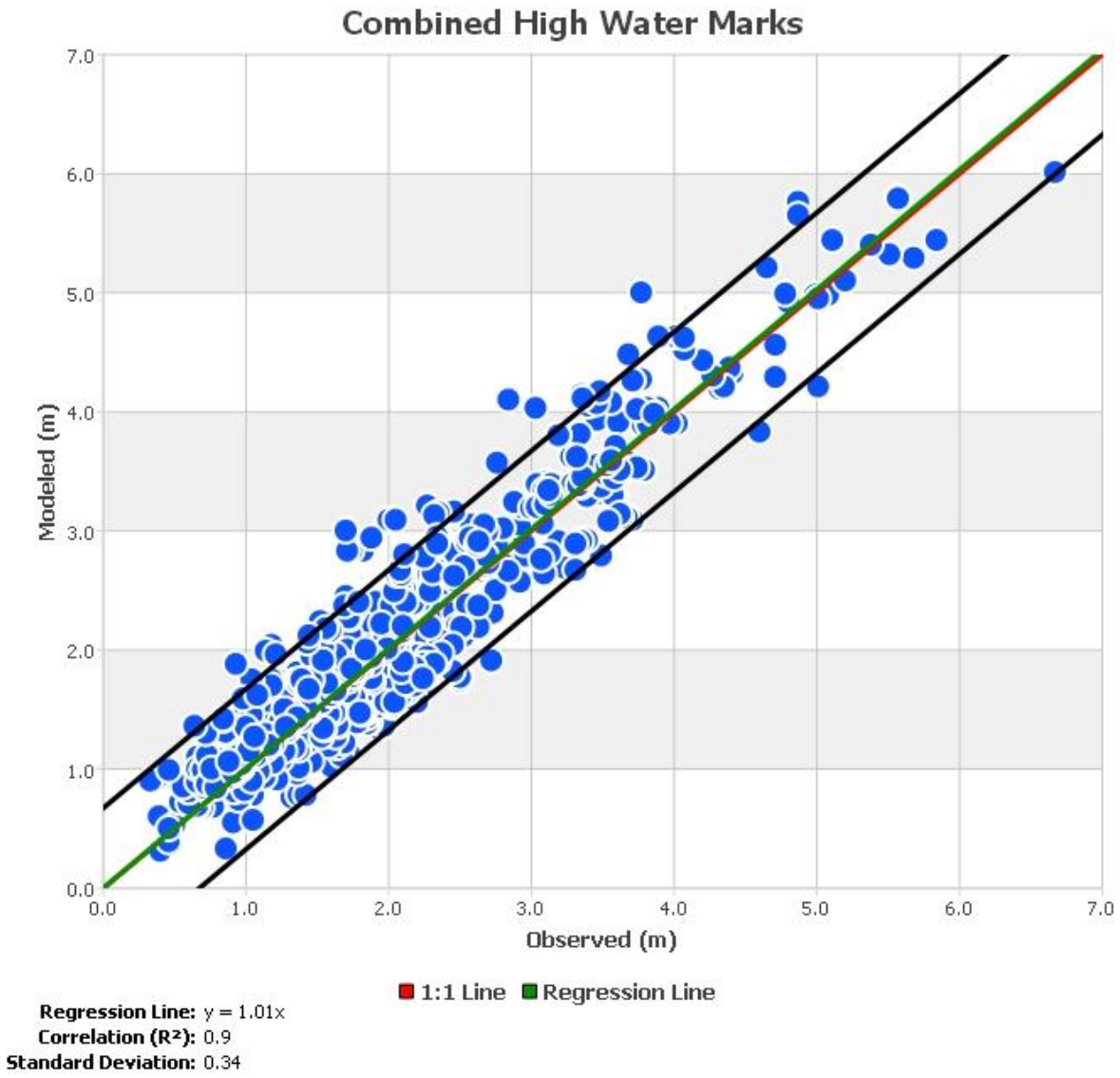

Figure 46: Regression Plot Comparing Measured High Water Marks for All Four Storms to CPRA 2017 Model Results.

References

Cobell, Z., H. Zhao, H.J. Roberts, F.R. Clark, and S. Zou. (2013). Surge and Wave Modeling for the Louisiana 2012 Coastal Master Plan. Journal of Coastal Research: Special Issue 67 – Louisiana's 2012 Coastal Master Plan Technical Analysis, pp. 88-108.

Dietrich, J.C., J.J. Westerink, A.B. Kennedy, J.M. Smith, R. Jensen, M. Zijlema, L.H. Holthuijsen, C.N. Dawson, R.A. Luettich, Jr., M.D. Powell, V.J. Cardone, A.T. Cox, G.W. Stone, H. Pourtaheri, M.E. Hope, S. Tanaka, L.G. Westerink, H.J. Westerink, and Z. Cobell. (2011) Hurricane Gustav Waves and Storm Surge: Hindcast, Synoptic Analysis and Validation in Southern Louisiana. Monthly Weather Review, Volume 139, pp. 2488-2522, DOI 10.1175/2011MWR3611.1.

Dietrich, J.C., S. Tanaka, J.J. Westerink, C.N. Dawson, R.A. Luettich, Jr., M. Zijlema, L.H. Holthuijsen, J.M. Smith, L.G. Westerink, and H.J. Westerink. (2012) Performance of the Unstructured-Mesh, SWAN+ADCIRC Model in Computing Hurricane Waves and Surge. Journal of Scientific Computing, Volume 52, Issue 2, pp. 468-497.

Ben C. Gerwick, Inc. (2012). Southeast Louisiana Flood Protection Authority – East: New Orleans East Land Bridge Study. Oakland, CA. 228pp.

Hope, M.E., J.J. Westerink, A.B. Kennedy, P.C. Kerr, C.N. Dawson, C.J. Bender, J.M. Smith, R.E. Jensen, M. Zijlema, L.H. Holthuijsen, R.A. Luettich, Jr., M.D. Powell, V.J. Cardone, A.T. Cox, H. Pourtaheri, H.J. Roberts, J.H. Atkinson, S. Tanaka, H.J. Westerink, and L.G. Westerink. (2013) Hindcast and Validation of Hurricane Ike Waves, Forerunner, and Storm Surge. Journal of Geophysical Research: Oceans, Volume 118, pp. 4424-4460.

Kennedy, A.B., U. Gravois, B.C. Zachry, J.J. Westerink, M.E. Hope, J.C. Dietrich, M.D. Powell, A.T. Cox, R.A. Luettich, Jr., and R.G. Dean. (2011) Origin of the Hurricane Ike Forerunner Surge. Geophysical Research Letters, Volume 38, Issue 8, L08608, DOI 10.1029/2011GL047090.

USACE (2008a). Louisiana Coastal Protection and Restoration Technical Report. Vicksburg, Mississippi: USACE, 98 pp.

USACE (2008b). Flood Insurance Study: Southeastern Parishes, Louisiana. Intermediate Submission 2: Offshore Water Levels and Waves. Vicksburg, Mississippi: USACE, 152 pp.

USACE (2008c). Flood Insurance Study: Southwestern Parishes, Louisiana. Intermediate Submission 2. Vicksburg, Mississippi: USACE, 697 pp.

USACE (2011). Flood Insurance Study: Coastal Counties, Texas Intermediate Submission 2, Vicksburg, Mississippi: USACE, 150 pp.

Appendix 2: Synthetic Storm Suite Simulations

In order to supply ADCIRC+SWAN model results for CLARA model improvements, the CPRA 2017 model was used to simulate all 446 synthetic storms that were developed as part of the Federal Emergency Management Agency Flood Insurance Rate Map studies in Louisiana (USACE, 2008b; USACE, 2008c). The storm tracks are shown in Figure 47. For each storm track, there are multiple storm parameters. These parameters are shown in Table 3. This storm suite includes both the FEMA low-frequency storms, which are the most powerful and generate the largest surge levels but happen more rarely, and the FEMA high-frequency storms, which are relatively less powerful and generate lower surge levels but happen more frequently. These simulations were completed on both the current conditions geometry from the 2012 Coastal Master Plan and the Less Optimistic (S13) future without action (FWOA) scenario 50 years into the future which takes into account future sea level rise (0.46 meter) and landscape changes.

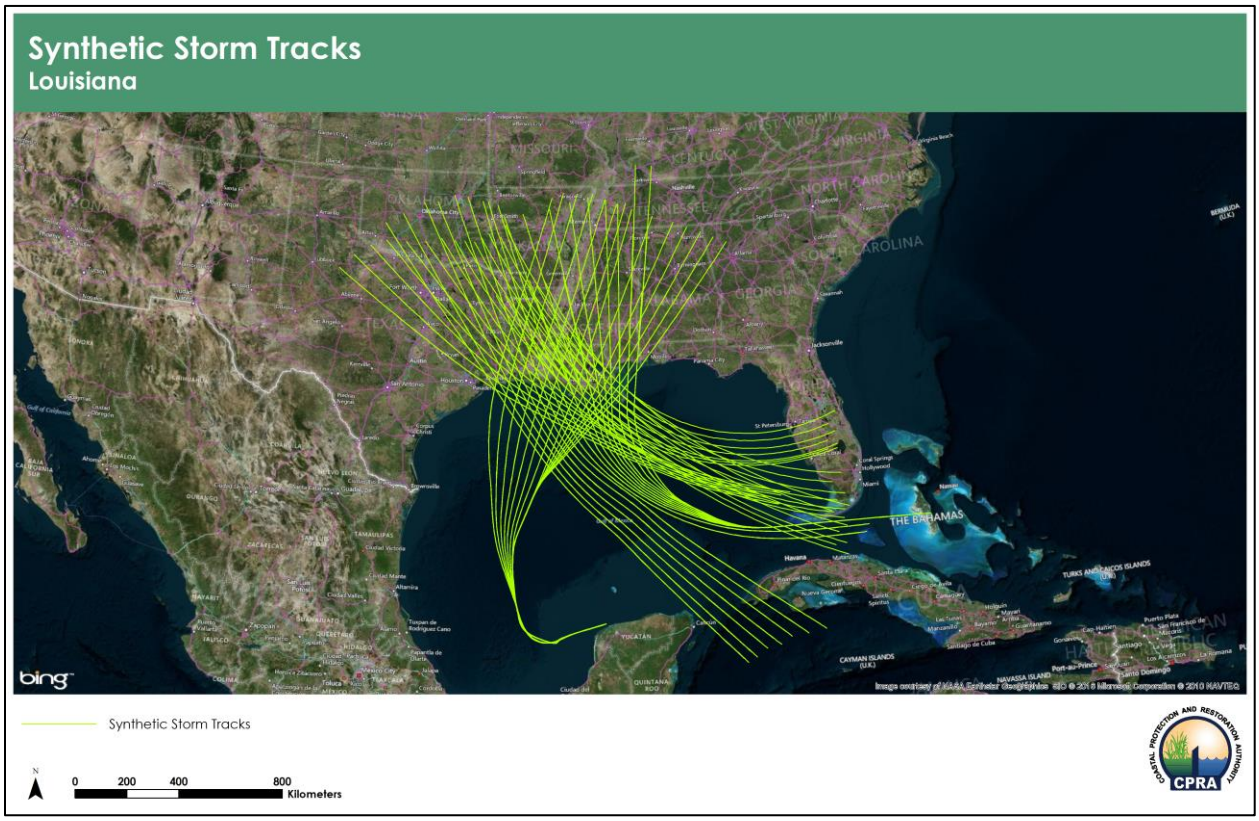

Figure 47: Synthetic Storm Tracks for Louisiana. Note that more than one storm lies on each track.

Model setup for these simulations mirrored that of the 2012 Coastal Master Plan with only a few changes:

1. Wave coupling occurred every 10 minutes as opposed to every 20 minutes. This provides a more detailed wave solution and quicker wave model numerical convergence;

2. The Powell (2006) wind drag formulation was used in ADCIRC and SWAN. More details about this can be found in Appendix 4; and

3. The ADCIRC model used was release version 50 where version 49 was used during the 2012 Coastal Master Plan.

Table 3: Louisiana Synthetic Storm Parameters.

Storm Number	Minimum Central Pressure (mb)	Radius To Maximum Winds (km)	Track	Forward Velocity (m/s)	Angle (°)	Landfall Location	
						Longitude	Latitude
1	960	20.4	E1	5.7	0	-91.2111	29.5000
2	960	38.9	E1	5.7	0	-91.2111	29.5000
3	960	65.9	E1	5.7	0	-91.2111	29.5000
4	930	14.8	E1	5.7	0	-91.2111	29.5000
5	930	32.8	E1	5.7	0	-91.2111	29.5000
6	930	47.8	E1	5.7	0	-91.2111	29.5000
7	900	11.1	E1	5.7	0	-91.2111	29.5000
8	900	27.6	E1	5.7	0	-91.2111	29.5000
9	900	40.4	E1	5.7	0	-91.2111	29.5000
10	960	20.4	E2	5.7	0	-90.4511	29.5000
11	960	38.9	E2	5.7	0	-90.4511	29.5000
12	960	65.9	E2	5.7	0	-90.4511	29.5000
13	930	14.8	E2	5.7	0	-90.4511	29.5000
14	930	32.8	E2	5.7	0	-90.4511	29.5000
15	930	47.8	E2	5.7	0	-90.4511	29.5000
16	900	11.1	E2	5.7	0	-90.4511	29.5000
17	900	27.6	E2	5.7	0	-90.4511	29.5000
18	900	40.4	E2	5.7	0	-90.4511	29.5000
19	960	20.4	E3	5.7	0	-89.8479	29.5000
20	960	38.9	E3	5.7	0	-89.8479	29.5000
21	960	65.9	E3	5.7	0	-89.8479	29.5000
22	930	14.8	E3	5.7	0	-89.8479	29.5000
23	930	32.8	E3	5.7	0	-89.8479	29.5000
24	930	47.8	E3	5.7	0	-89.8479	29.5000
25	900	11.1	E3	5.7	0	-89.8479	29.5000
26	900	27.6	E3	5.7	0	-89.8479	29.5000
27	900	40.4	E3	5.7	0	-89.8479	29.5000
28	960	20.4	E4	5.7	0	-89.2758	29.5000
29	960	38.9	E4	5.7	0	-89.2758	29.5000
30	960	65.9	E4	5.7	0	-89.2758	29.5000
31	930	14.8	E4	5.7	0	-89.2758	29.5000
32	930	32.8	E4	5.7	0	-89.2758	29.5000
33	930	47.8	E4	5.7	0	-89.2758	29.5000
34	900	11.1	E4	5.7	0	-89.2758	29.5000
35	900	27.6	E4	5.7	0	-89.2758	29.5000

Storm Number	Minimum Central Pressure (mb)	Radius To Maximum Winds (km)	Track	Forward Velocity (m/s)	Angle (°)	Landfall Location	
						Longitude	Latitude
36	900	40.4	E4	5.7	0	-89.2758	29.5000
37	960	20.4	E5	5.7	0	-88.6467	29.5000
38	960	38.9	E5	5.7	0	-88.6467	29.5000
39	960	65.9	E5	5.7	0	-88.6467	29.5000
40	930	14.8	E5	5.7	0	-88.6467	29.5000
41	930	32.8	E5	5.7	0	-88.6467	29.5000
42	930	47.8	E5	5.7	0	-88.6467	29.5000
43	900	11.1	E5	5.7	0	-88.6467	29.5000
44	900	27.6	E5	5.7	0	-88.6467	29.5000
45	900	40.4	E5	5.7	0	-88.6467	29.5000
46	960	33.7	E1	5.7	-45	-91.3677	29.5000
47	960	45.6	E1	5.7	-45	-91.3677	29.5000
48	900	23.2	E1	5.7	-45	-91.3677	29.5000
49	900	34.1	E1	5.7	-45	-91.3677	29.5000
50	960	33.7	E2	5.7	-45	-90.7238	29.5000
51	960	45.6	E2	5.7	-45	-90.7238	29.5000
52	900	23.2	E2	5.7	-45	-90.7238	29.5000
53	900	34.1	E2	5.7	-45	-90.7238	29.5000
54	960	33.7	E3	5.7	-45	-89.9208	29.5000
55	960	45.6	E3	5.7	-45	-89.9208	29.5000
56	900	23.2	E3	5.7	-45	-89.9208	29.5000
57	900	34.1	E3	5.7	-45	-89.9208	29.5000
58	960	33.7	E4	5.7	-45	-89.1054	29.5000
59	960	45.6	E4	5.7	-45	-89.1054	29.5000
60	900	23.2	E4	5.7	-45	-89.1054	29.5000
61	900	34.1	E4	5.7	-45	-89.1054	29.5000
66	960	33.7	E1	5.7	45	-90.9941	29.5000
67	960	45.6	E1	5.7	45	-90.9941	29.5000
68	900	23.2	E1	5.7	45	-90.9941	29.5000
69	900	34.1	E1	5.7	45	-90.9941	29.5000
70	960	33.7	E2	5.7	45	-90.2138	29.5000
71	960	45.6	E2	5.7	45	-90.2138	29.5000
72	900	23.2	E2	5.7	45	-90.2138	29.5000
73	900	34.1	E2	5.7	45	-90.2138	29.5000
74	960	33.7	E3	5.7	45	-89.6380	29.5000
75	960	45.6	E3	5.7	45	-89.6380	29.5000
76	900	23.2	E3	5.7	45	-89.6380	29.5000
77	900	34.1	E3	5.7	45	-89.6380	29.5000

Storm Number	Minimum Central Pressure (mb)	Radius To Maximum Winds (km)	Track	Forward Velocity (m/s)	Angle (°)	Landfall Location	
						Longitude	Latitude
78	960	33.7	E4	5.7	45	-89.0471	29.5000
79	960	45.6	E4	5.7	45	-89.0471	29.5000
80	900	23.2	E4	5.7	45	-89.0471	29.5000
81	900	34.1	E4	5.7	45	-89.0471	29.5000
82	960	32.8	E1	3.1	0	-91.1978	29.5000
83	900	32.8	E1	3.1	0	-91.1978	29.5000
84	960	32.8	E2	3.1	0	-90.4540	29.5000
85	900	32.8	E2	3.1	0	-90.4540	29.5000
86	960	32.8	E3	3.1	0	-89.8470	29.5000
87	900	32.8	E3	3.1	0	-89.8470	29.5000
88	960	32.8	E4	3.1	0	-89.2700	29.5000
89	900	32.8	E4	3.1	0	-89.2700	29.5000
90	960	32.8	E5	3.1	0	-88.6490	29.5000
91	900	32.8	E5	3.1	0	-88.6490	29.5000
92	930	32.8	E1	3.1	-45	-91.3729	29.5000
93	930	32.8	E2	3.1	-45	-90.7129	29.5000
94	930	32.8	E3	3.1	-45	-89.9200	29.5000
95	930	32.8	E4	3.1	-45	-89.0971	29.5000
97	930	32.8	E1	3.1	45	-90.9920	29.5000
98	930	32.8	E2	3.1	45	-90.2100	29.5000
99	930	32.8	E3	3.1	45	-89.6425	29.5000
100	930	32.8	E4	3.1	45	-89.0500	29.5000
101	930	32.8	E1	8.7	0	-91.2177	29.5000
102	930	32.8	E2	8.7	0	-90.4437	29.5000
103	930	32.8	E3	8.7	0	-89.8476	29.5000
104	930	32.8	E4	8.7	0	-89.2743	29.5000
105	930	32.8	E5	8.7	0	-88.6455	29.5000
106	930	32.8	E1	8.7	-45	-91.3730	29.5000
107	930	32.8	E2	8.7	-45	-90.7265	29.5000
108	930	32.8	E3	8.7	-45	-89.9205	29.5000
109	930	32.8	E4	8.7	-45	-89.1060	29.5000
111	930	32.8	E1	8.7	45	-90.9923	29.5000
112	930	32.8	E2	8.7	45	-90.2108	29.5000
113	930	32.8	E3	8.7	45	-89.6386	29.5000
114	930	32.8	E4	8.7	45	-89.0571	29.5000
115	960	32.8	E1B	5.7	0	-90.8224	29.5000
116	900	32.8	E1B	5.7	0	-90.8224	29.5000
117	960	32.8	E2B	5.7	0	-90.1267	29.5000

Storm Number	Minimum Central Pressure (mb)	Radius To Maximum Winds (km)	Track	Forward Velocity (m/s)	Angle (°)	Landfall Location	
						Longitude	Latitude
118	900	32.8	E2B	5.7	0	-90.1267	29.5000
119	960	32.8	E3B	5.7	0	-89.6000	29.5000
120	900	32.8	E3B	5.7	0	-89.6000	29.5000
121	960	32.8	E4B	5.7	0	-88.9500	29.5000
122	900	32.8	E4B	5.7	0	-88.9500	29.5000
123	960	32.8	E1B	5.7	-45	-91.0508	29.5000
124	960	32.8	E2B	5.7	-45	-90.3192	29.5000
125	960	32.8	E3B	5.7	-45	-89.5123	29.5000
126	900	32.8	E1B	5.7	-45	-91.0508	29.5000
127	900	32.8	E2B	5.7	-45	-90.3192	29.5000
128	900	32.8	E3B	5.7	-45	-89.5123	29.5000
131	960	32.8	E1B	5.7	45	-90.6000	29.5000
132	900	32.8	E1B	5.7	45	-90.6000	29.5000
133	960	32.8	E2B	5.7	45	-89.9267	29.5000
134	900	32.8	E2B	5.7	45	-89.9267	29.5000
135	960	32.8	E3B	5.7	45	-89.3457	29.5000
136	900	32.8	E3B	5.7	45	-89.3457	29.5000
137	960	32.8	E1B	3.1	0	-90.8100	29.5000
138	900	32.8	E1B	3.1	0	-90.8100	29.5000
139	960	32.8	E2B	3.1	0	-90.1380	29.5000
140	900	32.8	E2B	3.1	0	-90.1380	29.5000
141	960	32.8	E3B	3.1	0	-89.6000	29.5000
142	900	32.8	E3B	3.1	0	-89.6000	29.5000
143	960	32.8	E4B	3.1	0	-88.9520	29.5000
144	900	32.8	E4B	3.1	0	-88.9520	29.5000
145	930	32.8	E1B	3.1	-45	-91.0486	29.5000
146	930	32.8	E2B	3.1	-45	-90.3243	29.5000
147	930	32.8	E3B	3.1	-45	-89.5057	29.5000
149	930	32.8	E1B	3.1	45	-90.6050	29.5000
150	930	32.8	E2B	3.1	45	-89.9233	29.5000
151	930	32.8	E3B	3.1	45	-89.3500	29.5000
152	930	32.8	E1B	8.7	0	-90.8207	29.5000
153	930	32.8	E2B	8.7	0	-90.1300	29.5000
154	930	32.8	E3B	8.7	0	-89.6000	29.5000
155	930	32.8	E4B	8.7	0	-88.9548	29.5000
156	930	32.8	E1B	8.7	-45	-91.0470	29.5000
157	930	32.8	E2B	8.7	-45	-90.3185	29.5000
158	930	32.8	E3B	8.7	-45	-89.5195	29.5000

Storm Number	Minimum Central Pressure (mb)	Radius To Maximum Winds (km)	Track	Forward Velocity (m/s)	Angle (°)	Landfall Location	
						Longitude	Latitude
160	930	32.8	E1B	8.7	45	-90.6068	29.5000
161	930	32.8	E2B	8.7	45	-89.9217	29.5000
162	930	32.8	E3B	8.7	45	-89.3445	29.5000
201	960	20.4	W1	5.7	0	-94.2200	29.5000
202	960	38.9	W1	5.7	0	-94.2200	29.5000
203	960	65.9	W1	5.7	0	-94.2200	29.5000
204	930	14.8	W1	5.7	0	-94.2200	29.5000
205	930	32.8	W1	5.7	0	-94.2200	29.5000
206	930	47.8	W1	5.7	0	-94.2200	29.5000
207	900	11.1	W1	5.7	0	-94.2200	29.5000
208	900	27.6	W1	5.7	0	-94.2200	29.5000
209	900	40.4	W1	5.7	0	-94.2200	29.5000
210	960	20.4	W2	5.7	0	-93.5575	29.5000
211	960	38.9	W2	5.7	0	-93.5575	29.5000
212	960	65.9	W2	5.7	0	-93.5575	29.5000
213	930	14.8	W2	5.7	0	-93.5575	29.5000
214	930	32.8	W2	5.7	0	-93.5575	29.5000
215	930	47.8	W2	5.7	0	-93.5575	29.5000
216	900	11.1	W2	5.7	0	-93.5575	29.5000
217	900	27.6	W2	5.7	0	-93.5575	29.5000
218	900	40.4	W2	5.7	0	-93.5575	29.5000
219	960	20.4	W3	5.7	0	-92.9641	29.5000
220	960	38.9	W3	5.7	0	-92.9641	29.5000
221	960	65.9	W3	5.7	0	-92.9641	29.5000
222	930	14.8	W3	5.7	0	-92.9641	29.5000
223	930	32.8	W3	5.7	0	-92.9641	29.5000
224	930	47.8	W3	5.7	0	-92.9641	29.5000
225	900	11.1	W3	5.7	0	-92.9641	29.5000
226	900	27.6	W3	5.7	0	-92.9641	29.5000
227	900	40.4	W3	5.7	0	-92.9641	29.5000
228	960	20.4	W4	5.7	0	-92.3165	29.5000
229	960	38.9	W4	5.7	0	-92.3165	29.5000
230	960	65.9	W4	5.7	0	-92.3165	29.5000
231	930	14.8	W4	5.7	0	-92.3165	29.5000
232	930	32.8	W4	5.7	0	-92.3165	29.5000
233	930	47.8	W4	5.7	0	-92.3165	29.5000
234	900	11.1	W4	5.7	0	-92.3165	29.5000
235	900	27.6	W4	5.7	0	-92.3165	29.5000

Storm Number	Minimum Central Pressure (mb)	Radius To Maximum Winds (km)	Track	Forward Velocity (m/s)	Angle (°)	Landfall Location	
						Longitude	Latitude
236	900	40.4	W4	5.7	0	-92.3165	29.5000
237	960	20.4	W5	5.7	0	-91.6535	29.5000
238	960	38.9	W5	5.7	0	-91.6535	29.5000
239	960	65.9	W5	5.7	0	-91.6535	29.5000
240	930	14.8	W5	5.7	0	-91.6535	29.5000
241	930	32.8	W5	5.7	0	-91.6535	29.5000
242	930	47.8	W5	5.7	0	-91.6535	29.5000
243	900	11.1	W5	5.7	0	-91.6535	29.5000
244	900	27.6	W5	5.7	0	-91.6535	29.5000
245	900	40.4	W5	5.7	0	-91.6535	29.5000
246	960	33.7	W1	5.7	-45	-94.2600	29.5000
247	960	45.6	W1	5.7	-45	-94.2600	29.5000
248	900	23.2	W1	5.7	-45	-94.2600	29.5000
249	900	34.1	W1	5.7	-45	-94.2600	29.5000
250	960	33.7	W2	5.7	-45	-93.2636	29.5000
251	960	45.6	W2	5.7	-45	-93.2636	29.5000
252	900	23.2	W2	5.7	-45	-93.2636	29.5000
253	900	34.1	W2	5.7	-45	-93.2636	29.5000
254	960	33.7	W3	5.7	-45	-92.3845	29.5000
255	960	45.6	W3	5.7	-45	-92.3845	29.5000
256	900	23.2	W3	5.7	-45	-92.3845	29.5000
257	900	34.1	W3	5.7	-45	-92.3845	29.5000
258	960	33.7	W4	5.7	-45	-91.7515	29.5000
259	960	45.6	W4	5.7	-45	-91.7515	29.5000
260	900	23.2	W4	5.7	-45	-91.7515	29.5000
261	900	34.1	W4	5.7	-45	-91.7515	29.5000
266	960	33.7	W1	5.7	45	-94.2467	29.5000
267	960	45.6	W1	5.7	45	-94.2467	29.5000
268	900	23.2	W1	5.7	45	-94.2467	29.5000
269	900	34.1	W1	5.7	45	-94.2467	29.5000
270	960	33.7	W2	5.7	45	-93.2833	29.5000
271	960	45.6	W2	5.7	45	-93.2833	29.5000
272	900	23.2	W2	5.7	45	-93.2833	29.5000
273	900	34.1	W2	5.7	45	-93.2833	29.5000
274	960	33.7	W3	5.7	45	-92.3167	29.5000
275	960	45.6	W3	5.7	45	-92.3167	29.5000
276	900	23.2	W3	5.7	45	-92.3167	29.5000
277	900	34.1	W3	5.7	45	-92.3167	29.5000

Storm Number	Minimum Central Pressure (mb)	Radius To Maximum Winds (km)	Track	Forward Velocity (m/s)	Angle (°)	Landfall Location	
						Longitude	Latitude
278	960	33.7	W4	5.7	45	-91.4135	29.5000
279	960	45.6	W4	5.7	45	-91.4135	29.5000
280	900	23.2	W4	5.7	45	-91.4135	29.5000
281	900	34.1	W4	5.7	45	-91.4135	29.5000
282	960	32.8	W1	3.1	0	-94.2244	29.5000
283	900	32.8	W1	3.1	0	-94.2244	29.5000
284	960	32.8	W2	3.1	0	-93.5575	29.5000
285	900	32.8	W2	3.1	0	-93.5575	29.5000
286	960	32.8	W3	3.1	0	-92.9600	29.5000
287	900	32.8	W3	3.1	0	-92.9600	29.5000
288	960	32.8	W4	3.1	0	-92.3178	29.5000
289	900	32.8	W4	3.1	0	-92.3178	29.5000
290	960	32.8	W5	3.1	0	-91.6522	29.5000
291	900	32.8	W5	3.1	0	-91.6522	29.5000
292	930	32.8	W1	3.1	-45	-94.2500	29.5000
293	930	32.8	W2	3.1	-45	-93.2650	29.5000
294	930	32.8	W3	3.1	-45	-92.3800	29.5000
295	930	32.8	W4	3.1	-45	-91.7500	29.5000
297	930	32.8	W1	3.1	45	-94.2540	29.5000
298	930	32.8	W2	3.1	45	-93.2867	29.5000
299	930	32.8	W3	3.1	45	-92.3189	29.5000
300	930	32.8	W4	3.1	45	-91.4140	29.5000
301	930	32.8	W1	8.7	0	-94.2250	29.5000
302	930	32.8	W2	8.7	0	-93.5624	29.5000
303	930	32.8	W3	8.7	0	-92.9640	29.5000
304	930	32.8	W4	8.7	0	-92.3159	29.5000
305	930	32.8	W5	8.7	0	-91.6531	29.5000
306	930	32.8	W1	8.7	-45	-94.2567	29.5000
307	930	32.8	W2	8.7	-45	-93.2650	29.5000
308	930	32.8	W3	8.7	-45	-92.3771	29.5000
309	930	32.8	W4	8.7	-45	-91.7442	29.5000
311	930	32.8	W1	8.7	45	-94.2500	29.5000
312	930	32.8	W2	8.7	45	-93.2800	29.5000
313	930	32.8	W3	8.7	45	-92.3144	29.5000
314	930	32.8	W4	8.7	45	-91.4137	29.5000
315	960	32.8	W1B	5.7	0	-93.9253	29.5000
316	900	32.8	W1B	5.7	0	-93.9253	29.5000
317	960	32.8	W2B	5.7	0	-93.2294	29.5000

Storm Number	Minimum Central Pressure (mb)	Radius To Maximum Winds (km)	Track	Forward Velocity (m/s)	Angle (°)	Landfall Location	
						Longitude	Latitude
318	900	32.8	W2B	5.7	0	-93.2294	29.5000
319	960	32.8	W3B	5.7	0	-92.6065	29.5000
320	900	32.8	W3B	5.7	0	-92.6065	29.5000
321	960	32.8	W4B	5.7	0	-91.9718	29.5000
322	900	32.8	W4B	5.7	0	-91.9718	29.5000
323	960	32.8	W1B	5.7	-45	-93.7340	29.5000
324	960	32.8	W2B	5.7	-45	-92.8027	29.5000
325	960	32.8	W3B	5.7	-45	-92.0336	29.5000
326	900	32.8	W1B	5.7	-45	-93.7340	29.5000
327	900	32.8	W2B	5.7	-45	-92.8027	29.5000
328	900	32.8	W3B	5.7	-45	-92.0336	29.5000
331	960	32.8	W1B	5.7	45	-93.7278	29.5000
332	900	32.8	W1B	5.7	45	-93.7278	29.5000
333	960	32.8	W2B	5.7	45	-92.7953	29.5000
334	900	32.8	W2B	5.7	45	-92.7953	29.5000
335	960	32.8	W3B	5.7	45	-91.9044	29.5000
336	900	32.8	W3B	5.7	45	-91.9044	29.5000
337	960	32.8	W1B	3.1	0	-93.9233	29.5000
338	900	32.8	W1B	3.1	0	-93.9233	29.5000
339	960	32.8	W2B	3.1	0	-93.2344	29.5000
340	900	32.8	W2B	3.1	0	-93.2344	29.5000
341	960	32.8	W3B	3.1	0	-92.6133	29.5000
342	900	32.8	W3B	3.1	0	-92.6133	29.5000
343	960	32.8	W4B	3.1	0	-91.9733	29.5000
344	900	32.8	W4B	3.1	0	-91.9733	29.5000
345	930	32.8	W1B	3.1	-45	-93.7267	29.5000
346	930	32.8	W2B	3.1	-45	-92.8000	29.5000
347	930	32.8	W3B	3.1	-45	-92.0350	29.5000
349	930	32.8	W1B	3.1	45	-93.7278	29.5000
350	930	32.8	W2B	3.1	45	-92.7867	29.5000
351	930	32.8	W3B	3.1	45	-91.9040	29.5000
352	930	32.8	W1B	8.7	0	-93.9225	29.5000
353	930	32.8	W2B	8.7	0	-93.2320	29.5000
354	930	32.8	W3B	8.7	0	-92.6100	29.5000
355	930	32.8	W4B	8.7	0	-91.9723	29.5000
356	930	32.8	W1B	8.7	-45	-93.7327	29.5000
357	930	32.8	W2B	8.7	-45	-92.8012	29.5000
358	930	32.8	W3B	8.7	-45	-92.0317	29.5000

Storm Number	Minimum Central Pressure (mb)	Radius To Maximum Winds (km)	Track	Forward Velocity (m/s)	Angle (°)	Landfall Location	
						Longitude	Latitude
360	930	32.8	W1B	8.7	45	-93.7300	29.5000
361	930	32.8	W2B	8.7	45	-92.7932	29.5000
362	930	32.8	W3B	8.7	45	-91.9037	29.5000
401	975	20.4	W1	5.7	0	-94.2200	29.5000
402	975	38.9	W1	5.7	0	-94.2200	29.5000
403	975	65.9	W1	5.7	0	-94.2200	29.5000
404	975	20.4	W2	5.7	0	-93.5575	29.5000
405	975	38.9	W2	5.7	0	-93.5575	29.5000
406	975	65.9	W2	5.7	0	-93.5575	29.5000
407	975	20.4	W3	5.7	0	-92.9641	29.5000
408	975	38.9	W3	5.7	0	-92.9641	29.5000
409	975	65.9	W3	5.7	0	-92.9641	29.5000
410	975	20.4	W4	5.7	0	-92.3165	29.5000
411	975	38.9	W4	5.7	0	-92.3165	29.5000
412	975	65.9	W4	5.7	0	-92.3165	29.5000
413	975	20.4	W5	5.7	0	-91.6535	29.5000
414	975	38.9	W5	5.7	0	-91.6535	29.5000
415	975	65.9	W5	5.7	0	-91.6535	29.5000
416	975	33.7	W1	5.7	-45	-94.2600	29.5000
417	975	45.6	W1	5.7	-45	-94.2600	29.5000
418	975	33.7	W2	5.7	-45	-93.2636	29.5000
419	975	45.6	W2	5.7	-45	-93.2636	29.5000
420	975	33.7	W3	5.7	-45	-92.3845	29.5000
421	975	45.6	W3	5.7	-45	-92.3845	29.5000
422	975	33.7	W4	5.7	-45	-91.7515	29.5000
423	975	45.6	W4	5.7	-45	-91.7515	29.5000
424	975	33.7	W1	5.7	45	-94.2467	29.5000
425	975	45.6	W1	5.7	45	-94.2467	29.5000
426	975	33.7	W2	5.7	45	-93.2833	29.5000
427	975	45.6	W2	5.7	45	-93.2833	29.5000
428	975	33.7	W3	5.7	45	-92.3167	29.5000
429	975	45.6	W3	5.7	45	-92.3167	29.5000
430	975	33.7	W4	5.7	45	-91.4135	29.5000
431	975	45.6	W4	5.7	45	-91.4135	29.5000
432	975	32.8	W1	3.1	0	-94.2244	29.5000
433	975	32.8	W2	3.1	0	-93.5575	29.5000
434	975	32.8	W3	3.1	0	-92.9600	29.5000
435	975	32.8	W4	3.1	0	-92.3178	29.5000

Storm Number	Minimum Central Pressure (mb)	Radius To Maximum Winds (km)	Track	Forward Velocity (m/s)	Angle (°)	Landfall Location	
						Longitude	Latitude
436	975	32.8	W5	3.1	0	-91.6522	29.5000
437	975	32.8	W1	3.1	-45	-94.2500	29.5000
438	975	32.8	W2	3.1	-45	-93.2650	29.5000
439	975	32.8	W3	3.1	-45	-92.3800	29.5000
440	975	32.8	W4	3.1	-45	-91.7500	29.5000
441	975	32.8	W1	3.1	45	-94.2540	29.5000
442	975	32.8	W2	3.1	45	-93.2867	29.5000
443	975	32.8	W3	3.1	45	-92.3189	29.5000
444	975	32.8	W4	3.1	45	-91.4140	29.5000
445	975	32.8	W1	8.7	0	-94.2250	29.5000
446	975	32.8	W2	8.7	0	-93.5624	29.5000
447	975	32.8	W3	8.7	0	-92.9640	29.5000
448	975	32.8	W4	8.7	0	-92.3159	29.5000
449	975	32.8	W5	8.7	0	-91.6531	29.5000
450	975	32.8	W1	8.7	-45	-94.2567	29.5000
451	975	32.8	W2	8.7	-45	-93.2650	29.5000
452	975	32.8	W3	8.7	-45	-92.3771	29.5000
453	975	32.8	W4	8.7	-45	-91.7442	29.5000
454	975	32.8	W1	8.7	45	-94.2500	29.5000
455	975	32.8	W2	8.7	45	-93.2800	29.5000
456	975	32.8	W3	8.7	45	-92.3144	29.5000
457	975	32.8	W4	8.7	45	-91.4137	29.5000
458	975	32.8	W1B	5.7	0	-93.9253	29.5000
459	975	32.8	W2B	5.7	0	-93.2294	29.5000
460	975	32.8	W3B	5.7	0	-92.6065	29.5000
461	975	32.8	W4B	5.7	0	-91.9718	29.5000
462	975	32.8	W1B	3.1	0	-93.9233	29.5000
463	975	32.8	W2B	3.1	0	-93.2344	29.5000
464	975	32.8	W3B	3.1	0	-92.6133	29.5000
465	975	32.8	W4B	3.1	0	-91.9733	29.5000
466	975	32.8	W1B	3.1	-45	-93.7267	29.5000
467	975	32.8	W2B	3.1	-45	-92.8000	29.5000
468	975	32.8	W3B	3.1	-45	-92.0350	29.5000
469	975	32.8	W1B	3.1	45	-93.7278	29.5000
470	975	32.8	W2B	3.1	45	-92.7867	29.5000
471	975	32.8	W3B	3.1	45	-91.9040	29.5000
501	975	20.4	E1	5.7	0	-91.2111	29.5000
502	975	38.9	E1	5.7	0	-91.2111	29.5000

Storm Number	Minimum Central Pressure (mb)	Radius To Maximum Winds (km)	Track	Forward Velocity (m/s)	Angle (°)	Landfall Location	
						Longitude	Latitude
503	975	65.9	E1	5.7	0	-91.2111	29.5000
504	975	20.4	E2	5.7	0	-90.4511	29.5000
505	975	38.9	E2	5.7	0	-90.4511	29.5000
506	975	65.9	E2	5.7	0	-90.4511	29.5000
507	975	20.4	E3	5.7	0	-89.8479	29.5000
508	975	38.9	E3	5.7	0	-89.8479	29.5000
509	975	65.9	E3	5.7	0	-89.8479	29.5000
510	975	20.4	E4	5.7	0	-89.2758	29.5000
511	975	38.9	E4	5.7	0	-89.2758	29.5000
512	975	65.9	E4	5.7	0	-89.2758	29.5000
513	975	20.4	E5	5.7	0	-88.6467	29.5000
514	975	38.9	E5	5.7	0	-88.6467	29.5000
515	975	65.9	E5	5.7	0	-88.6467	29.5000
516	975	33.7	E1	5.7	-45	-91.3677	29.5000
517	975	45.6	E1	5.7	-45	-91.3677	29.5000
518	975	33.7	E2	5.7	-45	-90.7238	29.5000
519	975	45.6	E2	5.7	-45	-90.7238	29.5000
520	975	33.7	E3	5.7	-45	-89.9208	29.5000
521	975	45.6	E3	5.7	-45	-89.9208	29.5000
522	975	33.7	E4	5.7	-45	-89.1054	29.5000
523	975	45.6	E4	5.7	-45	-89.1054	29.5000
524	975	33.7	E1	5.7	45	-90.9941	29.5000
525	975	45.6	E1	5.7	45	-90.9941	29.5000
526	975	33.7	E2	5.7	45	-90.2138	29.5000
527	975	45.6	E2	5.7	45	-90.2138	29.5000
528	975	33.7	E3	5.7	45	-89.6380	29.5000
529	975	45.6	E3	5.7	45	-89.6380	29.5000
530	975	33.7	E4	5.7	45	-89.0471	29.5000
531	975	45.6	E4	5.7	45	-89.0471	29.5000
532	975	32.8	E1	3.1	0	-91.1978	29.5000
533	975	32.8	E2	3.1	0	-90.4540	29.5000
534	975	32.8	E3	3.1	0	-89.8470	29.5000
535	975	32.8	E4	3.1	0	-89.2700	29.5000
536	975	32.8	E5	3.1	0	-88.6490	29.5000
537	975	32.8	E1	3.1	-45	-91.3729	29.5000
538	975	32.8	E2	3.1	-45	-90.7129	29.5000
539	975	32.8	E3	3.1	-45	-89.9200	29.5000
540	975	32.8	E4	3.1	-45	-89.0971	29.5000

Storm Number	Minimum Central Pressure (mb)	Radius To Maximum Winds (km)	Track	Forward Velocity (m/s)	Angle (°)	Landfall Location	
						Longitude	Latitude
541	975	32.8	E1	3.1	45	-90.9920	29.5000
542	975	32.8	E2	3.1	45	-90.2100	29.5000
543	975	32.8	E3	3.1	45	-89.6425	29.5000
544	975	32.8	E4	3.1	45	-89.0500	29.5000
545	975	32.8	E1	8.7	0	-91.2177	29.5000
546	975	32.8	E2	8.7	0	-90.4437	29.5000
547	975	32.8	E3	8.7	0	-89.8476	29.5000
548	975	32.8	E4	8.7	0	-89.2743	29.5000
549	975	32.8	E5	8.7	0	-88.6455	29.5000
550	975	32.8	E1	8.7	-45	-91.3730	29.5000
551	975	32.8	E2	8.7	-45	-90.7265	29.5000
552	975	32.8	E3	8.7	-45	-89.9205	29.5000
553	975	32.8	E4	8.7	-45	-89.1060	29.5000
554	975	32.8	E1	8.7	45	-90.9923	29.5000
555	975	32.8	E2	8.7	45	-90.2108	29.5000
556	975	32.8	E3	8.7	45	-89.6386	29.5000
557	975	32.8	E4	8.7	45	-89.0571	29.5000
558	975	32.8	E1B	5.7	0	-90.8224	29.5000
559	975	32.8	E2B	5.7	0	-90.1267	29.5000
560	975	32.8	E3B	5.7	0	-89.6000	29.5000
561	975	32.8	E4B	5.7	0	-88.9500	29.5000
562	975	32.8	E1B	3.1	0	-90.8100	29.5000
563	975	32.8	E2B	3.1	0	-90.1380	29.5000
564	975	32.8	E3B	3.1	0	-89.6000	29.5000
565	975	32.8	E4B	3.1	0	-88.9520	29.5000
566	975	32.8	E1B	3.1	-45	-91.0486	29.5000
567	975	32.8	E2B	3.1	-45	-90.3243	29.5000
568	975	32.8	E3B	3.1	-45	-89.5057	29.5000
569	975	32.8	E1B	3.1	45	-90.6050	29.5000
570	975	32.8	E2B	3.1	45	-89.9233	29.5000
571	975	32.8	E3B	3.1	45	-89.3500	29.5000

Figures 48 and 49 show a single storm simulation that was conducted using the 2017 CPRA model, assuming the current conditions landscape. Figures 50 and 51 show the same storm for the Less Optimistic FWOA scenario. Finally, Figure 52 shows the difference between the surge levels in current conditions and the Less Optimistic FWOA scenario. Note in Figure 52 that, through much of the domain, the orange value is representative of the eustatic sea level rise applied to the model in Less Optimistic conditions. Contours other than orange represent a nonlinear storm surge response (e.g., a flood hazard change that differs from the eustatic sea level rise applied in the model).

Information from these simulations was extracted and packaged for analysis by the CLARA model. The CLARA model recieves input from the surge and waves model at four sets of locations: 1) Unprotected census blocks, 2) Semi-protected census blocks, 3) Surge and wave points, and 4) CLARA model grid points. Each set of points receives maximum surge elevation and maximum signficiant wave height information. Surge and wave points additionaly receive the peak wave period for the maximum wave significant height, as well as time series storm surge elevation.

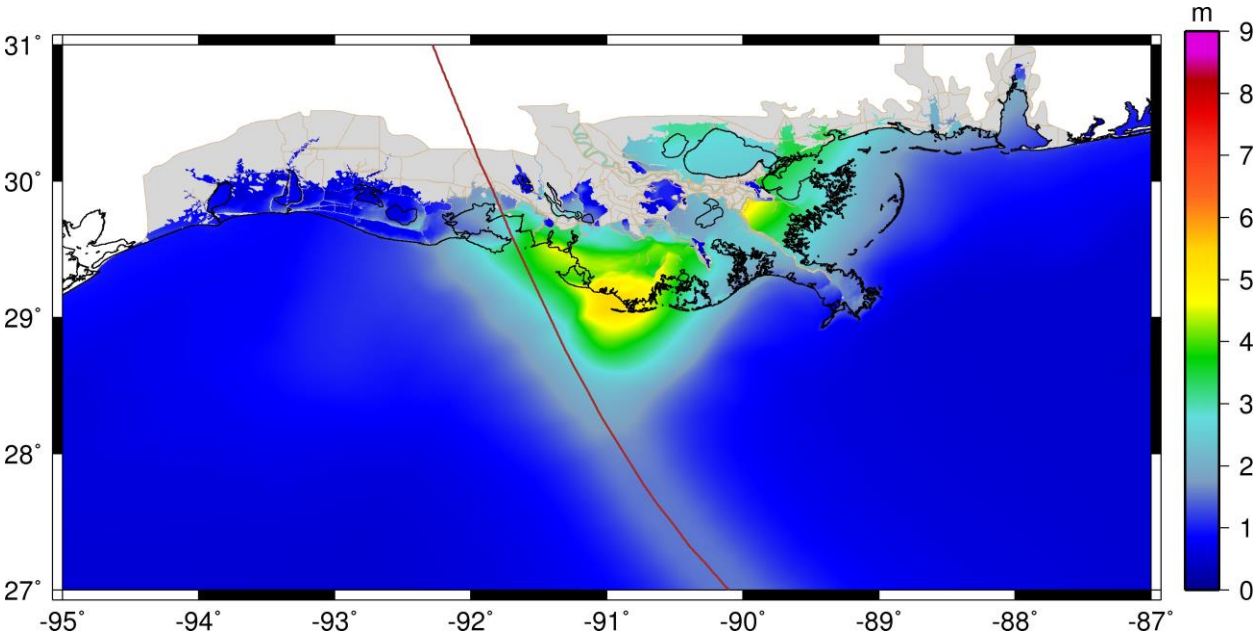

Figure 48: Maximum Storm Surge Elevation (meters [m], North American Vertical Datum of 1988 [NAVD88]) for Storm 245 Under the Current Conditions Scenario. Storm track shown in brown.

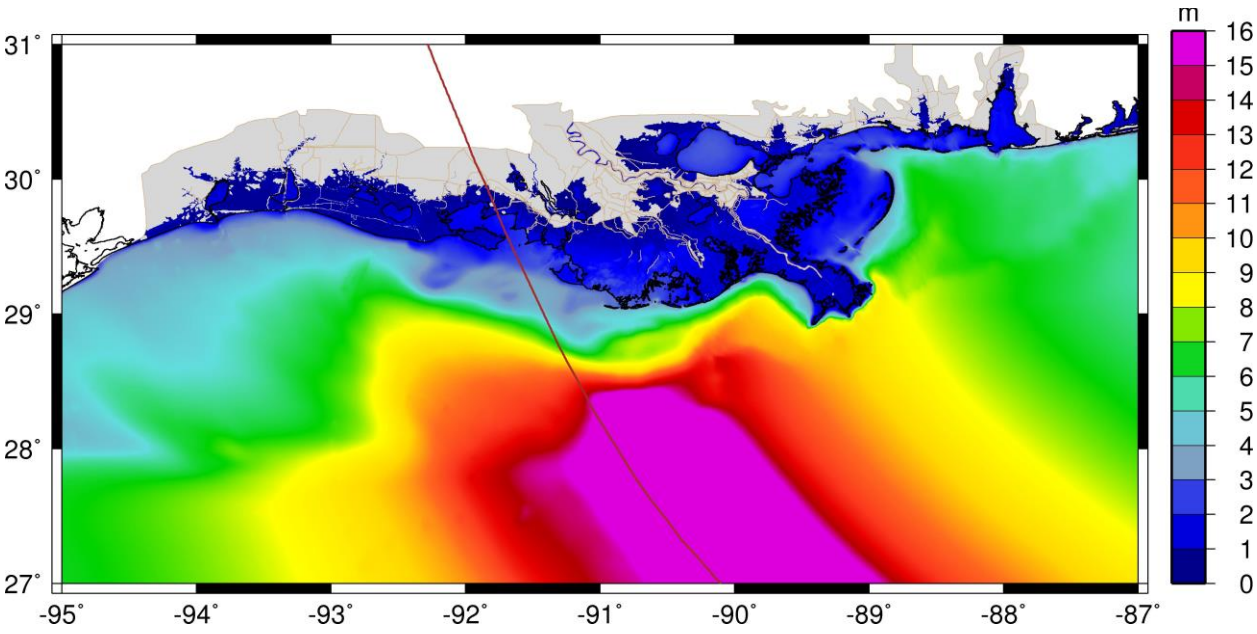

Figure 49: Maximum Significant Wave Height (m) for Storm 245 Under the Current Conditions Scenario. Storm track shown in brown.

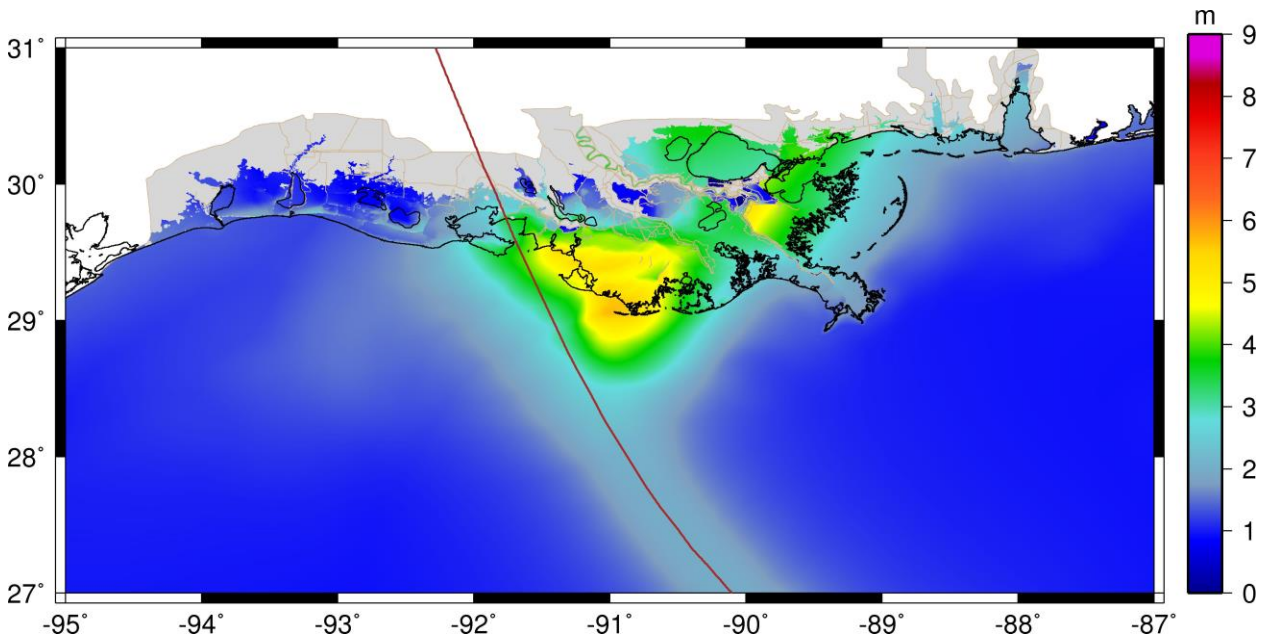

Figure 50: Maximum Storm Surge Elevation (m, NAVD88) for Storm 245 Under the Less Optimistic Scenario. Storm track shown in brown.

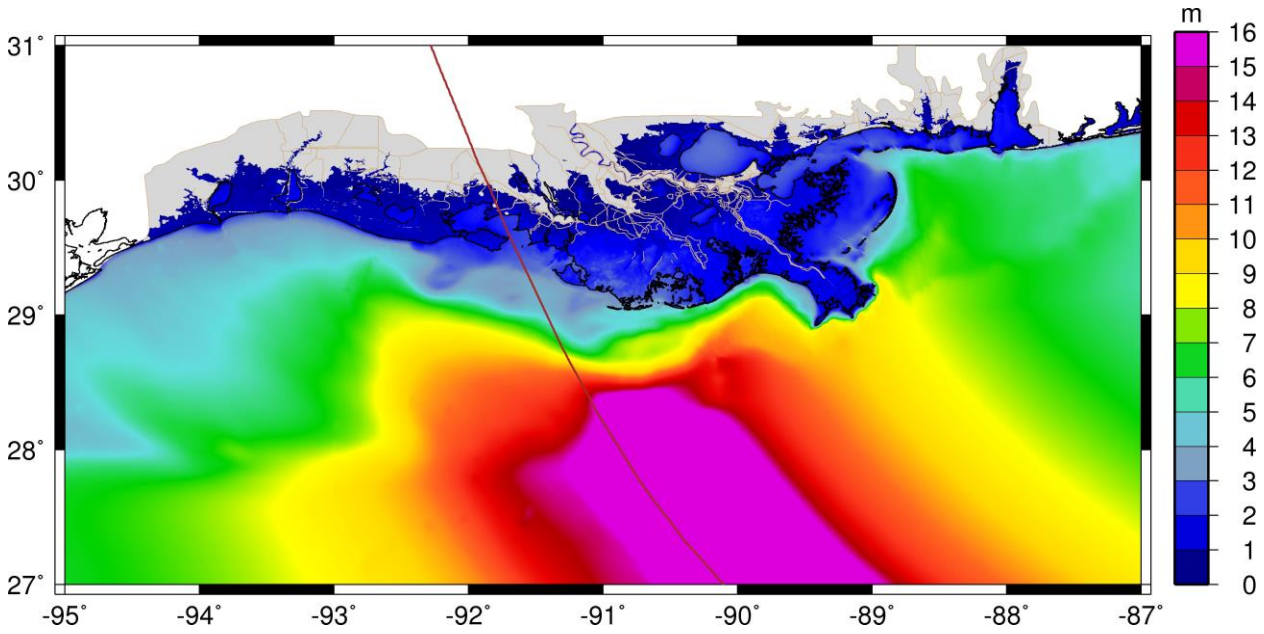

Figure 51: Maximum Significant Wave Height (m) for Storm 245 Under the Less Optimistic Scenario. Storm track shown in brown.

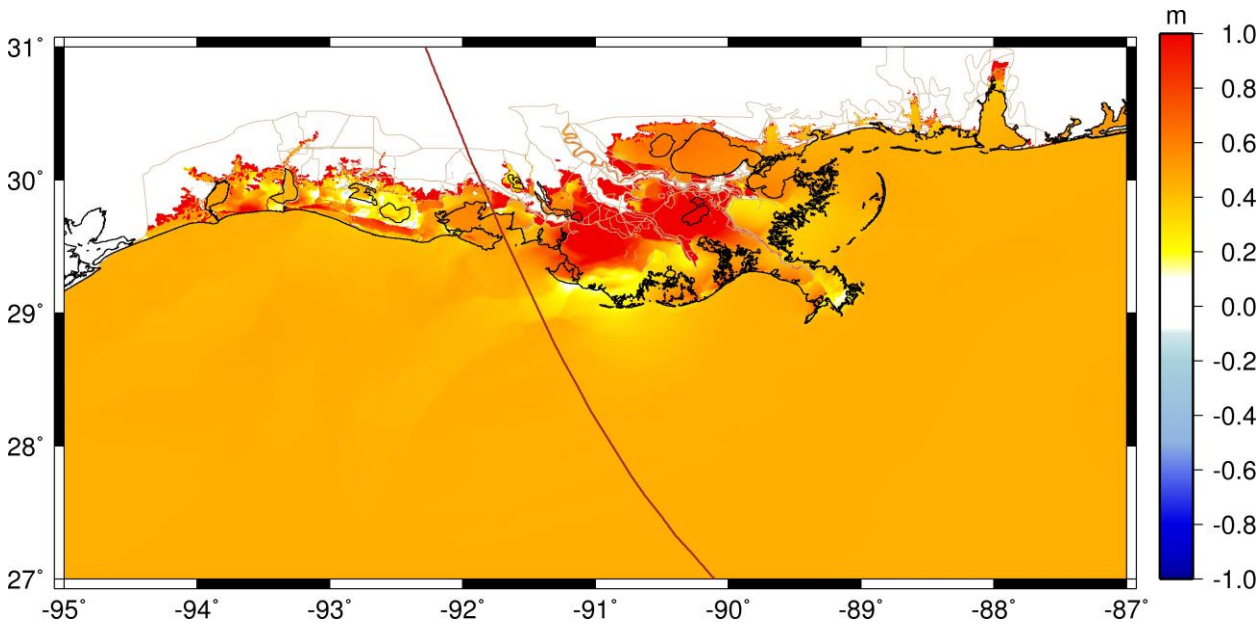

Figure 52: Difference in Water Levels (m) between the Less Optimistic Scenario and Current Conditions Scenario. Positive values indicate Less Optimistic elevations higher than current conditions. Strom track shown in brown.

References

Powell, M.D. (2006). Final Report to the National Oceanic and Atmospheric Administration (NOAA) Joint Hurricane Testbed (JHT) Program. 26 pp.

USACE (2008b). Flood Insurance Study: Southeastern Parishes, Louisiana. Intermediate Submission 2: Offshore Water Levels and Waves. Vicksburg, Mississippi: USACE, 152 pp.

USACE (2008c). Flood Insurance Study: Southwestern Parishes, Louisiana. Intermediate Submission 2. Vicksburg, Mississippi: USACE, 697 pp.

Appendix 3: Raised Feature Elevation Interpolation Sensitivity Analysis

In coastal Louisiana, there are many critical features included in a storm surge model to accurately predict the movement of water throughout the system. A portion of these are frequently surveyed levees, such as federally maintained levees. The application of levee elevations in the ADCIRC+SWAN model using levee crown surveys is a process that is as accurate as the survey itself. However, some critical hydraulic features (one meter or more above the surrounding landscape), such as local levees, roadways, dredge spoil mounds, and natural ridges lack site specific survey data gathered with the intention of capturing the feature's crown elevation. When site specific survey data are not available, the crown elevations of these features must be defined using LIDAR data which do not target specific locations (e.g., feature crown locations) on the landscape. The determination of accurate representative crown elevations for these features may reduce model uncertainty.

Crown elevations for critical raised features without site specific survey data have previously been estimated from LIDAR datasets using a control volume method to normalize the selection area for elevations based upon the size of elements in the numerical model (Cobell et al., 2013; USACE, 2008a; USACE, 2008b; USACE, 2008c). A schematic is shown in Figure 53. In this figure, the black lines represent the triangular finite elements of the ADCIRC mesh, with the red dot representing the vertex of concern. The blue triangles represent the centers of each finite element. The red box is an example of a control volume. The LIDAR data inside this control volume are selected for analysis.

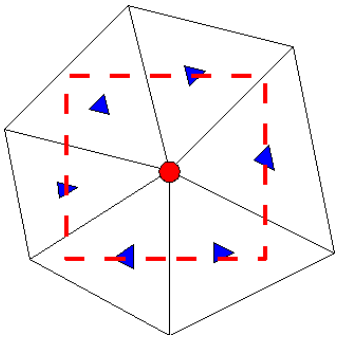

Figure 53: Schematic of a Control Volume Approach for Triangular Finite Elements.

Determining crown elevations of raised features, particularly at intersections of multiple features, can be difficult and is an ongoing research topic known as edge or ridge detection (Coggin, 2008).

For this analysis, three methods were applied to determine crown elevations of raised features that do not have individual survey data. These methods were applied in Barataria Basin and the Chenier Plain using the 2001 ATLAS LIDAR (Louisiana State University, 2004), shown in Figure 54. Barataria Basin has features that have relatively shorter lengths, on the order of a few kilometers, than the Chenier Plain, which has many roads and natural ridges extending over the broad floodplain for 80 kilometers or more. This analysis assumes that the LIDAR maintains enough resolution to adequately describe the crest of the feature and, therefore, all three methods were applied without any additional post-processing.

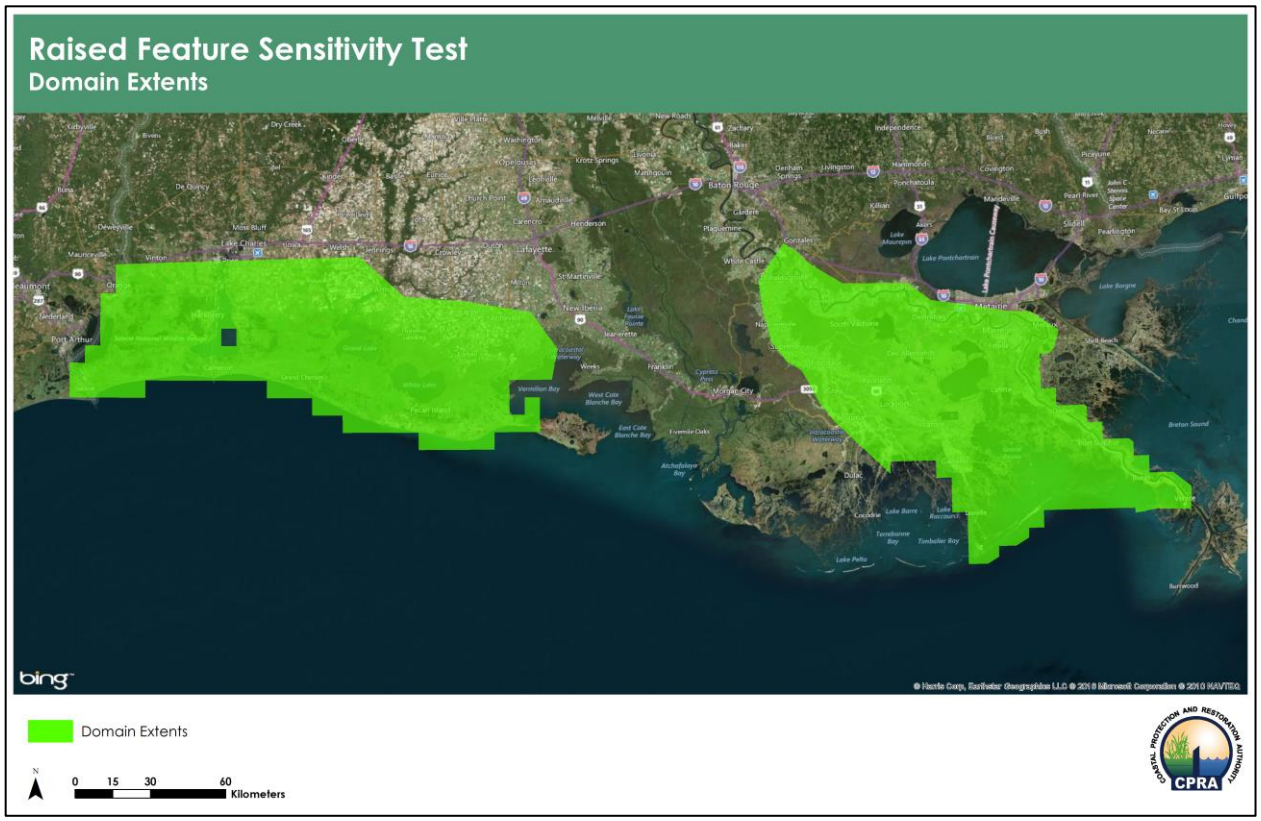

Figure 54: Raised Feature Sensitivity Test Domains.

Note that more recent LIDAR is available in coastal Louisiana than the 2001 ATLAS data. However, other data were not readily available during the study. Because this analysis is an evaluation of the sensitivity of interpolation methodologies and not the data themselves, these data were applied rather than more recent LIDAR.

For each of the methods, the suite of 40 storms utilized during the 2012 Coastal Master Plan was simulated on ADCIRC model meshes with modified raised feature elevations. As was done with the full suite of 446 storms from Appendix 2, information regarding storm surge and waves was extracted at discrete locations and passed to the CLARA model for analysis. Results are used as part of the CLARA model development tasks to assess the uncertainty related to the ADCIRC model development, specifically the translation of continuous, two-dimensional data onto linear features defined by discrete points. The appliciation of elevation data onto the model vertices is believed to be one of the largest sources of uncertainty in ADCIRC model development.

Maximum Value Method

The maximum value method extracts the maximum topographic elevation within a defined control volume around each model vertex aligned along a given raised feature. The sampling is performed on a diameter equal to the maximum finite element size that is connected to the vertex. As an example, if the vertex is connected to a 100 meter element, the searching radius will be 50 meters in any direction. The 1:1 size selection was used to ensure that the crown elevation along a suitable raised feature length is captured, even in instances where the model vertices are not aligned exactly along the raised feature crown as it is defined by LIDAR.

This method has the benefit of always finding the highest topography in the area and has generally been used for applying values to previous versions of USACE and CPRA ADCIRC models throughout coastal Louisiana since the Louisiana Coastal Protection and Restoration analysis, including the 2012 Coastal Master Plan. In this way, crown elevations are not underestimated, ensuring that hydraulic controls are fully captured. However, the risk of an approach like this is that crown elevations can be overstated by outliers in the data that are either not filtered in LIDAR post-processing or are high ground along an adjacent feature.

Based on comparisons to available site specific data, this technique has generally provided a reasonable representation of crown elevations along a feature, with the exception of feature reaches adjacent to other high land that can unintentionally set a crown elevation that is significantly higher than is actually present on the feature itself. Overstated elevations (e.g., those 0.3 meters above crown elevations determined through manual quality check procedures) have been manually adjusted in previous ADCIRC mesh development efforts. However, when numerous model scenarios are simulated, particularly for state wide analyses like the master plan, improved automation helps limit model setup errors and reduces the human time necessary for quality control.

Averaging Method

The averaging method, similar to the maximum value method, considers all LIDAR data within a selected control volume. LIDAR elevations within a diameter one half the maximum element size are averaged. For example, a vertex that is connected to a 100 meter element would search 25 meters in any direction. This method makes use of a smaller control volume than the maximum value method in order to reduce the number of low-lying LIDAR data (e.g., those in the floodplain immediately adjacent to the raised feature) included in the control volume. As the control volume becomes larger, the greater number of points selected from LIDAR will be from the floodplain, unintentionally lowering the crown elevation extracted at the mesh vertex.

The primary disadvantage of this approach is that some features, particularly those with narrow widths relative to the control volume size, will potentially be defined with too low of a crown elevation. However, the potential pitfall of overstating elevations in the maximum value method is addressed.

2σ Averaging Method

The 2σ averaging method was developed with the intent to leverage the benefits of the maximum value and averaging methods while limiting the impacts of the disadvantages associated with each method. The control volume size used is the same as the maximum value method.

This method assumes that the points that lie within each control volume resemble a normal distribution. To determine a representative crown elevation, only points with an elevation of 2σ or higher are considered, as shown in the red box in Figure 55. The aim is to isolate only those LIDAR points that are part of some raised features and not part of the surrounding floodplain.

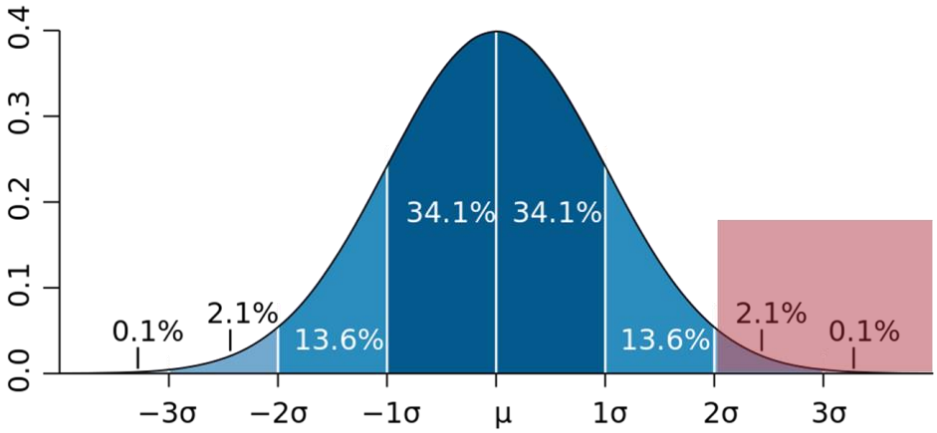

Figure 55: A Normal Distribution. Points within the control volume are assumed to follow a normal distribution, with the raised features falling outside positive 2σ from the mean, as shown by the red box.

Figures 56 and 58 show vertices with representative crown elevations determined through the 2σ averaging method and plotted with the same contour range as the LIDAR behind them. Similarly, Figures 57 and 59 show vertices with the representative crown elevations defined by the maximum value method. Figures 56 and 57 show a roadway that is higher than the surrounding topography. The applied crown elevations follow the trend of the raised feature in general for both methods. The maximum value method shows slightly higher elevations than the 2σ averaging method. Because the roadway has a generally consistent elevation, the slight difference in interpolation methods is expected, rather than more substantial differences.

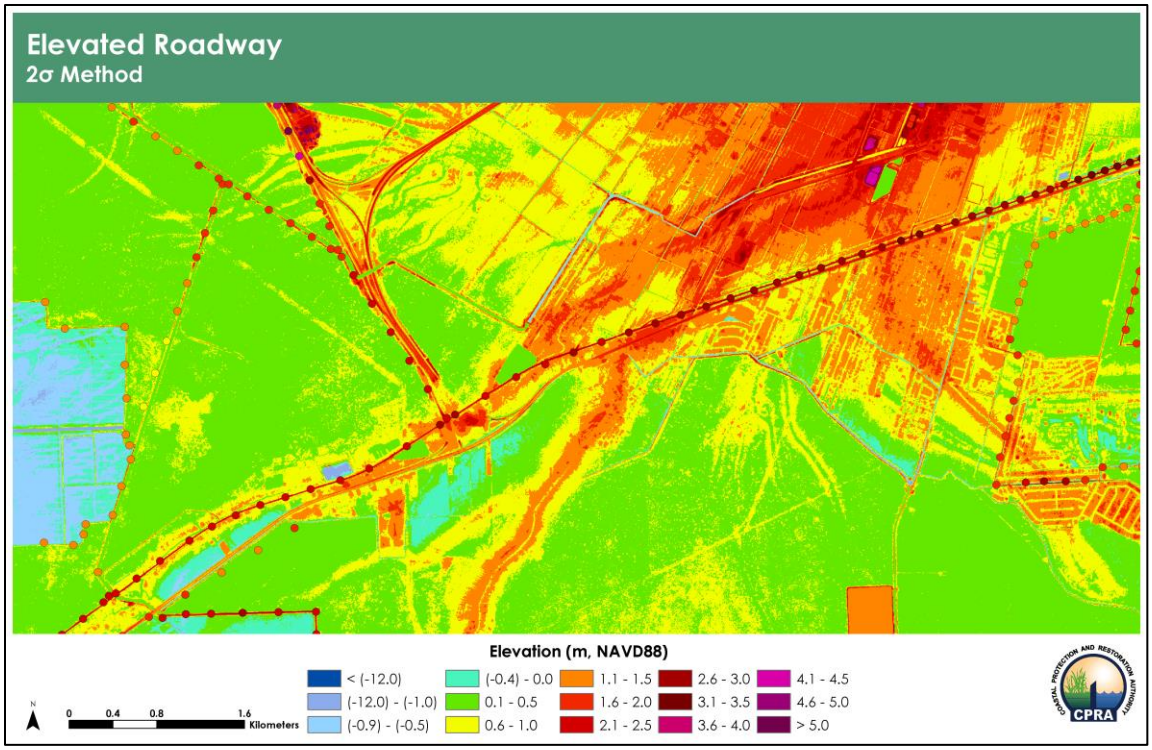

Figure 56: An Example of an Elevated Roadway. LIDAR data is shown as a background. Circles show the elevations prescribed by the 2σ averaging method.

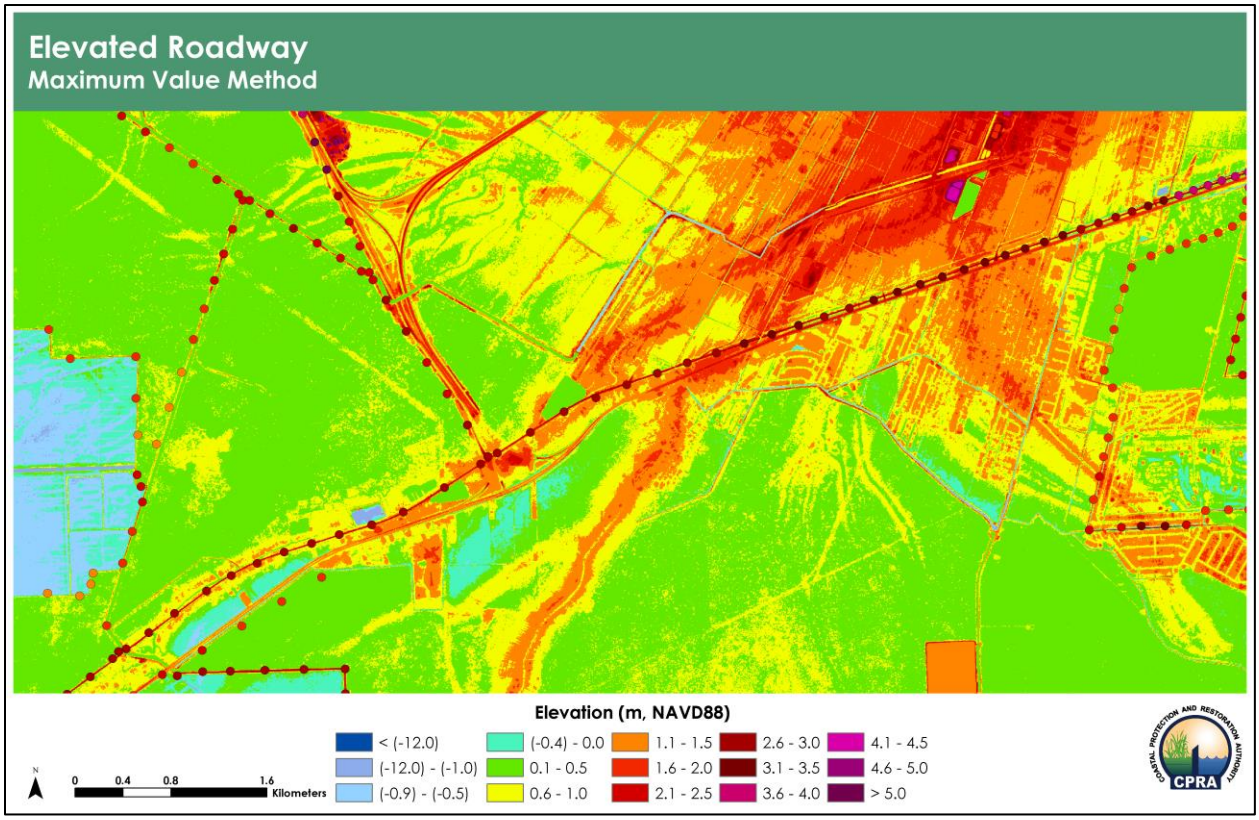

Figure 57: An Example of an Elevated Roadway. LIDAR data is shown as a background. Circles show the elevations prescribed by the maximum value method.

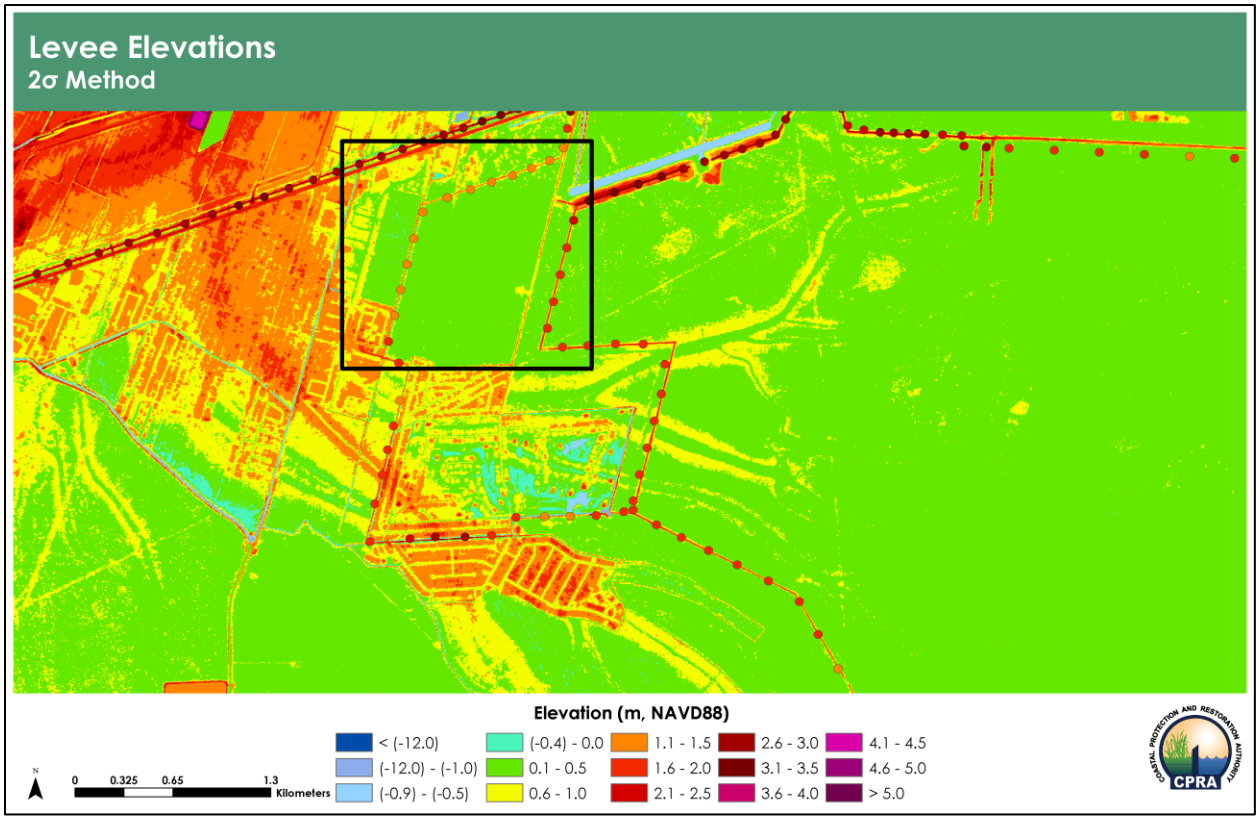

Figure 58: An Example of a Local Levee with Variable Elevation. LIDAR data is shown as a background. Circles show the elevations prescribed by the 2σ averaging method.

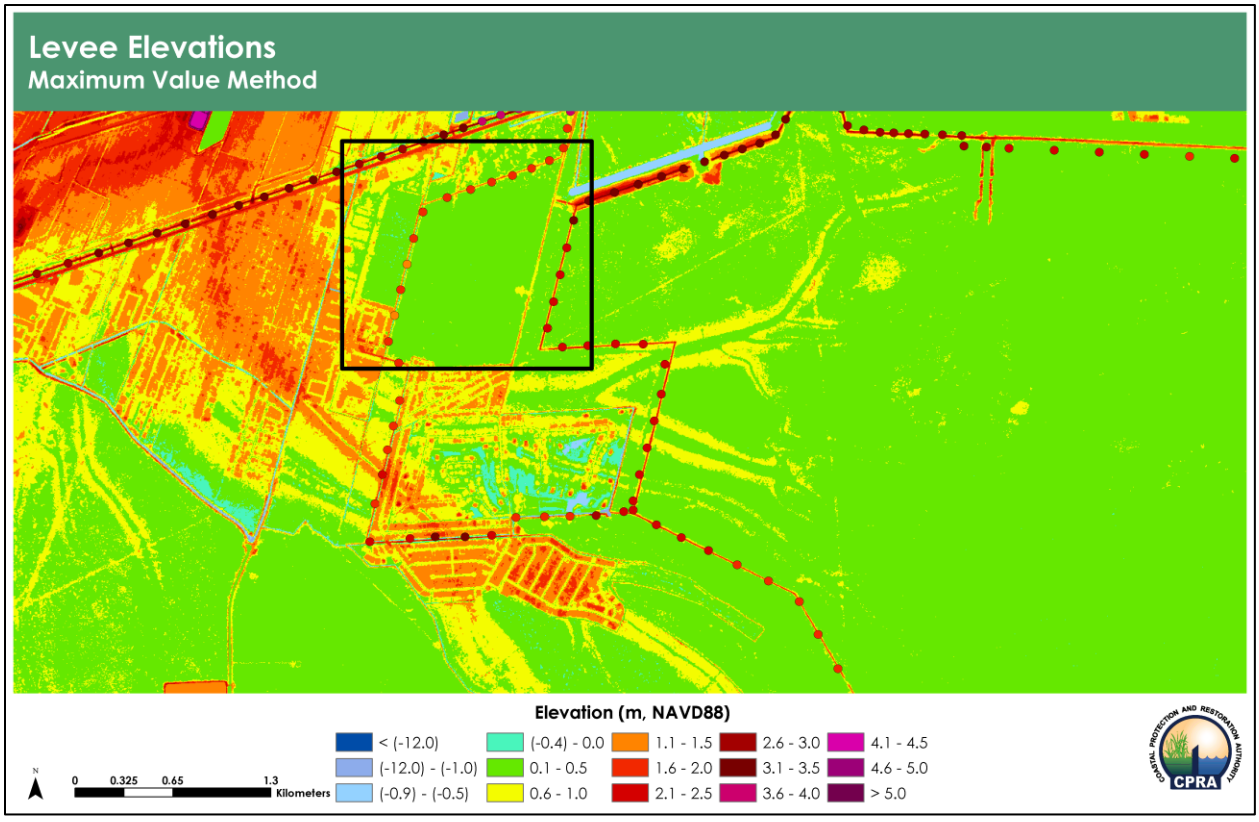

Figure 59: An Example of a Local Levee with Variable Elevation. LIDAR data is shown as a background. Circles show the elevations prescribed by the maximum value method.

Figures 58 and 59 highlight a local levee. The LIDAR data contains high variability in topography along the feature. In the outlined region specifically, variability in LIDAR results in higher crown elevations when the maximum value approach is applied, as highlighted by the different interpolated elevations shown in Figures 58 and 59. The colored vertices in Figure 58 show that these high adjacent ground elevations are being filtered from the data to provide more realistic elevations for the targeted feature while Figure 59 shows that the maximum value overstates the elevation of the feature.

Simulation Results

Figure 60 shows the difference when surge elevations computed for the averaging method is subtracted from maximum value method. As expected, the averaging method increases surge behind most raised features because these features are comparatively lower. Surge is higher on the unprotected side of many raised features when using the maximum value method because the water builds up against the higher features. This comparison shows the level of difference that can be created by different methods of selecting elevation values for raised features.

The 2σ averaging method, however, results in only minor differences when compared to the maximum value method. Figure 61 shows this comparison. This is due to the small portion of data in the LIDAR that could artificially raise the elevation of a raised feature when applying a maximum value method.

The results demonstrate that the averaging method greatly understates the protection of features while the 2σ averaging method generates surges very near the maximum value method that had been generally applied previously. For future mesh development, the 2σ averaging method is recommended because it will not overstate protection. However, the simulations have shown that the maximum value method is reasonable as well, but would be a slightly more conservative estimate of protection.

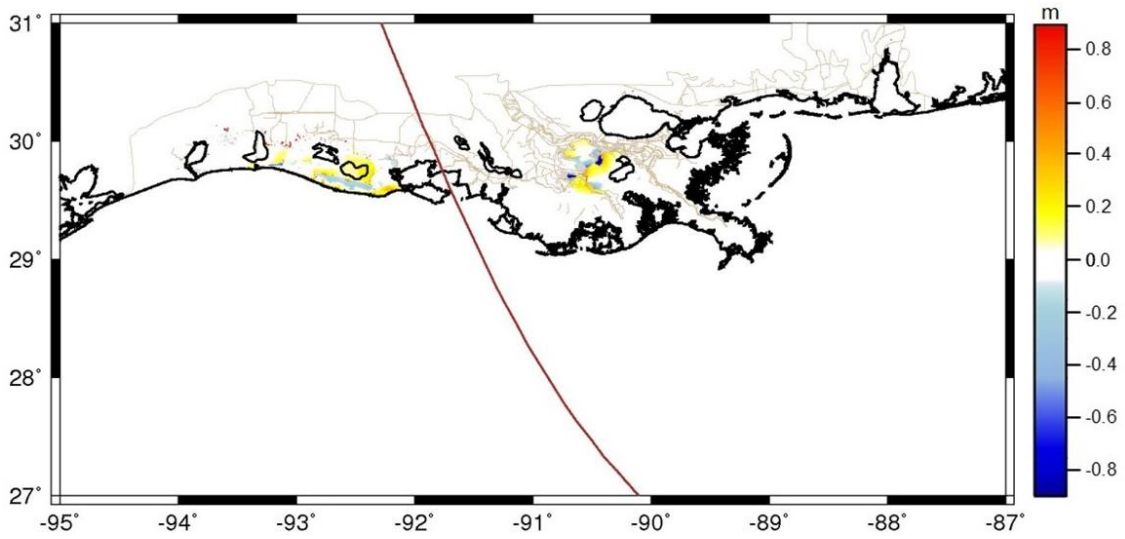

Figure 60: Difference in Maximum Surge Elevation for Maximum Value Method Minus Averaging Method. Positive values indicate maximum value method has a higher surge in the area.

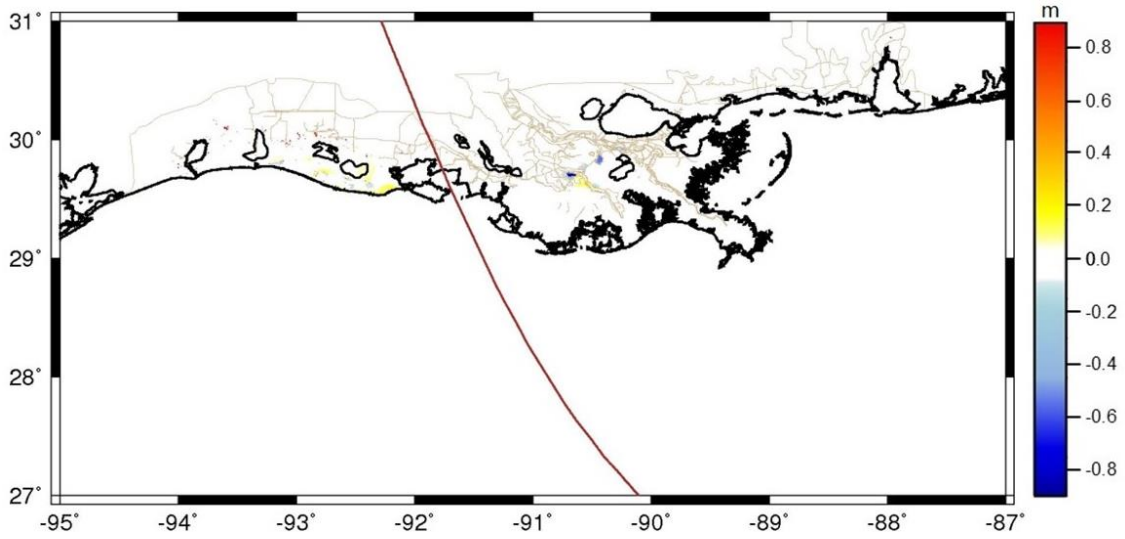

Figure 61: Difference in Maximum Surge Elevation for Maximum Value Method Minus 2σ Averaging Method. Positive values indicate maximum value method has a higher surge in the area.

References

Cobell, Z., H. Zhao, H.J. Roberts, F.R. Clark, and S. Zou. (2013). Surge and Wave Modeling for the Louisiana 2012 Coastal Master Plan. Journal of Coastal Research: Special Issue 67 – Louisiana's 2012 Coastal Master Plan Technical Analysis, pp. 88-108.

Coggin, D. (2008). LIDAR in Coastal Storm Surge Modeling: Modeling Linear Raised Features, Unpublished Masters Thesis, University of Central Florida, Orlando, Florida.

Louisiana State University (LSU) (2004). Louisiana LIDAR. http://atlas.lsu.edu/LIDAR/.

USACE (2008a). Louisiana Coastal Protection and Restoration Technical Report. Vicksburg, Mississippi: USACE, 98 pp.

USACE (2008b). Flood Insurance Study: Southeastern Parishes, Louisiana. Intermediate Submission 2: Offshore Water Levels and Waves. Vicksburg, Mississippi: USACE, 152 pp.

USACE (2008c). Flood Insurance Study: Southwestern Parishes, Louisiana. Intermediate Submission 2. Vicksburg, Mississippi: USACE, 697 pp.

Appendix 4: Sector-Based Wind Drag Analysis

Until recently, storm surge and wave simulations utilizing the ADCIRC model have applied a wind drag coefficient from Garratt (1977), as shown in Equation 1. Similarly, SWAN applied a nearly identical drag coefficient from Wu (1982), as shown in Equation 2.

$$C_d = \frac{1}{1000}\left(\frac{15}{20} + \frac{40}{600}U_{10}\right) \quad (1)$$

$$C_d = \frac{1}{1000}\left(\frac{16}{20} + \frac{39}{600}U_{10}\right) \quad (2)$$

However, Powell (2006) observed an azimuthal dependence of wind drag based upon dropsonde data. Later, Black et al. (2007) parameterized this dependence into storm sectors. This parameterization is shown in Figure 62.

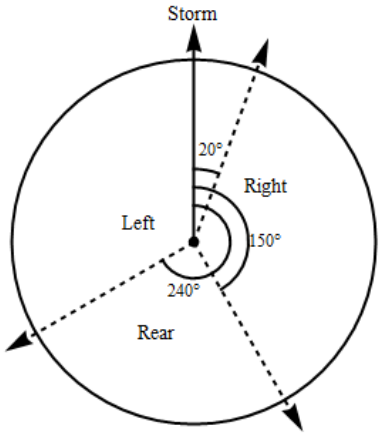

Figure 62: Parameterization of Storm Sectors.

This parameterization aims to recreate the dependence of wind drag upon not only the speed of the wind but also the mean direction of wave travel. For waves that are moving in the same direction as the wind, the drag will be lower than when the waves are moving in the opposite direction as the wind. Figure 63 shows the wind drag scheme applied. The behavior in the right and rear sectors is similar to medium and low speed winds where the maximum drag coefficient is set at 0.002 with the right sector receiving a boost for high speed winds to 0.003. For these storm sectors, the counterclockwise winds, direction of storm travel, and mean wave directions are approximately aligned. By contrast, the left sector sees significantly increased wind drag. On the left side of the storm, the winds and waves are aligned in opposite directions. In this sector, wind drag is allowed to increase to 0.0045.

This wind drag algorithm is available to ADCIRC+SWAN model versions 50 and greater.

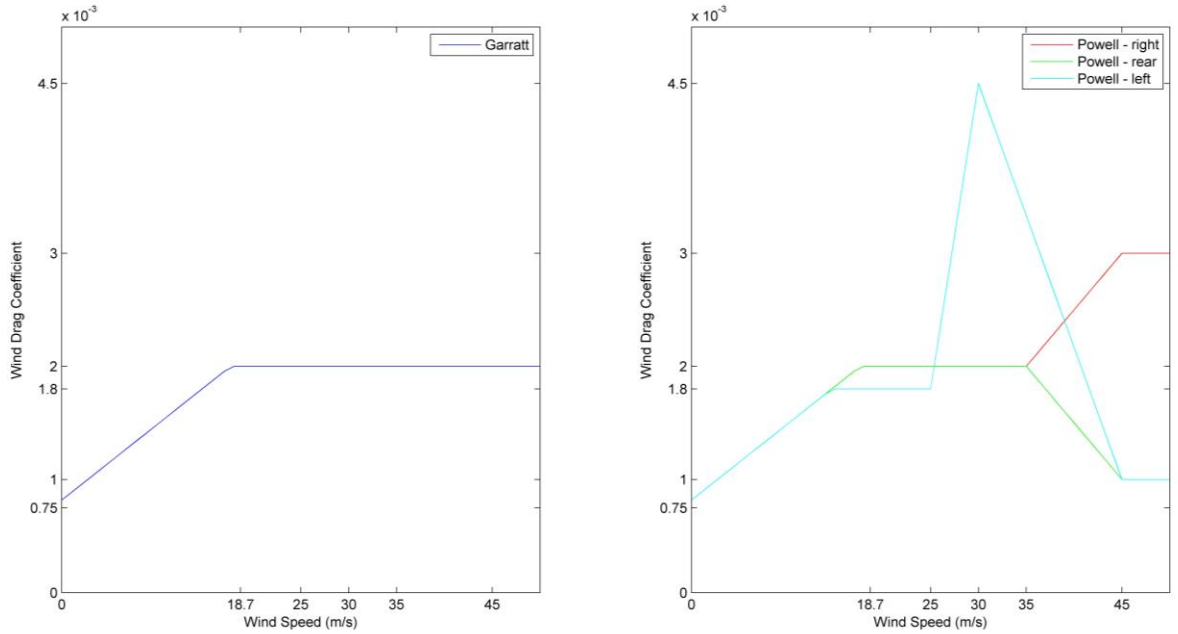

Figure 63: Garratt Wind Drag Parameterization (left) and Parameterization of Hurricane Wind Drag Based Upon Storm Sectors (right).

Before finalizing validations for Gustav (Dietrich et al., 2011) and Katrina, Rita, and Ike (Dietrich et al., 2012), Dietrich et al. implemented this new wind drag formulation into the ADCIRC model to optimize the validation of storm surge elevations and wave parameters. The Powell drag formulation, however, does create significant differences in storm surge response compared to the Garratt formulation. Figures 65 and 66 show the differences in storm surge elevations using the current conditions landscape created by simulating ADCIRC+SWAN considering the two wind drag formulations. For individual storms, the Powell wind drag formulation produces results that differ from both the 2012 Coastal Master Plan analysis and many other previous analyses, including the FEMA studies from 2008. However, based on model validation, described in Appendix 1, and to embrace the state of the science, the Powell sector based wind drag formulation is recommended for implementation in the 2017 Coastal Master Plan.

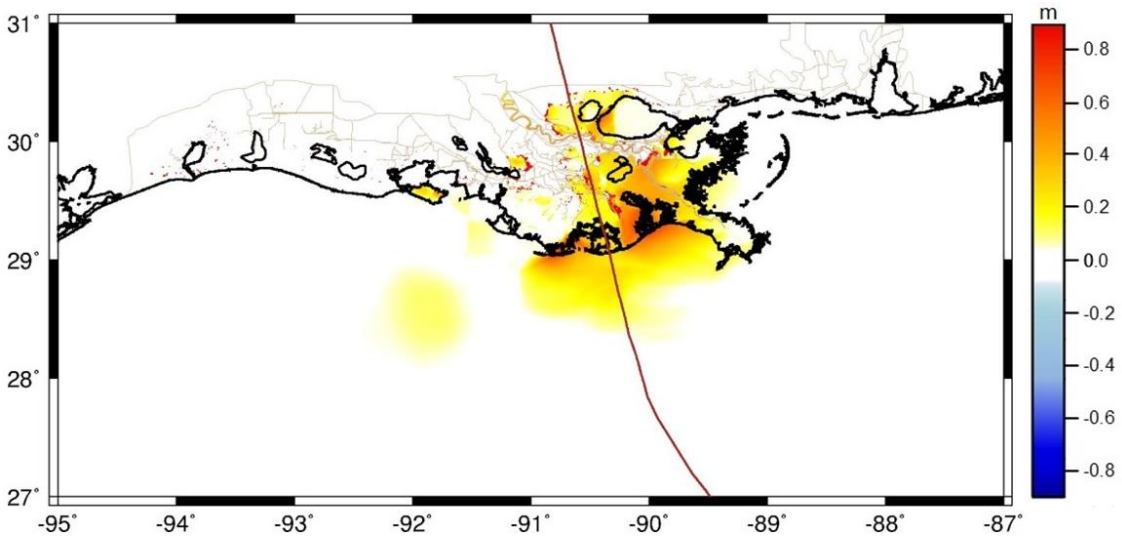

Figure 64: Surge Elevation Change for Storm 18 with Powell Wind Drag. Warm colors indicate greater surge when Powell wind drag is active.

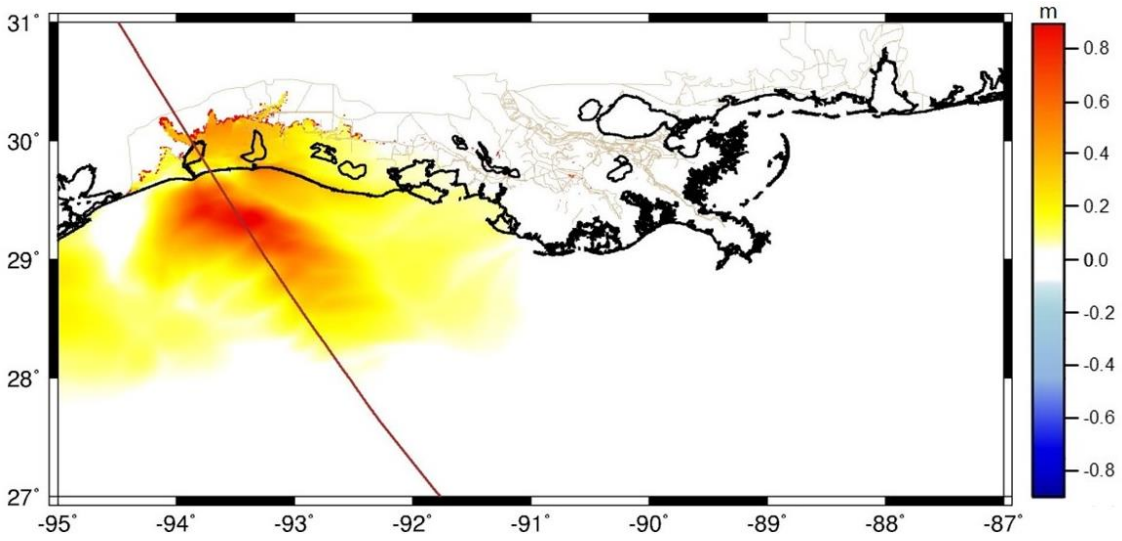

Figure 65: Surge Elevation Change for Storm 218 with Powell Wind Drag. Warm colors indicate greater surge when Powell wind drag is active.

References

Black, P.G., E.A. D'Asaro, W.M. Drennan, J.R. French, P.P. Niiler, T.B. Sanford, E.J. Terrill, E.J. Walsh, and J.A. Zhang. (2007). Air-Sea Exchange in Hurricanes: Synthesis of Observations from the Coupled Boundary Layer Air-Sea Transfer Experiment. Bulletin of the American Meteorological Society, Volume, 88, Issue 3, pp. 357-374.

Dietrich, J.C., J.J. Westerink, A.B. Kennedy, J.M. Smith, R. Jensen, M. Zijlema, L.H. Holthuijsen, C.N. Dawson, R.A. Luettich, Jr., M.D. Powell, V.J. Cardone, A.T. Cox, G.W. Stone, H. Pourtaheri, M.E. Hope, S. Tanaka, L.G. Westerink, H.J. Westerink, and Z. Cobell. (2011). Hurricane Gustav Waves and Storm Surge: Hindcast, Synoptic Analysis and Validation in Southern Louisiana. Monthly Weather Review, Volume 139, pp. 2488-2522, DOI 10.1175/2011MWR3611.1.

Dietrich, J.C., S. Tanaka, J.J. Westerink, C.N. Dawson, R.A. Luettich, Jr., M. Zijlema, L.H. Holthuijsen, J.M. Smith, L.G. Westerink, and H.J. Westerink. (2012). Performance of the Unstructured-Mesh, SWAN+ADCIRC Model in Computing Hurricane Waves and Surge. Journal of Scientific Computing, Volume 52, Issue 2, pp. 468-497.

Garratt, J.R. (1977). Review of Drag Coefficients over Oceans and Continents. Monthly Weather Review, Volume 105, pp. 915-929.

Powell, M.D. (2006). Final Report to the National Oceanic and Atmospheric Administration (NOAA) Joint Hurricane Testbed (JHT) Program. 26 pp.

Wu, J. (1982). Wind-Stress Coefficients over Sea Surface from Breeze to Hurricane. Journal of Geophysical Research, Volume 87, Issue C12, pp. 9704-9706.

Appendix 5: Asymmetric Hurricane Literature Review

At the 2013 ADCIRC model users meeting, Dr. Rick Luettich presented work that he has been pursuing related to asymmetric parametric hurricane wind models used in real time forecasting applications. The surge and waves team felt it would be important to understand how this related to statistical applications and better understand the treatment of asymmetry in the Planetary Boundary Layer (PBL) model used during the 2008 FEMA study in Louisiana and 2012 Coastal Master Plan.

Storm asymmetry plays an important part in determining how storm surge and waves will affect an area. Figure 66 shows Hurricane Isabel, which has a high level of symmetry, and Hurricane Bob, which has a high level of asymmetry. Storms with high asymmetry have greater distance to wind isotachs on one side of the storm than the other. This storm asymmetry is largely linked to the distortion that occurs due to greater translation speed (Tang & Liu, 2009). Figure 67 shows wind composites generated from data collected between 2000 and 2007 in the Northern Hemisphere. This data is normalized to the storm direction. The tangential component shows that, when storms have a greater translation speed, a left-right asymmetry is induced. The authors conclude that this asymmetry is an important component of hurricane weakening because it acts like a natural speed brake.

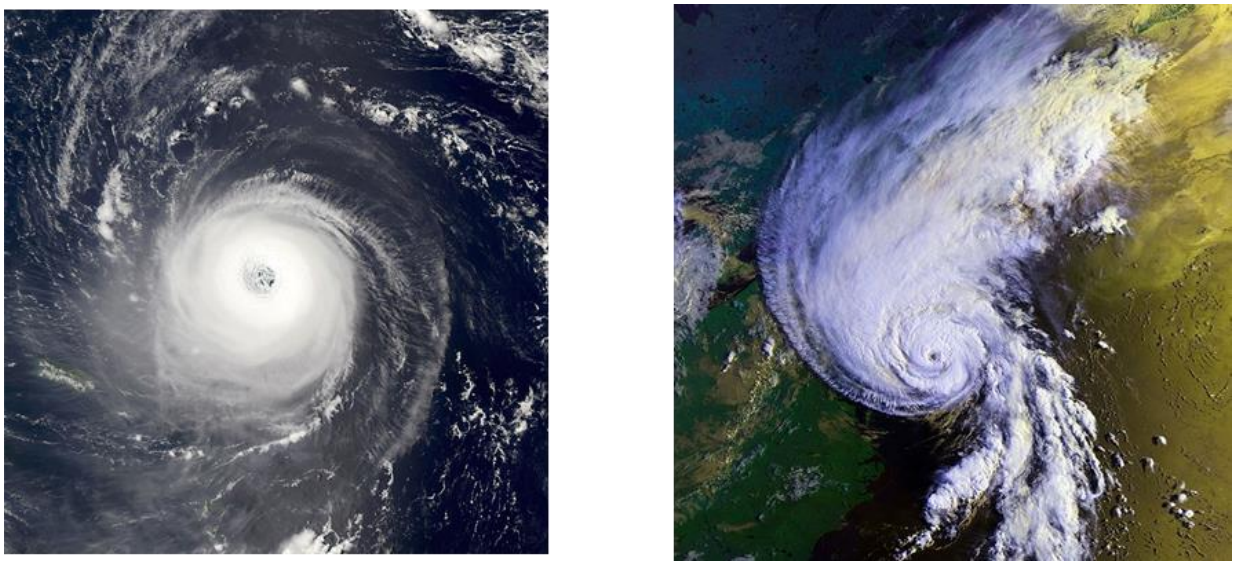

Figure 66: Hurricane Isabel (left), which is Symmetric, and Hurricane Bob (right), which is Highly Asymmetric.

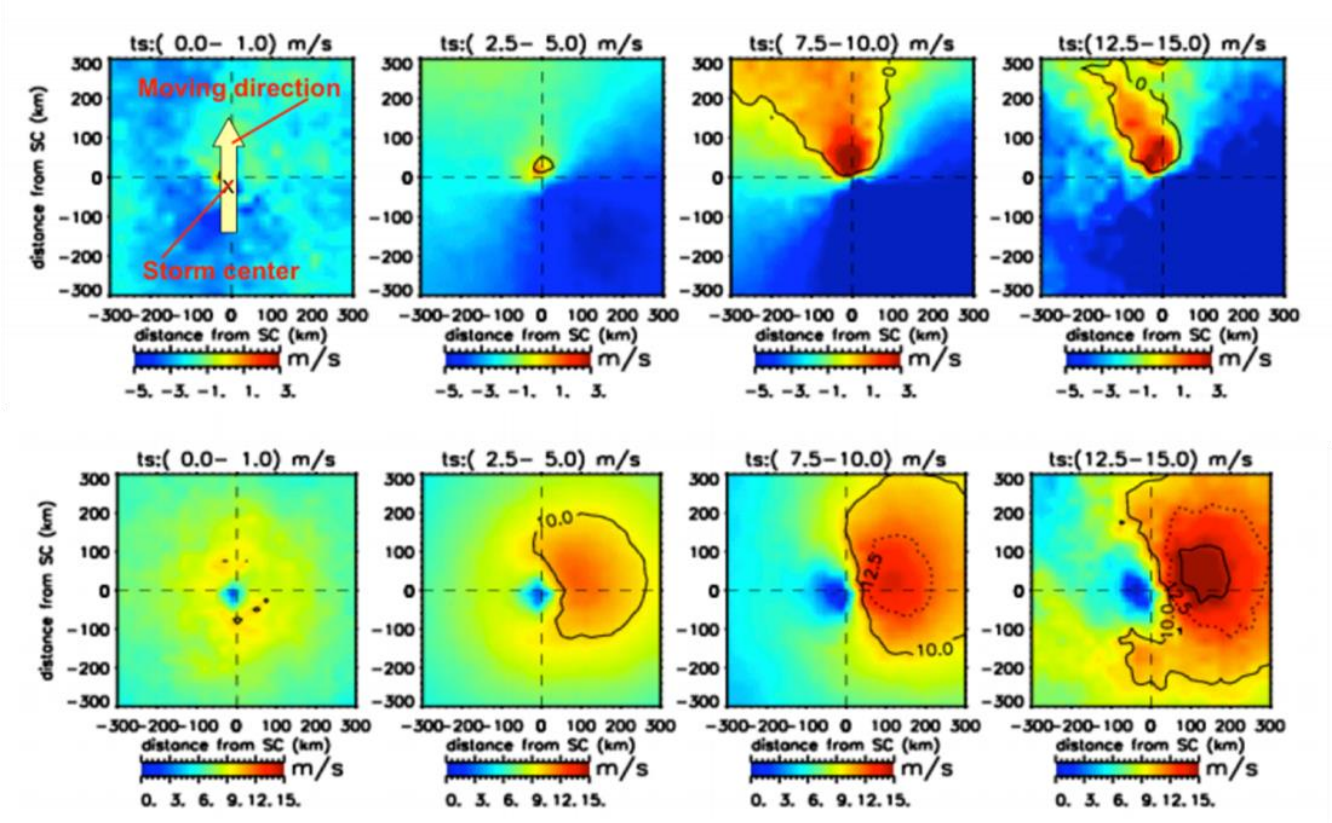

Figure 67: Radial (top) and Tangential (bottom) Wind Composites for Varying Storm Translation Speeds in the Northern Hemisphere between 2000 and 2007 (Tang & Liu 2009).

Hurricane asymmetry has important implications to a hurricane storm surge model. The surge model used in the master plan suite of simulations is primarily driven by wind and pressure forcing. Therefore, it is important to select storms that represent the diversity of storms that can occur. For instance, a fast-moving, symmetric storm, even with identical maximum wind speeds as a slow moving, asymmetric storm, might inundate an area to a significantly lower level. The slow-moving storm will give water much more time to move through narrow channels and ultimately inundate the broader floodplain to a greater elevation, which may be accentuated in some instances due to the asymmetry.

Upon review, the PBL model takes into account some of these asymmetries. Figure 68 shows two storms on identical tracks within the full storm suite discussed in Appendix 2. The storm on the top is moving significantly slower than the storm on the bottom. Notice the difference in structure. The storm on the top is a near perfect set of concentric rings while the storm on the bottom is asymmetric.

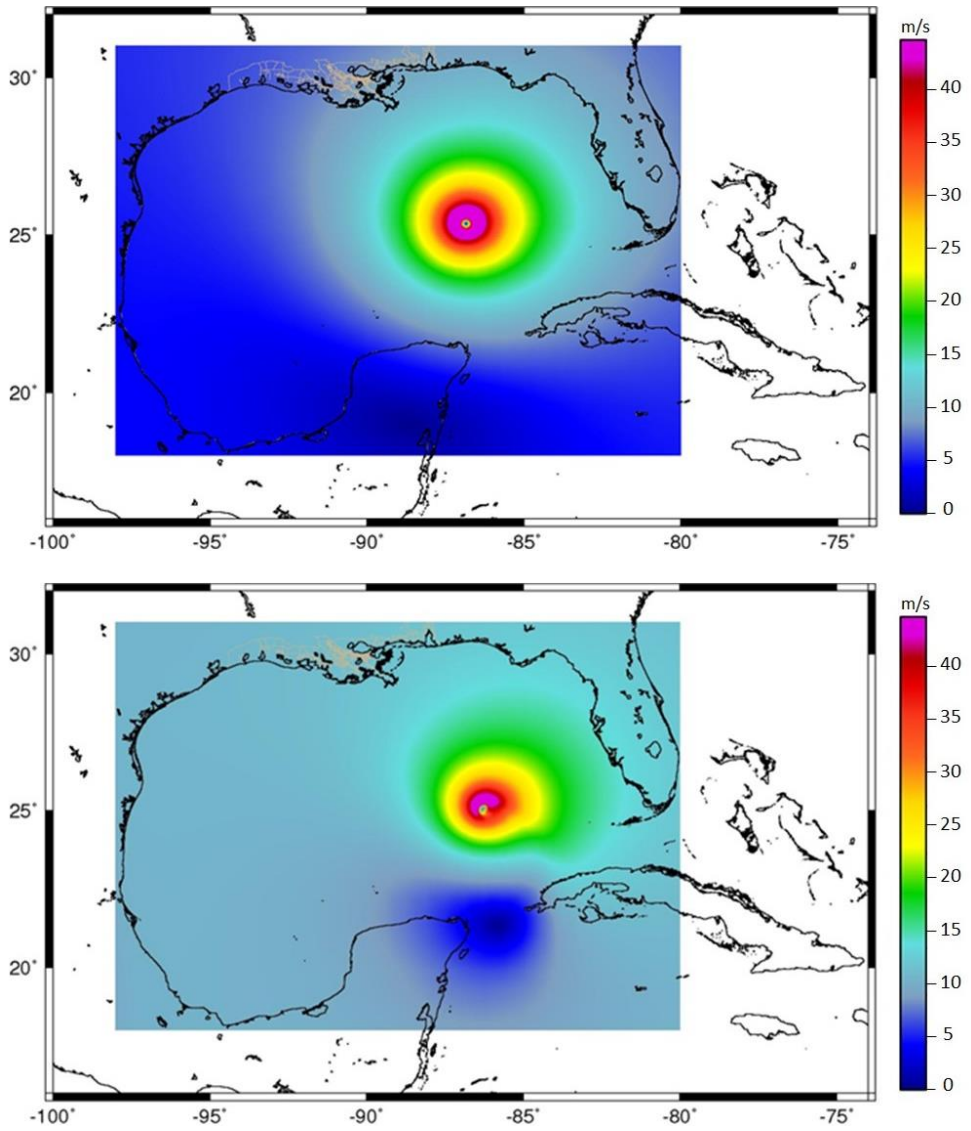

Figure 68: Hurricane Wind Symmetry (top) and Asymmetry (bottom) in the PBL Model.

At the onset of this task, the team assumed that all storms in the suite from the 2008 FEMA study were symmetric. The intention was to better understand the impacts of storm asymmetry to make a recommendation whether CPRA should consider regenerating wind fields with an updated wind model that better incorporates asymmetry patterns into the storm suite. However, upon evaluating the existing storm suite more closely, it has been determined that some faster moving storms already include asymmetry.

Rather than evaluating the topic of asymmetry further, it is recommended that storms with varying forward speed, and thus greater degrees of asymmetry, are incorporated into the final selected suite of storms used in the 2017 Coastal Master Plan.

References

Tang, W., and W.T. Liu. (2009). Dependence of Hurricane Asymmetry and Intensification on Translation Speed Revealed by a Decade of QuikSCAT Measurements. NASA Ocean Vector Wind Science Team Meeting, Boulder, Colorado.

Appendix 6: Initial Water Levels for Surge and Waves Simulations in the 2017 Coastal Master Plan

As part of updates to the ADCIRC model for the 2017 Coastal Master Plan, new topographic, bathymetric, and levee elevation information has been applied to the model. These data have been provided in the North American Vertical Datum of 1988 (NAVD88) 2009.55 datum. Previous ADCIRC studies have used the NAVD88 2004.65 datum and have developed model initial conditions accordingly. In July 2014, USACE examined the differences between these datums in an effort to update their ADCIRC models. The report states:

> 0.05 m was subtracted from the previous water surface elevation of 0.37 m (all other considerations, including steric adjustment, uncertainty, rounding, etc. were again left unchanged), yielding a starting water surface elevation of +0.32 m NAVD88 2009.55.

An identical adjustment has been made for the 2017 Coastal Master Plan modeling efforts. The initial water level for production simulations will be set to +0.31 meter, which will be incrementally raised due to sea level rise for future conditions scenarios. Validation simulations will use an initial water level representative of the period in which each storm occurred to adjust for the seasonal oscillations in mean sea level.

References

Agnew, Maxwell E., Joshua T. Hardy, Whitney J. Hickerson, Julie Z. LeBlanc, P.E., and William C. Veatch. 2014. Sensitivity Analysis on Storm Surge Modeling Results for the Lake Pontchartrain and Vicinity (LPV), West Bank and Vicinity (WBV) and New Orleans to Venice (NOV)/Non-Federal Levee (NFL) Incorporation into NOV Hurricane Storm Damage and Risk Reduction (HSDRRS) Projects due to the Vertical Datum Update from NAVD88 (2004.65) to NAVD88 (2009.55). Mark W. Huber, C.H. (AGC), Richard A. Luettich, Jr., ScD (UNC), Nancy J. Powell, P.E., D.WRE (ARCADIS), Hugh J. Roberts, P.E. (ARCADIS), Jane McKee Smith, Ph.D., P.E. (ERDC-CHL), and Ty Wamsley, Ph.D. (ERDC-CHL), eds. U.S. Army Corps of Engineers. July.

Appendix 7: River Stages for Production Simulations in the 2017 Coastal Master Plan

As part of the model improvement plan implementation, Mississippi and Atchafalaya River flows used in the 2012 Coastal Master Plan modeling have been reviewed and lessons learned from other modeling efforts have been examined. The 2012 Coastal Master Plan model setup used river flows consistent with those in the FEMA study completed in 2007 (USACE, 2008a, b). FEMA selected river flows similar to flows that occurred during Hurricanes Katrina and Rita.

Work by the New Orleans District USACE for the Hurricane and Storm Damage Risk Reduction System (HSDRRS) levee design and accreditation showed that river flow has a substantial effect on surge propagation in the Mississippi River. Higher river flows can result in higher river stages during a tropical event; the extent of the effect is dependent on the storm track in relation to the river levees. To incorporate the effect of river flow on surge response in determination of the 1% annual exceedance water level along the Mississippi River, USACE modified the ADCIRC model grid, recalibrated the model, revised the Joint Probability Method Optimal Sampling (JPM-OS) to incorporate river flow as an independent variable and modeled multiple storm sets, with different river flows, to develop input for the revised JPM-OS.

Modification of JPM-OS and modeling multiple storm sets are beyond the scope of the 2017 Coastal Master Plan modeling effort. If one flow per river is used to represent river conditions, the flow should be characteristic of flow conditions when tropical events occur. Considering daily river flow records during hurricane season for the period 1976 through 2014 and the USACE analysis, it is apparent that flows used in the FEMA study, and hence the 2012 Coastal Master Plan, are low and need to be revised.

To ensure that the peak surge in the river is effectively captured in the modeling, it is recommended that the median river flows, 9,175 m^3/s for the Mississippi River and 3,936 m^3/s for the Atchafalaya River, be used for the 2017 Coastal Master Plan modeling. These flows represent a more realistic representation of river flow throughout hurricane season, allowing the 2017 Coastal Master Plan modeling effort to better capture surge response in the river.

Attached is a summary of the New Orleans District analysis and documentation of the determination of the recommended flows.

References

USACE. 2008a. "Flood Insurance Study: Southeastern Parishes, Louisiana - Intermediate Submission 2." New Orleans District, Mississippi Valley Division. July

USACE. 2008b. "Flood Insurance Study: Southwestern Parishes, Louisiana - Intermediate Submission 2." New Orleans District, Mississippi Valley Division. October

Attachment: New Orleans District U.S. Amy Corps of Engineers River Flow Analysis

During the HSDRRS design process, the New Orleans District USACE reviewed the ADCIRC modeling used in the HSDRRS levee design to assess the 1% annual exceedance water levels in the Mississippi River to determine if the Mississippi River levees within the HSDRRS area could be accredited. The review revealed that all storms had a constant low discharge, water levels in the Mississippi River were not calibrated or validated, and the JPM-OS analysis did not consider discharge variation throughout the hurricane season. Thus, it was apparent that additional work was required to establish 1% annual exceedance design elevations for the Mississippi River levees within the HSDRRS area and identify possible deficiencies. The work included compilation and evaluation of historical tropical events and associated water levels along the Mississippi River, modification of the ADCIRC model grid to add resolution in the Mississippi River and Head of Passes area, calibration of the ADCIRC model for different river flows, re-running the ADCIRC model with a set of synthetic storms and multiple river flows, and revision of the JPM-OS to incorporate river flow as an independent variable in the computation of 1% exceedance water levels in the Mississippi River.

The Effect of Mississippi River Flow on Surge

Figures 70 and 71 show peak water levels in the Mississippi River for historical tropical events, supplemented by water surface profiles created using ADCIRC model output for similar events. The storms shown on these figures occurred with different river flows ranging from 5,012 to 26,900 m^3/s.

For tracks that pass the Mississippi River Bird's Foot Delta to the east, surge can enter the river downstream of the New Orleans to Venice Reach C levee system. Surge levels peak downstream of the New Orleans area but also push water upstream. When the New Orleans to Venice levees are overtopped, as occurred during Hurricane Katrina, surge can enter the river in more locations, affecting the water surface profile. For tracks that pass to the west of the Bird's Foot Delta, the water surface profile is smoother, likely because of the predominant wind direction.

Figures 70 and 71 demonstrate that river flow has an effect on surge propagation in the Mississippi River. The extent of the effect is dependent on the location of the storm in proximity to the river levees and the magnitude of the flow.

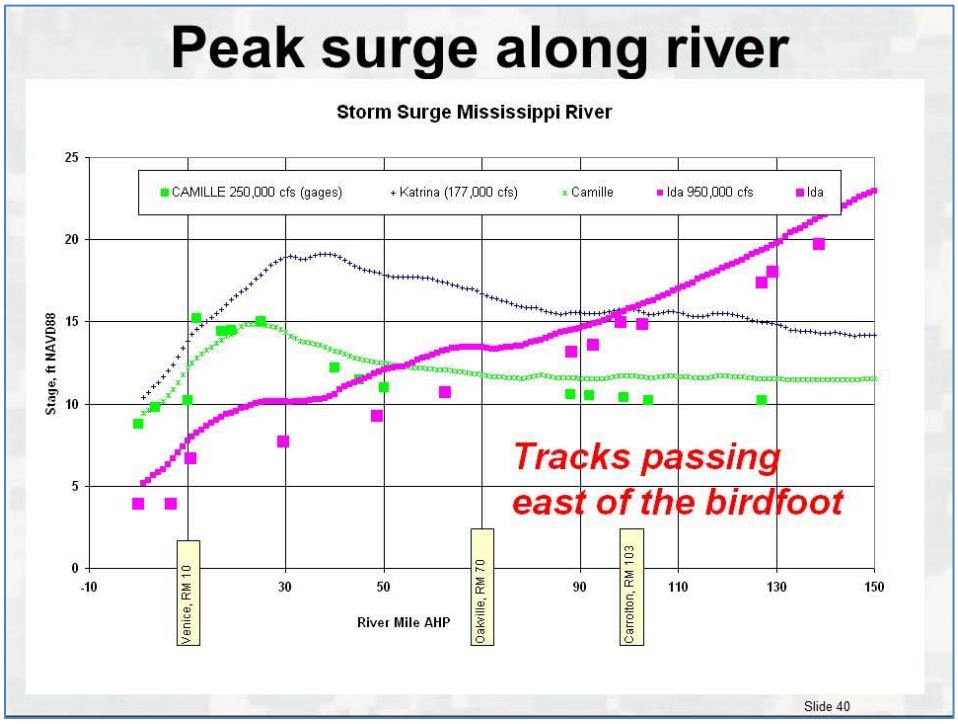

Figure 69: Mississippi River Water Surface Profiles for Tropical Events Passing to the East of the Bird's Foot Delta.

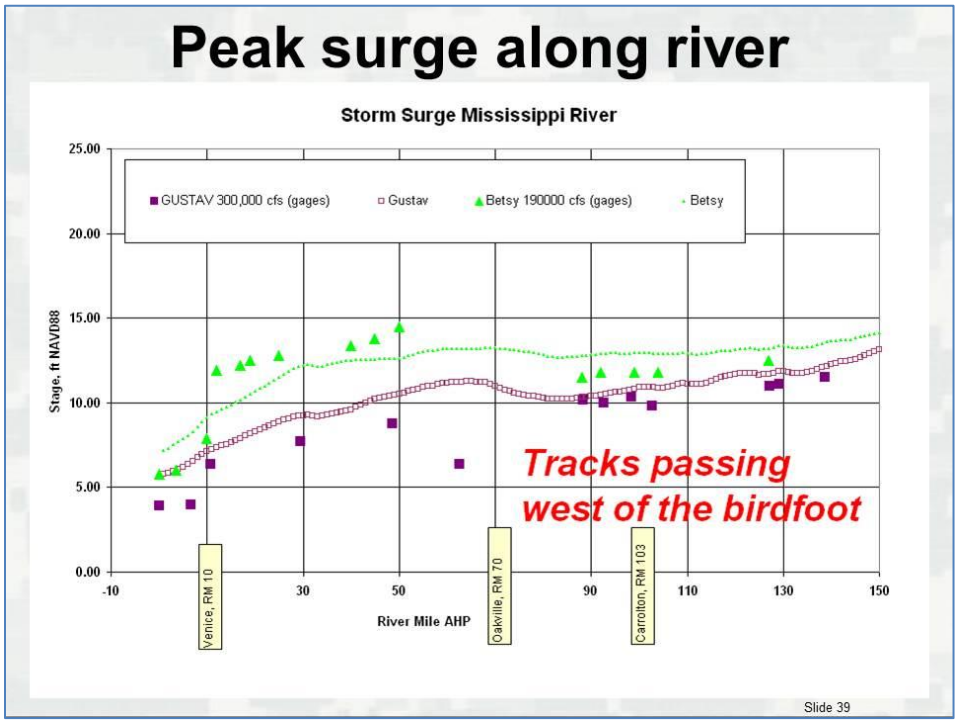

Figure 70: Mississippi River Water Surface Profiles for Tropical Events Passing to the West of the Bird's Foot Delta.

Table 4 shows peak stages for the Mississippi River at the Carrollton gage for several tropical events, demonstrating the effect of flow and surge on peak stages.

Table 4: Mississippi River at Carrollton Stages for Different Tropical Events.

Tropical Event	Mississippi River Flow (m^3/s)	Stage Prior to Event (m, Gage)	Peak Stage (m, Gage)
Hurricane Betsy, 1965	5,380	0.61	3.66
Hurricane Camille, 1969	7,079	0.91	3.05
Hurricane Katrina, 2005	5,012	0.61	4.57
Hurricane Gustav, 2008	8,495	0.91	3.05
Hurricane Ida, 2009	26,901	3.66	4.57

The original FEMA ADCIRC modeling, also used for the Louisiana Coastal Protection and Restoration Program and HSDRRS, used Mississippi River and Atchafalaya River flows that occurred at the time of Hurricanes Katrina and Rita. The modeled flow in the Mississippi River, 4,729 m^3/s, was lower than the flow in the river for other major hurricanes such as Hurricanes Camille, Gustav, and Betsy. The modeled flow was also significantly lower than the average and median flows in the Mississippi River for hurricane season, June through November. Figure 71 shows flow variation for the Mississippi River at the time of the USACE river analysis.

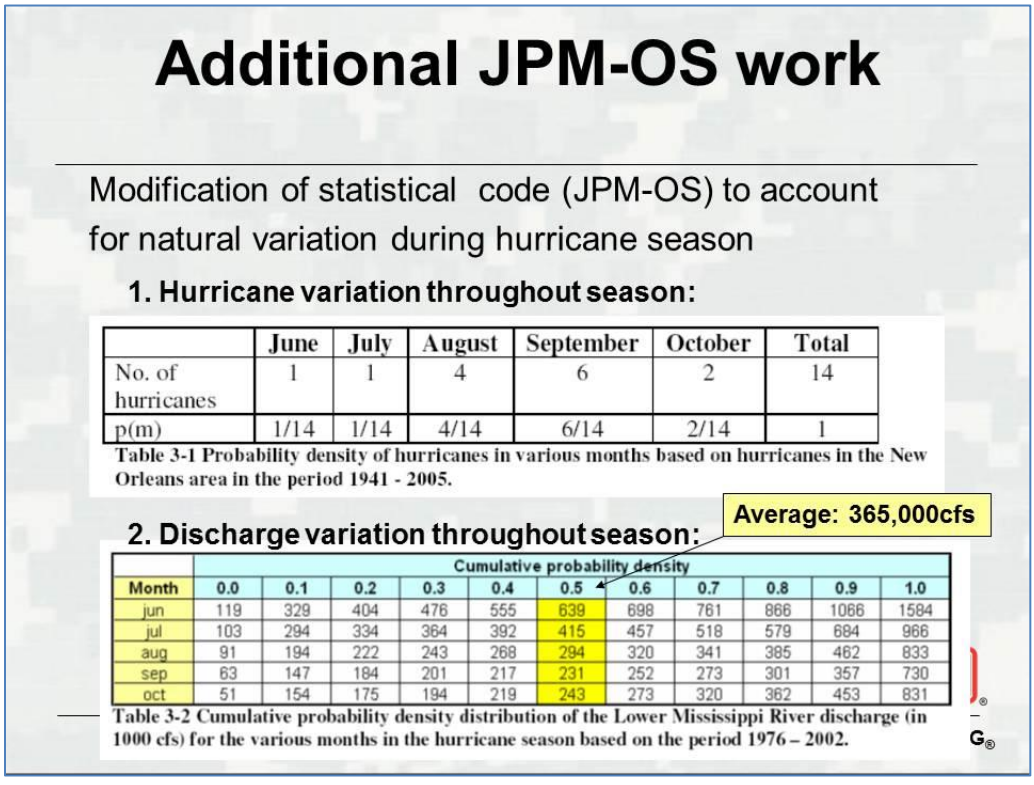

	June	July	August	September	October	Total
No. of hurricanes	1	1	4	6	2	14
p(m)	1/14	1/14	4/14	6/14	2/14	1

Table 3-1 Probability density of hurricanes in various months based on hurricanes in the New Orleans area in the period 1941 - 2005.

	Cumulative probability density										
Month	0.0	0.1	0.2	0.3	0.4	0.5	0.6	0.7	0.8	0.9	1.0
jun	119	329	404	476	555	639	698	761	866	1066	1584
jul	103	294	334	364	392	415	457	518	579	684	966
aug	91	194	222	243	268	294	320	341	385	462	833
sep	63	147	184	201	217	231	252	273	301	357	730
oct	51	154	175	194	219	243	273	320	362	453	831

Table 3-2 Cumulative probability density distribution of the Lower Mississippi River discharge (in 1000 cfs) for the various months in the hurricane season based on the period 1976 – 2002.

Figure 71: Hurricane Variation and Mississippi River Flow Variation.

In determining the 1% annual exceedance water level in the Mississippi River, river flow can be considered to be independent of hurricane activity. Figure 72 shows this independence.

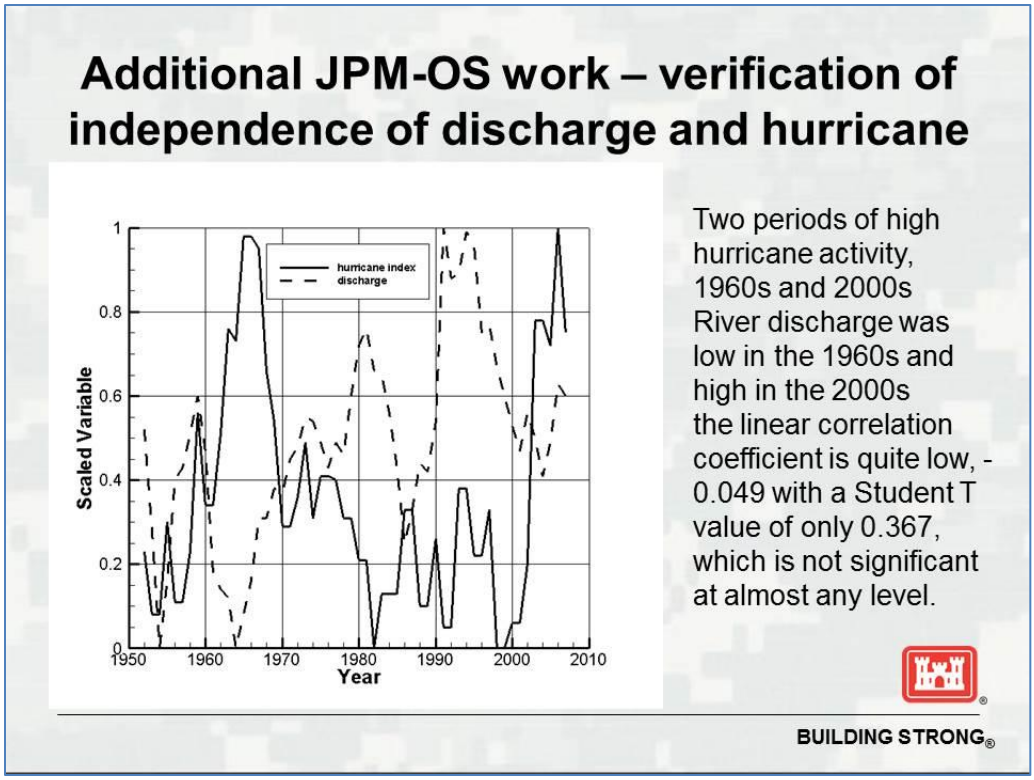

Figure 72: Verification of Independence of Mississippi River Flow and Hurricane Occurrence.

It was apparent that additional modeling and improvements to the JPM-OS code were needed to appropriately define the 1% annual exceedance water surface elevation for the Mississippi River for the HSDRRS effort. USACE improved the resolution of the grid of the lower Mississippi River, calibrated the model to several river flows, and ran several storms with three different river flows: 4,729 m^3/s, 18,916 m^3/s, and 33,102 m^3/s.

The JPM-OS code was revised to add flow as an independent variable to the probability functions, as shown on Figure 73. Assumptions made in the JPM-OS analysis are listed below.

- Hurricane strength is uncorrelated with river discharge.
- Hurricane activity and river discharge are independent phenomena.
- Three probability density functions need to be known to compute the probability of the surge level if the river discharge can vary.
  - The probability density of the surge level given a certain discharge (from ADCIRC model runs).
  - The hurricane probability density for each hurricane month (from NOAA data).
  - The discharge probability density for each hurricane month (from river data).

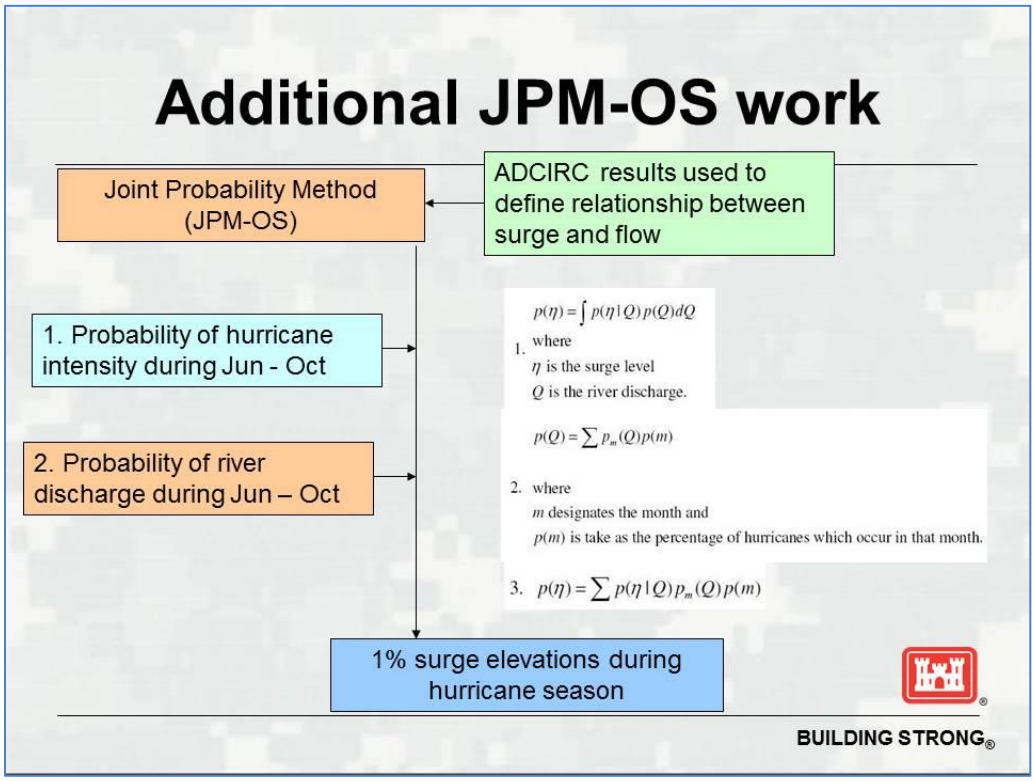

Figure 73: Revisions to JPM-OS.

Figure 74 shows an example of the water surface profiles for one storm, storm 124, with different river discharges, again demonstrating that flow has an effect on surge propagation and peak water levels in the river. Ultimately, USACE ran the ADCIRC model with two different river flows, 4,729 m^3/s and 11,327 m^3/s, and utilized the revised JPM-OS code to develop 1% annual exceedance water surface elevations in the river for HSDRRS design and accreditation.

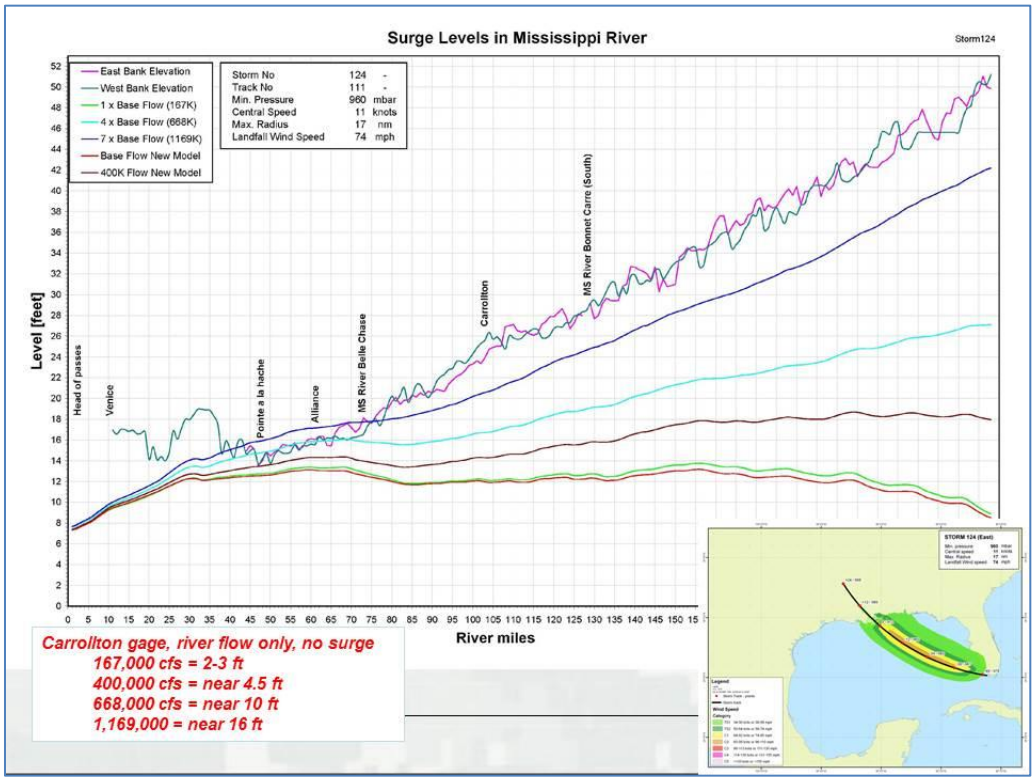

Figure 74: Peak Stages in the Mississippi River for Storm 124.

Note: For the accreditation investigation of the Atchafalaya Basin Floodway levees, a similar analysis was initiated, running storms with multiple river flows and revising JPM-OS to account for river flow as a variable. As of the date of this memorandum, the analysis is incomplete.

River Flow Analysis and Recommendation

Daily computed flow data for the Mississippi River and Atchafalaya River can be found on the USACE Rivergages.com web page. The daily flow data for the USACE stations Mississippi River at Tarbert Landing and Atchafalaya River at Simmesport for the period of record 1976 through 2014 were acquired from the web page. The year 1976 is the year that USACE began to allocate flow at the Old River Control Complex to 70% Mississippi and 30% Atchafalaya on a daily basis. Although flows have been computed at these locations on a daily basis since 1930, statistics based on the record from 1976 to date are more reflective of current USACE water control practices.

Table 5 shows the average and median flows for the Mississippi River and Atchafalaya River for the period of record 1976 through 2014 for the months June through November and the months August through October, which are considered the peak of hurricane season. Note the difference between the average flow rates and the median flow rates.

Table 5: Average and Median Flow Rates, Mississippi and Atchafalaya Rivers.

Period of Record 1976 through 2014		Mississippi River at Tarbert Landing Flow (m^3/s)	Atchafalaya River at Simmesport Flow (m^3/s)
June through November	Average Flow	10,987	4,672
	Median Flow	9,175	3,936
August through October	Average Flow	8,325	3,511
	Median Flow	7,532	3,200

Consideration should be given to using the median flow rates for June through November in the ADCIRC modeling as representative of flow throughout the hurricane season. The revised JPM-OS utilizes a probability density function for flow. Using the median flow rate is more consistent with the revised JPM-OS methodology than if the average flow rate is used.

References

USACE. 2011. Presentation to St Bernard Parish Officials.

USACE. 2011. Presentation at USACE Infrastructure Conference. Atlanta, Georgia.

USACE. 2012. Presentation to General Peabody of MVD.

Appendix 8: Interpolation of Land Use Data for the 2017 Coastal Master Plan

Land use data are critical for determining frictional parameters for use within the ADCIRC model. Manning's *n* bottom roughness and a direction-specific reduction factor applied to the wind vectors are both derived from land use data.

Two datasets were distributed for the initial landscape condition. First, a 15 meter resolution land use dataset containing 67 land use classes generated by the USGS (shown in Figures 75 and 76) and a 500 meter resolution containing seven land use classes generated by the Integrated Compartment Model (ICM) model (shown on Figure 77).

Two issues, described below, prevent the ADCIRC model from using the ICM land classification data directly. First, on Figure 77, the pink area shows the "Upland/Developed/Not Modeled" category, or areas that will not be updated by the ICM model. These are areas that the surge and waves model does consider and will need to have values derived from an alternate data source. Second, the 500 meter resolution of the land use data provided by the ICM model is significantly greater than the ADCIRC model, which resolves features as small as 30 meters.

To solve these issues, a hybrid approach will be applied. First, the 15 meter land use data will be interpolated to the ADCIRC mesh and validated. Then, the 500 meter land use data will be applied to the same ADCIRC mesh. This secondary interpolation will serve as a basis for future runs. When a future scenario is set up, the same interpolation method of the 500 meter data will be completed on the future data. Next, the initial conditions ADCIRC Manning's *n* bottom roughness and direction-specific reduction factors based on the 500 meter land use data and the future conditions ADCIRC Manning's *n* bottom roughness and direction-specific reduction factors based on the 500 meter land use data will be subtracted from each other. This will generate the difference between the two scenarios. This difference can then be applied to the initial conditions ADCIRC model frictional parameters derived from the 15 meter dataset to reflect future conditions. Finally, the values in the new mesh will be checked for values outside a reasonable range. For instance, if a difference was shown inside a channel that already had the minimum Manning's *n* value, the difference would not be applied in that area.

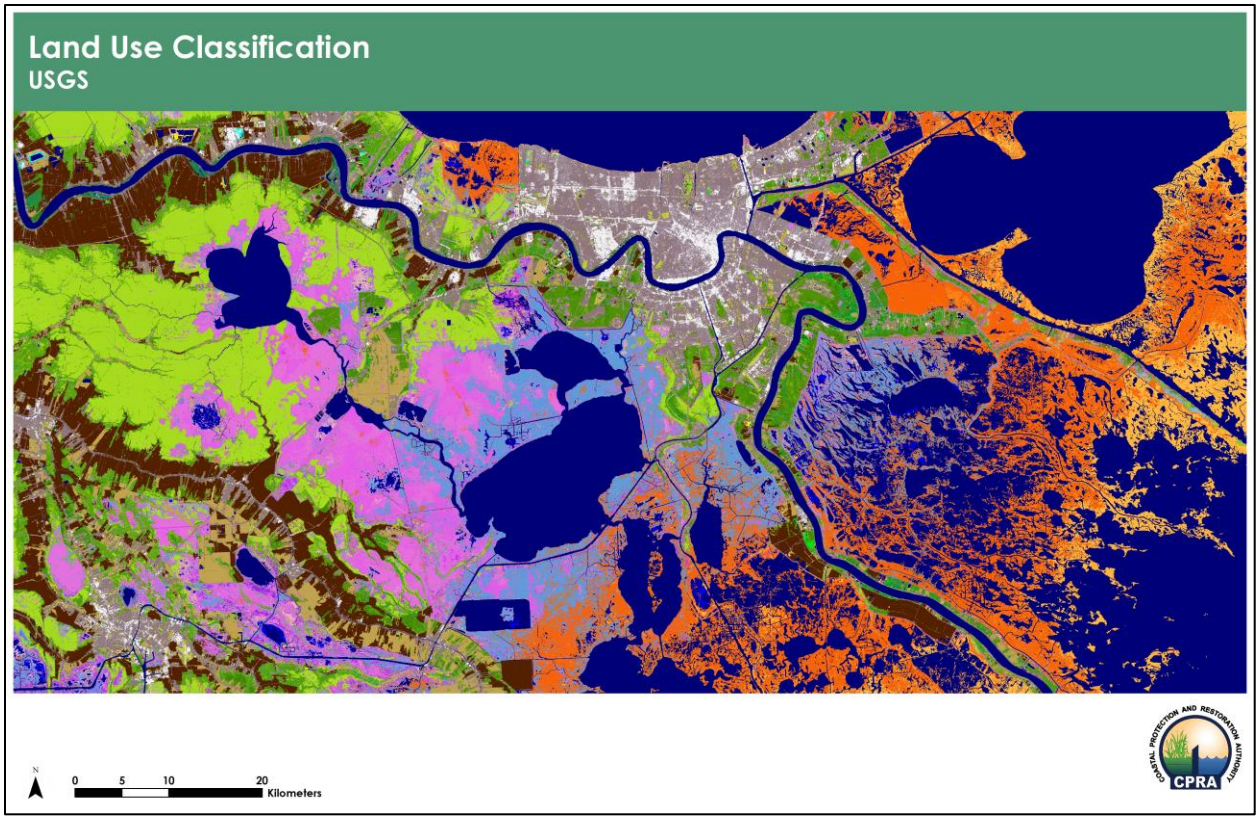

Figure 75: USGS Land Classification Dataset.

Figure 76: USGS Land Classification Categories.

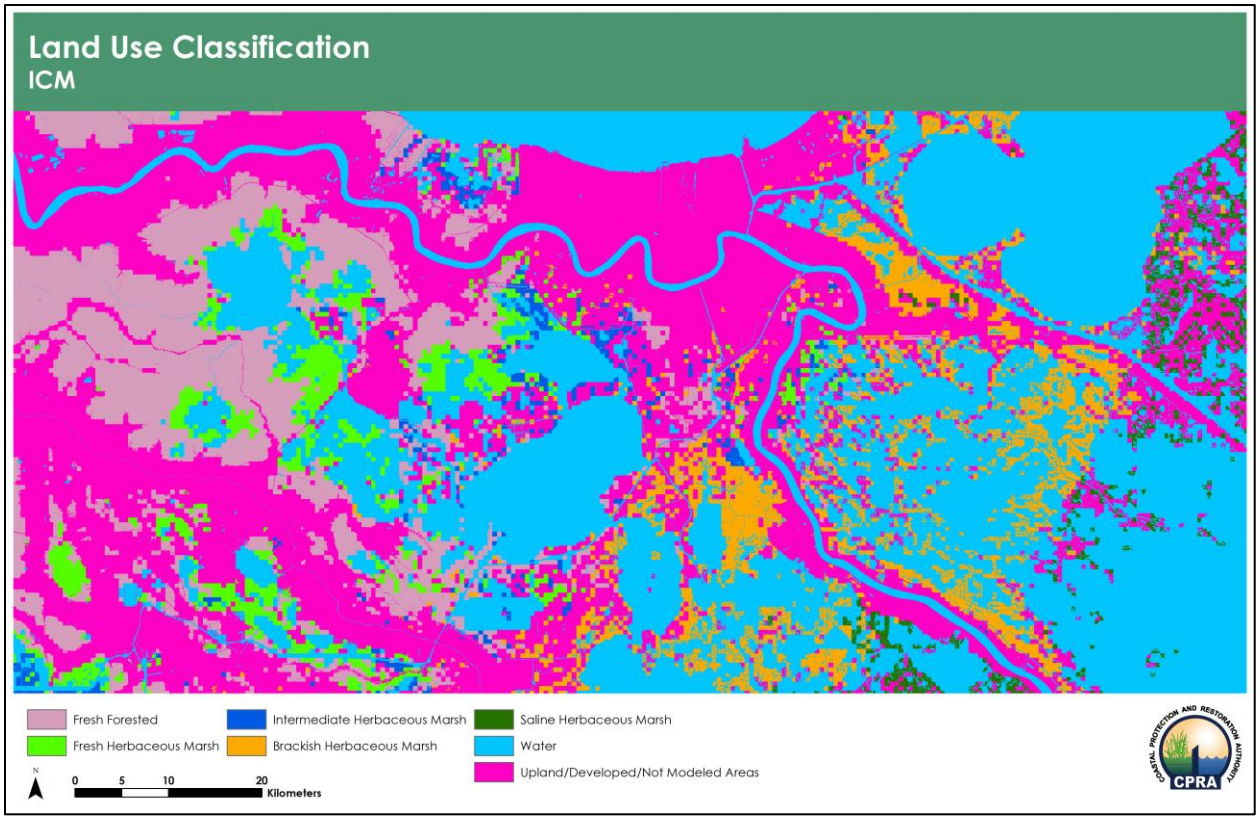

Figure 77: ICM Land Classification Dataset.

Appendix 9: Treatment of Waves in the Mississippi River for the 2017 Coastal Master Plan

Major drivers of overtopping rates and subsequent damages in enclosed areas in the CLARA model are wave heights and periods determined by the ADCIRC+SWAN model. For most enclosed areas, waves at the ADCIRC+SWAN model extraction locations generally approach perpendicular to the enclosing structures. Accordingly, model outputs extracted from ADCIRC+SWAN and passed to the CLARA model assume that the extracted maximum wave heights and associated wave periods occur at a direction perpendicular to the flood protection features. However, because of the levee and river geometries, the maximum wave heights and periods extracted from the ADCIRC+SWAN model do not necessarily align perpendicular to Mississippi River levees. The wind fetch along the river drives the development of the largest waves, and in the river, the longest fetches are in line with the river and thus parallel to many of the levees along the bank (Figure 78). Consequently, the assumption that maximum wave heights arrive perpendicular to the river levees leads to overestimates of overtopping rates in the CLARA model for the adjacent enclosed areas.

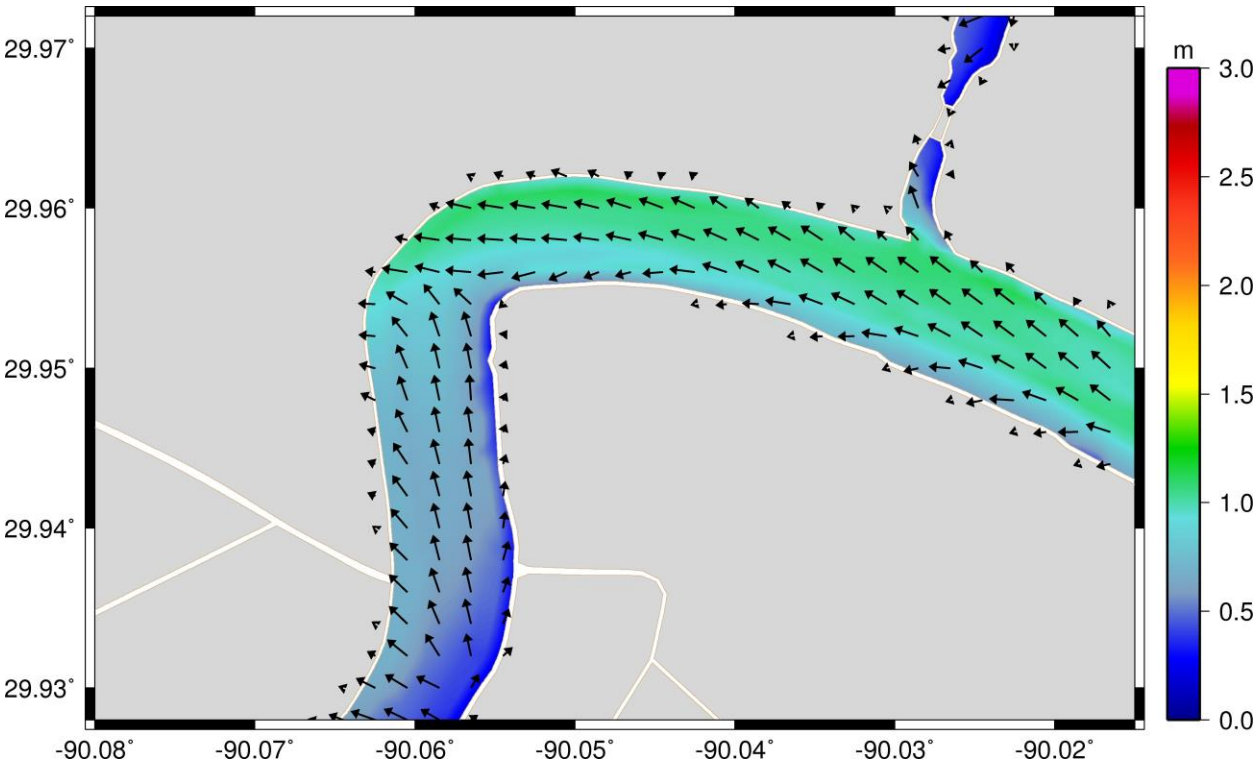

Figure 78: An Example of Wave Heights (contour colors) and Wave Directions (arrows) Near Algiers Point in New Orleans, Louisiana, for a Storm Simulation. Note that the waves do not approach perpendicular to the river levees at many locations.

To better estimate overtopping within adjacent enclosed areas, an approach developed by USACE was applied to adjust wave heights for oblique waves (USACE, 2012). At each time snap in the ADCIRC+SWAN model, wave heights were calculated based on reduction factors that account for the angle between the wave direction and the nearest river levee. The product of the modeled wave heights and the reduction factors created effective wave heights, and the

maximum effective wave height during each storm and the associated peak period were used in overtopping calculations. An example of the time series with and without the reduction factor and the resulting maximum wave heights passed to the CLARA model for a sample storm are presented on Figure 79.

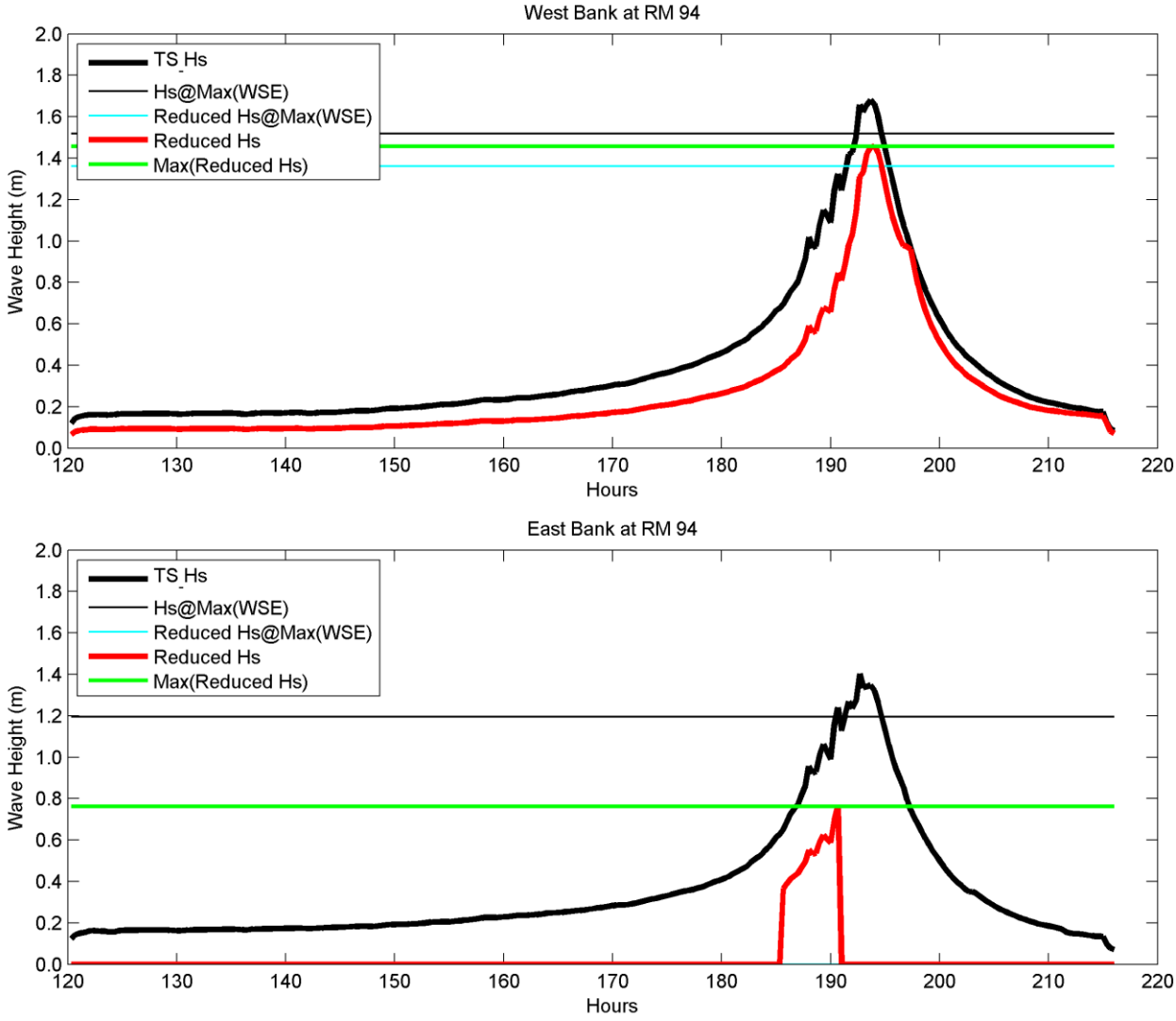

Figure 79: Wave Height Time Series with and without the Directional Correction Factor Near Algiers Point in New Orleans, Louisiana. The thick black line is the modeled wave height time series. The thin black line is the wave height at maximum water surface elevation. Red is the effective wave height time series with directional correction factor applied. Blue is the effective wave height at maximum water surface elevation. Green is the maximum effective wave height passed to the CLARA model.

References

USACE. 2012. Hurricane and Storm Damage Risk Reduction System Design Guidelines. USACE New Orleans District Engineering Division, New Orleans, LA. 606p.